General Disclaimer

One or more of the Following Statements may affect this Document

- This document has been reproduced from the best copy furnished by the organizational source. It is being released in the interest of making available as much information as possible.

- This document may contain data, which exceeds the sheet parameters. It was furnished in this condition by the organizational source and is the best copy available.

- This document may contain tone-on-tone or color graphs, charts and/or pictures, which have been reproduced in black and white.

- This document is paginated as submitted by the original source.

- Portions of this document are not fully legible due to the historical nature of some of the material. However, it is the best reproduction available from the original submission.

Produced by the NASA Center for Aerospace Information (CASI)

NASA Technical Memorandum 84570

Research and Technology

1982 Annual Report of the Langley Research Center

(NASA-TM-84570) RESEARCH AND TECHNOLOGY REPORT OF THE LANGLEY RESEARCH CENTER Annual Report (NASA) 91 p HC A05/MF A01 CSCL 05B

N83-15248

Unclas
G3/99 02320

National Aeronautics and Space Administration

Langley Research Center
Hampton, Virginia 23665

FOREWORD

The role of the Langley Research Center is to engage in the basic and applied research necessary for the advancement of aeronautics and space flight, to generate new and advanced concepts for the accomplishment of related national goals, and to provide research advice, technological support, and assistance to other NASA installations, other government agencies, and industry. This Langley Research Center 1982 Annual Report on Research and Technology contains highlights of our major accomplishments and applications made during the past year. The highlights illustrate both the broad range of the research and technology activities at the Langley Research Center and the contributions of this work toward maintaining United States leadership in aeronautics and space research. For further information about the report contact Robert H. Tolson, Chief Scientist, Mail Stop 103, Langley Research Center, Hampton, Virginia 23665, (804) 827-3316.

Donald P. Hearth
Director

AVAILABILITY INFORMATION

The research and technology accomplishments in this report are arranged according to the NASA program office sponsoring the work and the Agencywide Research and Technology Objectives and Plans (RTOP) work breakdown structure. For additional information on any summary, contact the individual identified with the highlight. Commercial telephone users may dial the listed extension preceded by (804) 827. Telephone users with access to the Federal Telecommunications System (FTS) may dial the extension preceded by 928.

CONTENTS

Aeronautics and Space Technology

Space Science and Applications

Space Transportation Systems

ORIGINAL PAGE IS
OF POOR QUALITY

Aeronautics and Space Technology

Advantages of Spectral Methods in Potential-Flow Airfoil Calculations

A spectral collocation method for computing solutions to the potential equation for transonic flow about a two-dimensional lifting airfoil has been developed that is competitive in computation time with existing finite-difference airfoil codes. The high accuracy attainable with spectral methods for a relatively small number of mesh points offers the possibility of obtaining good scientific results with far less computer storage than is required with finite-difference methods. Alternatively, solutions of higher accuracy can be produced with the same number of mesh points and storage. Previous spectral methods have been impractical for engineering use due to excessive machine times required for solution of the equations. The current scheme offers a significant reduction in computer time required.

Computed surface pressures are compared using 20 and 40 node points about an NACA 0012 airfoil. The spectral solution using 40 points agrees to within four decimal places with a similar computation (not shown) by FL036, a finite-difference code developed by Jameson at Princeton University that uses 192 points about the airfoil. Note that the section lift coefficient C_ℓ predicted by the 20-point solution is within 0.11 percent of that from the 40-point solution. The 40-point spectral solution required approximately the same computer time as the previously mentioned fine-grid finite-difference solution and used less than one-third the computer storage.

The spectral airfoil code is capable of producing solutions for supercritical flow with shocks using an artificial density approach. Some loss in accuracy near the shock is suffered in such cases.

Craig L. Streett, 2627 505-31-13

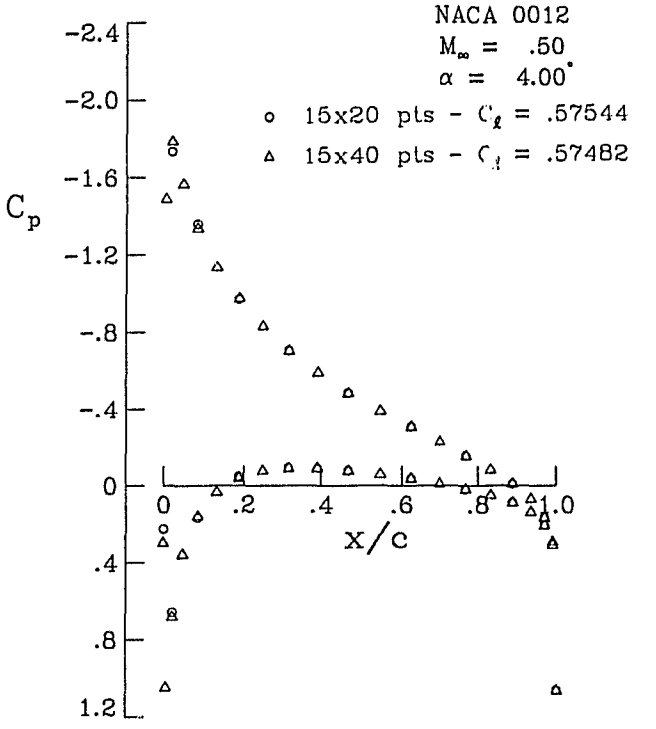

Comparison of predicted pressure distributions on coarse and fine grid.

Efficient 3-D Transonic Wing Calculations on CYBER 205

It has been found that with new vectorizable algorithms for numerically solving three-dimensional transonic potential flows, solutions can be obtained 20 times faster on the recently developed Control Data CYBER 205 computer than on the CYBER 175. The use of the new "supercomputer" and the new family of algorithms will allow aircraft designers to use the computer codes on a routine, affordable basis.

Most three-dimensional transonic computer codes are expensive to use as routine design tools. One way to reduce the cost of running these codes is through improvements in calculation rate by using "supercomputers" such as the CYBER 203 and CYBER 205. These machines are known as vector processors and

ORIGINAL PAGE IS
OF POOR QUALITY

can perform millions of operations per second in special cases where vector instructions are used. An active research area is the search for new algorithms that are readily "vectorized," in order to take better advantage of the design of the new vector processors.

To explore the application of vector processing to transonic aerodynamic calculations, a widely used transonic potential-flow computer code, FL022 (developed by Jameson and Caughey at New York University), was implemented on both a CYBER 203 and a CYBER 205. First the code was put on the CYBER 203 in serial form, and, using various programming techniques, a speedup of over 500 percent was obtained over a serial CYBER 175. Very little additional speedup was obtained when the program was vectorized, due to the inherently serial nature of the existing algorithm (SLOR) used to solve the finite-difference equations in FL022.

To make better use of the vector capabilities of the CYBER 203 and 205, the SLOR algorithm was replaced with a more readily vectorizable implicit line algorithm (ZEBRA I, developed at Langley). Although it has not yet been implemented in a fully efficient manner, projections based on runs that have been made show that a significantly higher computational rate could be obtained using this algorithm, as shown in the table.

N. Duane Melson, 2627 505-31-13

Solution Times for Various Implementations of FL022

Program	Machine	Solution time, sec
Scalar FL022*	CY 175	2300
	CY 203	470
Vector FL022	CY 203	430
Fully efficient FL022 ZEBRA I (projected)	CY 203	364
	CY 205	115

*Scalar FL022 calculation on the CYBER 175 was for a 192 × 32 × 24 grid. All other calculations were for a 192 × 32 × 32 grid.

On the Nonuniqueness of the Transonic Potential-Flow Equation

Recently it was shown that in a certain range of angle of attack and Mach number the numerical solutions of the equation for the velocity potential describing flow past a two-dimensional transonic airfoil are not unique. It was conjectured that the nonuniqueness was related to the buffeting phenomenon observed experimentally in the same Mach number range. However, ongoing research on the solution to the more exact Euler equations, which account for rotational effects, indicates that this is not the case. It appears that the nonuniqueness

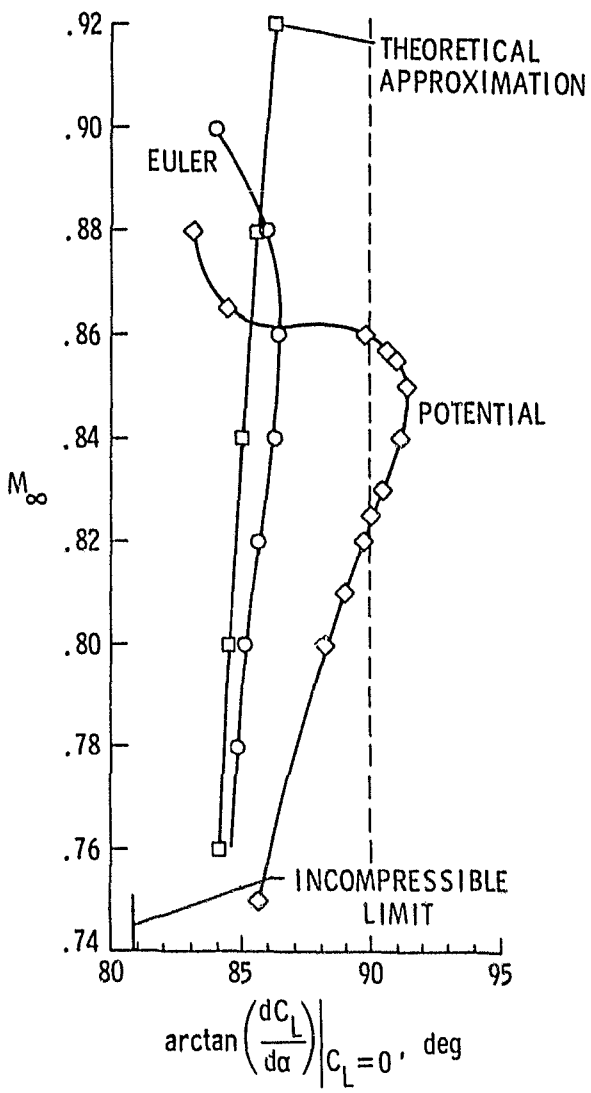

Comparison of Euler and potential solutions for flow past NACA 0012 airfoil.

ORIGINAL PAGE IS
OF POOR QUALITY

stems from the assumption of isentropic irrotational flow upon which the potential approximation is based.

A comparison between the results of a potential code and an Euler code for flow past an NACA 0012 airfoil is shown in the figures. As the free-stream Mach number increases beyond 0.76, the slope at $C_L = 0$ of the section lift coefficient (C_L) versus the angle-of-incidence (α) curve predicted by the potential solutions deviates considerably from that predicted by the Euler calculations. In the range of free-stream Mach numbers between 0.823 and 0.860, the potential exhibits multiple solutions at zero incidence, as shown in the second figure for a Mach number of 0.83. In this figure the Euler solutions do not show any anomaly, indicating that the phenomenon of multiple solutions is a problem associated only with the potential approximation.

Manuel D. Salas, 2627 505-31-13

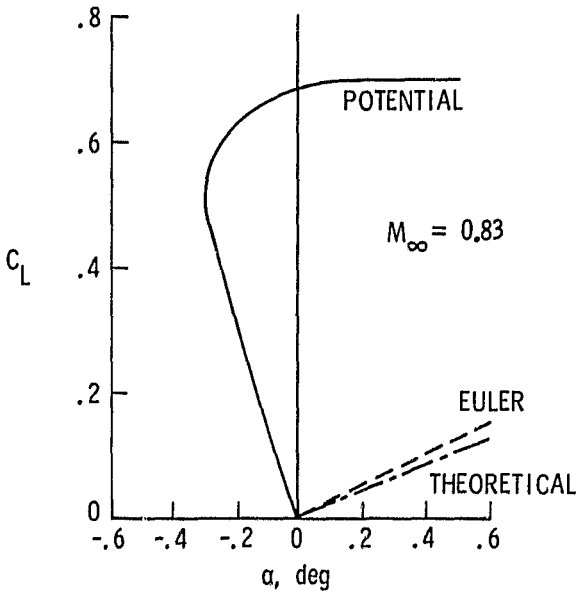

Lift coefficient as a function of angle of attack for flow past NACA 0012 airfoil.

Improving the Convergence Rate of Factored Implicit Schemes

In recent years alternating-direction implicit finite-difference schemes have become quite popular for solution of Euler and Navier-Stokes equations. The most commonly used form of these schemes is the approximate factorization (AF) method developed at NASA Ames Research Center. A theoretical advantage of the AF method is its unconditional stability, allowing an arbitrary choice of the time step. In practice, however, this algorithm has proven to be quite sensitive to a number of factors, including the choice of the time step. For calculations made with a constant time step, an "optimum" time step value, which gives the fewest iterations to convergence, can be found experimentally. A recent analysis at Langley has led to a successful analytical prediction of this complete convergence behavior for the AF scheme for the two-dimensional heat conduction equation, including the optimal time step.

As a result of the insight gained in this analysis, it was noted that combining a one-step explicit finite-difference scheme with the AF method in a predictor-corrector fashion should both accelerate the convergence of the scheme and greatly reduce the time step sensitivity. These results have been verified computationally, as shown in the figure. The curve labeled AF shows the sensitivity to time step λ (here normalized by the explicit stability limit) of the original AF scheme for the two-dimensional heat conduction equation on a 17 × 17 uniform grid. The number of time steps (N) needed to converge the solution to steady state is seen to depend strongly on λ. The curve labeled modified AF is from the new predictor-corrector scheme. The improvement in iterative efficiency and the reduction in time step sensitivity are apparent from the figure.

Douglas L. Dwoyer, 3171 505-31-13

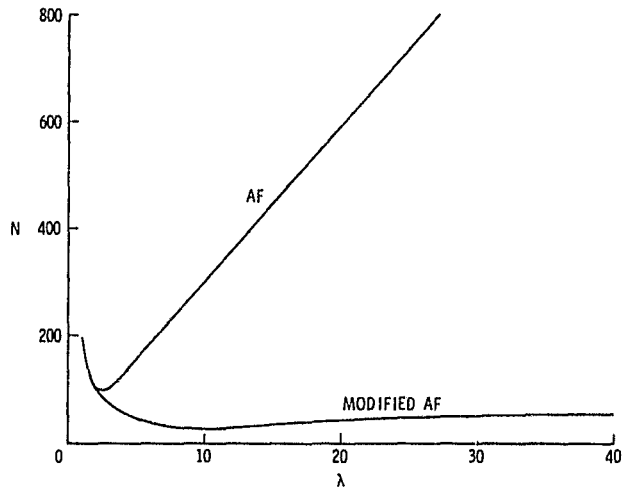

Variation of number of time steps to converge with choice of time step for AF and modified AF schemes.

ORIGINAL PAGE IS
OF POOR QUALITY

Successful Ground Simulation of Supersonic-Flight Boundary Layer Transition

Ground simulation of supersonic-flight boundary layer transition phenomena has heretofore been severely compromised by free-stream flow disturbances generated in turbulent wind tunnel sidewall boundary layers. Two new research tools have been developed that significantly enhance the quality and validity of ground simulation for the supersonic-flight boundary layer transition problem; these are a new concept for a "quiet" supersonic wind tunnel and a user-oriented compressible three-dimensional boundary layer stability code.

A Mach-3.5 Pilot Quiet Tunnel has been developed that incorporates a rapid-expansion contoured nozzle and boundary layer bleed slots upstream of the nozzle throat to produce extremely low background free-stream noise levels in the upstream portion of the test rhombus. The modifications result in noise levels that are an order of magnitude lower than those in conventional supersonic wind tunnels. Recent boundary layer transition measurements on a sharp-tip cone in this facility agree for the first time with those obtained in flight, as shown in the figure.

A new user-oriented stability code (COSAL) developed under contract with High Technology, Inc., for supersonic boundary layer flow over axisymmetric bodies and swept, tapered wings has been used to analyze the available supersonic-flight transition data as well as these recent Mach-3.5 Pilot Quiet Tunnel data. The results indicate that the compressible (supersonic) stability theory correlates well with both the quiet wind tunnel and flight results, and therefore can be utilized for design in such areas as thermal protection systems (TPS) and laminar flow control.

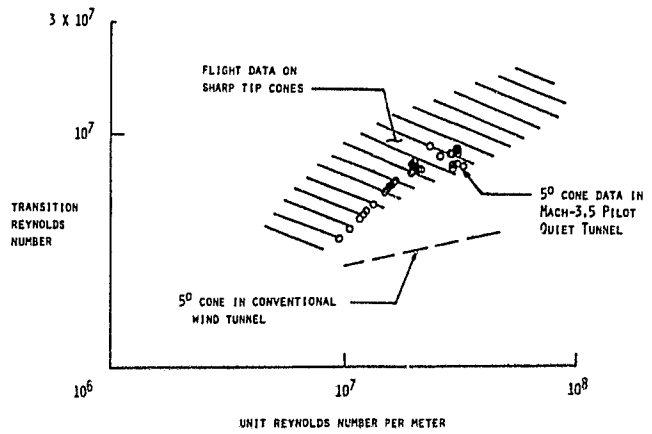

Transition Reynolds number on sharp cones in supersonic ground and flight experiments.

Ivan E. Beckwith, 4546 505-31-23

Simulation of Transition in Plane Channel Flow

Recent experiments conducted under a grant with Old Dominion University have shown that transition to turbulence in plane channel flow follows a sequence of events similar to that observed in the boundary layer transition. In this work, a direct numerical integration of the time-dependent three-dimensional Navier-Stokes equations is performed in an attempt to simulate these events in plane channel flow during the later stages of transition. The solution procedure is a second-order semi-implicit method that uses the pseudo-spectral technique along the homogeneous directions and finite differences along the nonhomogeneous direction. The finite-difference equations are transformed into wave-number space along the homogeneous directions and the resulting equations are solved by block-tridiagonal matrix inversion along the nonhomogeneous direction.

Contour plots of equishear lines, which correspond to the approximate spanwise vorticity in the x_1-x_2 plane at the position of maximum perturbation velocity, are presented and compared to the one-spike stage of the experiment. Measurements were made at a fixed streamwise location within the channel over a time period t; thus they represent the evolution of the flow field in space. The numerical simulation marches in time and tracks the growth of the vortex structure across a computational box including all of x_1. Comparisons can be made between the two sets of data because the experiment will be equivalent to a time-like evolution of the flow field when the development of an initial disturbance is followed over a period of time.

In both the experiment and the computation, the typical head of the shear layer appears very clearly, indicating the formation of a shear layer away from the wall about midway between the wall and the channel centerline.

ORIGINAL PAGE IS
OF POOR QUALITY

This is due to the induced velocity from the streamwise vortex system. Although the comparison is very favorable, inadequate mesh resolution in the outer portions of the flow field results in lower vorticity levels in the computation than are indicated by the laboratory flow. However, since the mesh is finely clustered along x_2 close to the wall, vorticity concentrations in this region are adequately resolved by the numerical simulation.

William D. Harvey, 2631 505-31-33

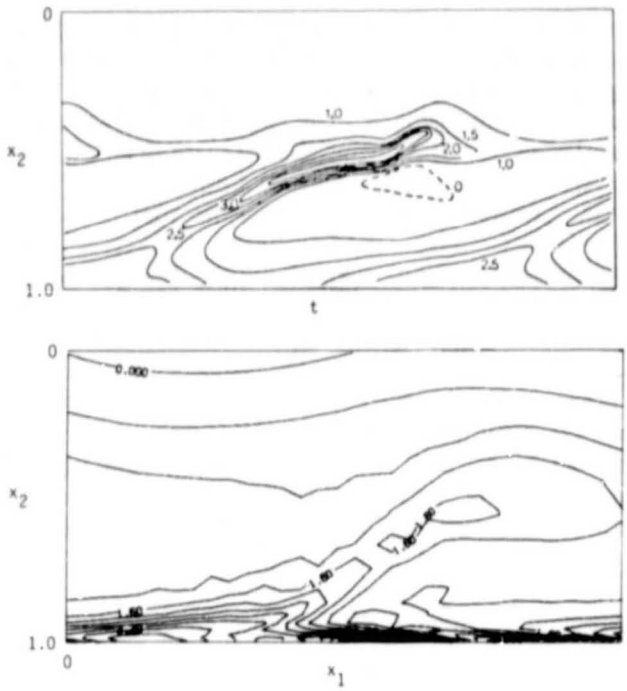

Contour plots of spanwise vorticity.

Wind Tunnel Model of Laminar-Flow-Control Airfoil

A large-chord swept-airfoil model has been developed with active suction provisions to maintain laminar flow about the airfoil at transonic conditions. Research requirements led to unique design and fabrication features not previously included in conventional transonic wind tunnel models. Specifically, these unique features included: 1) a large-chord (7-ft) airfoil that is manufactured to extremely close tolerance (±0.001 in. on airfoil ordinate) and extremely smooth surface conditions (waviness in streamwise direction); 2) very narrow (0.002 in. wide) sharp-edged suction slots in the spanwise direction spaced accurately on the upper and lower surface of the airfoil; and 3) precisely located and smoothly contoured internal flow passages to provide the required suction distribution over the model's surface. To meet these requirements the model substructure with internal flow passages was accurately machined by numerically controlled milling methods. A thin skin (1/32-in.-thick aluminum) was bonded over the substructure to form the airfoil aerodynamic surface, the precision suction slots were cut through the outer skin connecting to the internal flow passages by a unique sawcut operation, and the final surface finish was hand polished and treated with a special hard-surface anodized coating. The complete model, including the suction system and research instrumentation, has been calibrated, and the model is undergoing research evaluation in the Langley 8-Foot Transonic Pressure Tunnel.

Joseph D. Pride, 4666 505-31-33

LFC airfoil mounted in 8-ft TPT.

Variable Choke for 8-Foot Transonic Pressure Tunnel

Research evaluation of the laminar-flow-control (LFC) airfoil model in the Langley 8-Foot Transonic Pressure Tunnel (TPT) necessitated the development of a choke (sonic throat) that would operate from the sidewalls of the tunnel

ORIGINAL PAGE IS
OF POOR QUALITY

immediately downstream of the airfoil model. The two-wall variable sonic choke generates a normal shock downstream of the model that prevents upstream progression of the noise generated in the diffuser, turning vanes, and fan. The acoustic disturbance of the laminar boundary layer at the LFC model experiment is minimized.

The development of a variable choke that is remotely controlled during tunnel operation and is capable of producing sonic conditions over a test Mach number range from 0.77 to 0.84 while maintaining a specified aerodynamic shape to minimize pressure losses was a significant design challenge. The variable choke is constructed of fiberglass/epoxy composite material that varies in thickness from 0.42 in. to 0.72 in. from the upstream to the downstream end. The composite structure is flexible enough to allow displacement of up to 1.2 in. by a linear actuator, yet is strong enough to sustain the high-pressure loading encountered and maintain the smooth aerodynamic surface required to prevent flow disturbance and tunnel pressure losses. The choke planform spans the tunnel sidewall (5.5 ft) and has an overall length in the streamwise direction of 6 ft. The two-wall variable sonic choke is presently installed in the 8-ft TPT, where it is functioning as designed for the LFC wind tunnel test program.

Joseph D. Pride, 4666 505-31-33

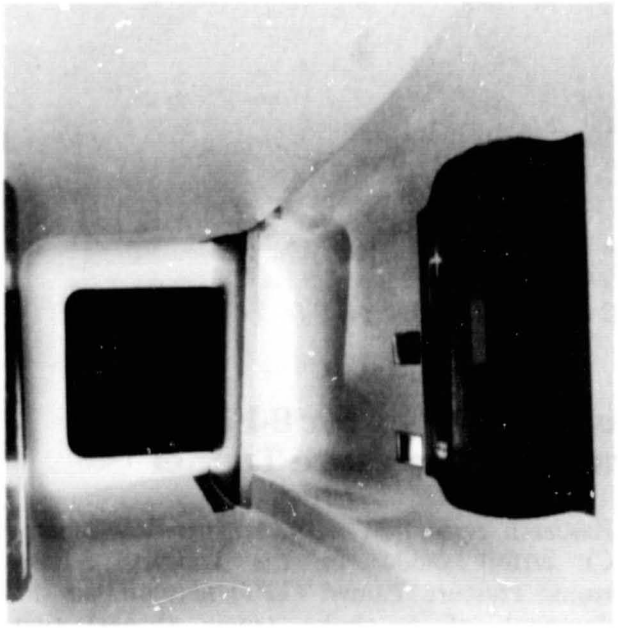

Variable sonic choke in 8-ft TPT.

Three-Dimensional Euler Solutions for Long-Duct Nacelles

Current transonic computational methods for complicated configurations have mainly been limited to inviscid, potential-flow solutions. Solutions of the more complete Euler equations, which allow for the capture of rotational effects, have been concentrated in the areas of two-dimensional airfoils, axisymmetric flows, and forebodies.

An Euler equation computational technique is being developed to numerically solve for the transonic flow past wing-pylon-nacelle configurations. The technique employs an implicit numerical algorithm and a radiation boundary condition at the outflow and far-field boundaries. To date, the resulting computer code has been developed to the point that it can handle three-dimensional flow-through nacelles. Calculations were made with the code for axisymmetric bodies and for long-duct turbofan engine nacelles at a free-stream Mach number of 0.80 and at angles of attack of 0^{o} and 4^{o}. The solutions at 0^{o} angle of attack were axisymmetric even though the code is three-dimensional, while at 4^{o} angle of attack the solution had a definite three-dimensional character. The calculations at both 0^{o} and 4^{o} angle of attack agreed well with wind tunnel data.

William B. Compton III, 2673 505-31-43

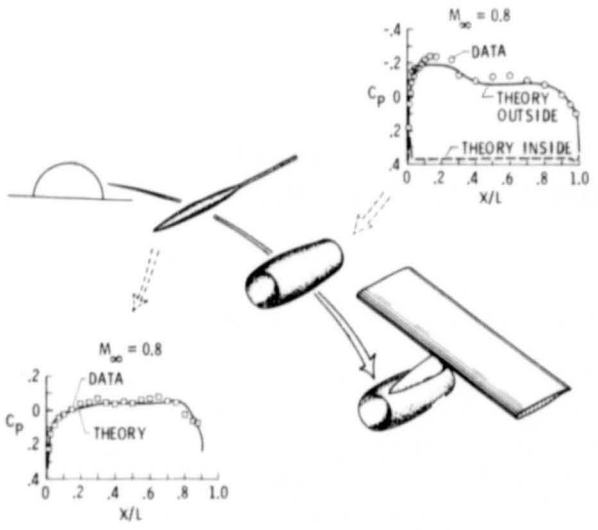

Comparisons of 3-D Euler solutions with wind tunnel data.

ORIGINAL PAGE IS
OF POOR QUALITY

Vortex Flap Technology

Vortex flaps are variable-geometry devices located at the leading edges of highly swept wings to exploit the naturally occurring leading-edge vortices present on these wings. As shown in the figure, these devices, when properly designed, can completely capture the leading-edge vortex on the flap and provide well-organized attached flow on the wing aft of the hinge line. As a result, the wing not only generates the additional lift associated with leading-edge vortices, but also achieves reduced drag because of the axial force generated by the vortex acting on the vortex flap. The increase in performance is particularly important for aircraft that are climbing or executing sustained transonic maneuvers. Vortex flaps can also be used to provide extra lift at low angles of attack so that takeoff roll distance can be reduced and visibility can be improved during landing approach. In addition, the vortex flap can be deflected downward so that a vortex is trapped behind it to produce drag and hence reduce landing rollout. The drag coefficient of a vortex flap is the same order of magnitude as that of a drogue chute. The vortex flap can be made more effective in its operation by employing suitable trailing-edge flap deflection as well.

The vortex flap concept has now been validated experimentally through extensive parametric studies conducted at subsonic speeds on a variety of planar delta-wing models. The studies were done both at Langley and under contract with Vigyan Research Assoc., Inc.

John E. Lamar, 2601 505-31-43

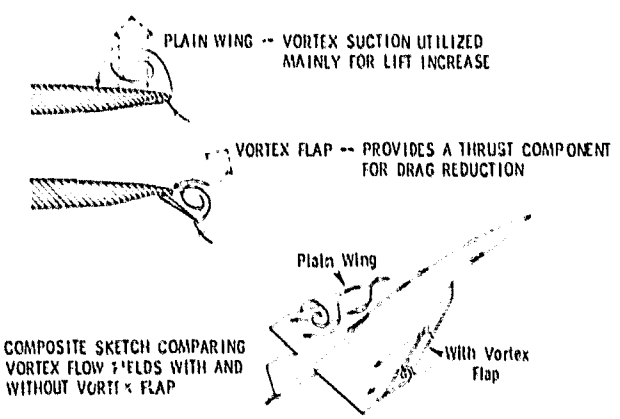

Vortex flap concept.

Laser Velocimeter/Hot Wire Turbulence Intensity Study

A comparative study was conducted between a laser velocimeter and a single-component hot wire to develop a base level of confidence in the laser velocimeter as a tool for measuring turbulence parameters in wind tunnel flow fields. The study was conducted in the free jet exiting from a fully developed turbulent pipe. Great care was taken to reduce the known measurement uncertainties in both instruments. The possible measurement uncertainties in the hot wire were reduced by frequent calibrations of the hot wire, low-velocity flow (15 m/sec) to maintain isothermal conditions, and the determination of the effects of seeded flows. Since the use of an rms meter to measure the nonlinear output voltage will yield inaccurate results, direct digitization of the hot-wire signal was performed and the results converted, point by point, to velocity via a spline-fit calibration curve. These velocity measurements were then statistically averaged to yield the turbulence intensity of the flow. The errors in the laser velocimeter were reduced to less than 1 percent by using very small particles (0.5 μm in diameter) as the seed material. Off-axis forward-scatter location of the collecting optics increased the output signal to noise while keeping the sample volume small (0.62 mm in length).

Typical results of this study are shown in the figure. Within the core region (flow turbulence intensities less than 20 percent, the

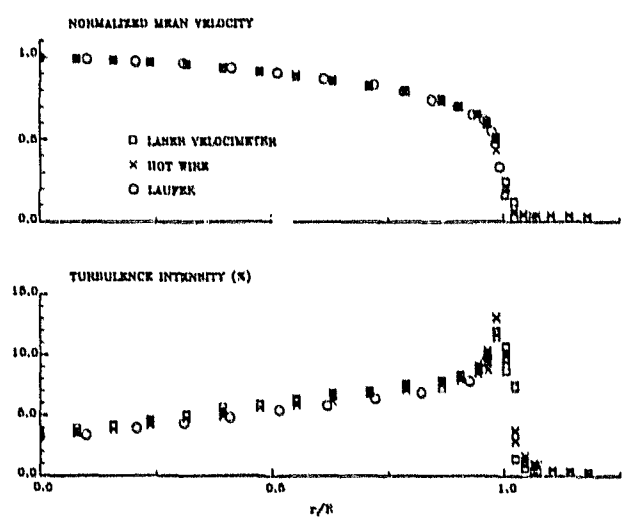

Laser velocimeter turbulence intensity measurements.

practical upper limit of the hot wire) the laser velocimeter and the hot-wire turbulence intensity measurements agree within ±0.8 percent in turbulence intensity. Although the present study was conducted in a jet flow, the results agreed within 0.4 percent in turbulence intensity with Laufer's classic work and are well within the scatter of similar hot-wire studies used to measure turbulence intensity in a pipe flow. The results of this study indicate that the laser velocimeter can be used to measure turbulence intensity with accuracy at least equal to hot-wire anemometry. Further, with the inclusion of a Bragg cell to account for flow reversal, the laser velocimeter may be used to measure turbulence intensities of much higher amplitude than are possible to measure with a hot wire.

J. F. Meyers, 2791 505-31-53

National Transonic Facility

The National Transonic Facility (NTF) represented a unique and complex engineering challenge. Operation at temperatures from +175°F to -320°F and pressures from 8.3 psia to 130 psia resulted in many design problems requiring state-of-the-art development in materials and techniques and the utilization of novel design concepts. Some typical design problems encountered and their solutions are discussed in this summary.

LN_2 Storage Tank Inlet Location

The NTF uses a 250,000-gallon tank for the storage of liquid nitrogen (LN_2). The tank is a thin-walled vessel designed for a maximum pressure of 5 psig and a minimum pressure of 4.0 in. of water. The geometry of the tank is such that a large ullage volume can exist. If a low level of LN_2 exists in the tank, the nitrogen gas (GN_2) will tend to stratify. An analysis was performed to determine what happens when the tank is refilled after stratification of the GN_2 has taken place. The LN_2 usually comes into the tank at the top, where it is poured onto a splash plate. If the GN_2 temperature is above the saturation temperature of LN_2 (140°R), some LN_2 will evaporate. If enough evaporation occurs the GN_2 pressure could drop fast enough to cause the tank to collapse.

A computer program was developed to model the tank filling process. A complete range of filling rates was simulated for various initial temperatures of the stratified GN_2. The results showed that the tank could collapse under certain conditions; consequently, the inlet design was changed to bring the LN_2 in at the bottom of the tank.

Gate Valves

The gate valves permit access to the model in the test chamber without depressurizing the entire tunnel circuit. To gain access to the plenum and model area the flow is stopped, the clamps on the movable contraction and high-speed diffuser are released, and the two structures are retracted from the plenum. The gate valves are then elevated and positioned to close the openings in the plenum bulkheads. The valves, approximately 14 ft in diameter, are moved on a track system using four electric-motor-driven mechanical actuators. Two lift actuators raise the gates to the top of the track and two positioning actuators push the gate into position, where the clamps can engage and seal against the bulkhead flange. After the gates are in their closed position and are sealed, the plenum volume is vented to the atmosphere and conditioned for personnel entry for the model change.

Side Access Housings

The side access housings allow personnel to work on a test model without environmentally conditioning the entire plenum section to obtain safe working conditions. This results in a significant reduction in operating cost.

The housings are 7 ft high and 11 ft wide inside, with 6-in. thick insulated walls. The construction is aluminum alloy with urethane insulation. Two cables on each housing pull the housings into the tunnel and two cables pull the housing out. (as one set of cables reels out, the other set reels in). When the housings are retracted, they stop inside the plenum-to-housing seal but allow the plenum doors to close. When the housings are inserted, they meet at the tunnel centerline and a seal is made between the housings and the model sting. The housings are then purged of the cold nitrogen gas with low-pressure air and heated with an electrical resistance heater. When the oxygen level is 19 percent and the temperature is about 40°F, the end doors of the housings may be opened for access to the model. The end doors are manually operated for safety purposes.

Internal Insulation System

A highly efficient insulation system was required to protect the steel pressure shell from excessive thermal stresses and to minimize energy losses. The goal was to limit heat transfer from external air to the tunnel interior to 300 BTU/sec for the 40,000 ft^2 of tunnel surface area. The insulation material was required to operate over the previously mentioned temperature and pressure ranges and also to be nonflammable in air at 130 psia.

An intensive development program was initiated to produce a system with the required characteristics. The resulting system consists of a high-density closed-cell modified polyurethane material laminated into blocks and machined to the required shape, along with an aero liner that serves as a backup retention system for the insulation material. The prefabricated blocks were individually filled on site and bonded to the tunnel shell. The aero liner is made up of fiberglass polyester "T"-shaped structural longerons bolted to the tunnel shell, 3/8-in.-thick aluminum liner panels, and a fiberglass polyester cap strip that retains the liner panels. A two-part polyurethane adhesive, Crest 391, and a layer of fiberglass cloth were used throughout the system for laminating the blocks, bonding the insulation blocks to the shell, and as a final cover over the blocks and joints.

Fan Blades

The main-drive fan blades for the National Transonic Facility were designed to produce test section Mach numbers from 0.1 to 1.2 and Reynolds numbers up to 120 million. The 25 blades are attached to a disk near the outer rim of the fan, and rotate at speeds up to 600 rpm.

Because of the severe operating environment and the relative inaccessibility for inspection, very rigid design criteria were established using specialized organic-matrix resins that were certified acceptable for cryogenic applications. The blade is fabricated using styles 7781 and 7576 preimpregnated E-glass. Ply thickness ranges from 1.341 in. at the attachment point to 0.315 in. at the tip. The fabrication is done in three basic operations. The main structural component, consisting of 100 plies of prepreg, is molded first. This lay-up is accomplished on a mandrel consisting of a vulcanized gum rubber bag over a wash-out plaster core. The assembly is placed in a matched metal mold and molded in an autoclave after removing the plaster core. Epoxy foam leading and trailing edges are bonded in place. This assembly is then overwrapped with 44 additional plies of prepreg, placed in a mold, and molded in the autoclave. Five additional plies are added after this molding. Machining operations are then performed to fit mating parts, which are bonded in place.

The finished blade is approximately 47.7 in. long from pin to tip, has a tip twist angle of 47°, and weighs 238 lb. The maximum principal stress is approximately 20 percent of the ultimate material strength at operating temperature.

Duct Acoustic Lining

Aeroacoustic estimates of the noise generated by the 25-blade fan in the NTF indicate a broadband noise spectrum with a maximum overall sound pressure level of 155 dB. The maximum sound pressure level is estimated to peak at the fan blade passage frequency of 150 Hz. These estimates were made over the operational temperature and pressure ranges. Attenuation of this noise by 10 to 20 dB was required for environmental purposes and for reducing fan-induced noise in the test section to less than 150 dB.

Parametric analyses were performed with impedance and acoustic performance prediction models for a duct lining filled with a bulk absorber and a duct lining in the form of a dual-cavity resonator (one each positioned upstream and downstream of the fan). The analyses predicted superior performance by the dual-cavity resonator. Final design of the panels was based on cavity depths arrived at by tuning one cavity to just above the blade-passage frequency and the other to a higher frequency.

Dual-cavity sandwich panels were constructed of 3/8-in.-cell Al honeycomb bonded to Al perforated face and septum sheets with a solid Al backing plate. The honeycomb was bonded to the sheets and plate with a reticulating structural adhesive. The panels are estimated to reduce the maximum test section sound pressure level to about 142 dB.

Evaluation of Heavy Welding of Invar

The design of large structures for cryogenic service requires a careful selection of materials and fabrication processes to prevent brittle failure and to minimize the effects of thermal distortion at operating temperatures. In the

ORIGINAL PAGE IS
OF POOR QUALITY

design of the NTF, several major supports for the internal structures were fabricated from a 36-percent nickel iron alloy (Invar 36).

Parts made from this alloy are usually small instrument-grade machinings, and there is very little information in the literature dealing with the machining and welding of heavy sections. The recommended weld filler material for this alloy is the same as for the base metal with the addition of 0.75 percent Ti and 2 percent Mn to enhance welding properties. This filler alloy is no longer readily available, and this necessitated the examination of technically acceptable alternatives.

A test program was initiated to evaluate the feasibility of using non-Invar filler materials for heavy Invar welds and to identify potential candidates alloys. A series of tests was conducted both on "as welded" specimens and on weld specimens that had been subjected to 50 thermal cycles between -300°F and +200°F. The tests included tensile, Charpy V-notch, and guided-bend tests, in accordance with the ASME Pressure Vessel Code. Two readily available alloys were found to be acceptable substitutes, ARCOS Corporation 308L and 8N12, corresponding to AWS/ASME composition E3089-15 and ENiCrFe-3, respectively. They had basically the same strength in the "as welded" condition as did the parent material.

The NTF is expected to be ready for operation in January 1983.

Ralph Muraca, 4539 505-31-63

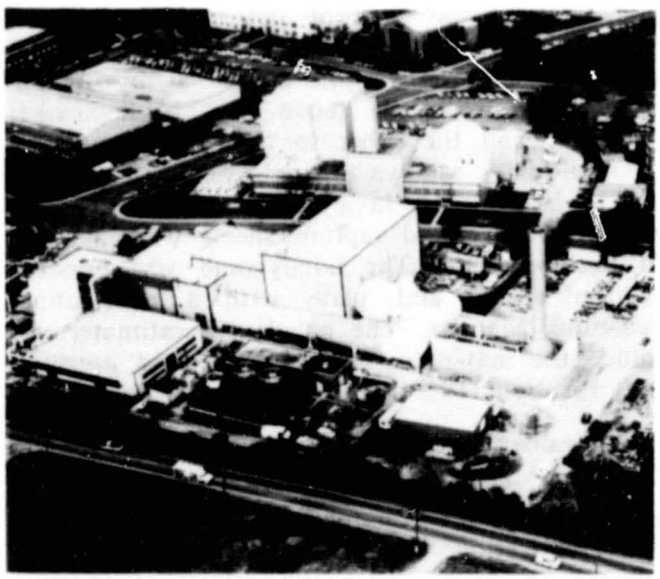

National Transonic Facility.

Prediction of Wind Tunnel Minimum Operating Temperatures

The benefits of cryogenic tunnel operation, such as greater Reynolds number or reduced LN_2 consumption, are maximized at the lowest temperatures at which the tunnel is operated. However, the operating temperature cannot be less than the temperature at which the test gas begins to condense. Condensation effects may result either from the presence of pre-existing seed particles or from seeds formed from the gas itself (self-nucleation). In many circumstances the pre-existing seed particles may be disregarded, so that the minimum operating temperatures depend only on the onset of self-nucleation.

Classical liquid droplet theory (CLDT), which was developed to predict self-nucleation, includes several assumptions that are only approximate. To correct CLDT, various modifications have been proposed by Lothe of the Fysisk Institute, Norway, and Pound of Stanford University (CLDT-LP), Reiss of Bell Telephone Laboratories and Kikuchi of Hughes Research Laboratories (CLDT-RK), and Tolman of the California Institute of Technology (CLDT-T). The problem has been to determine which correction is appropriate for the cryogenic wind tunnels at Langley Research Center. To this end, a CAST-10 airfoil was tested in the 0.3-Meter Transonic Cryogenic Tunnel. Deviations in pressure coefficient (ΔC_p) were then measured to determine the temperatures at which condensation effects occurred. Computational comparisons were made using CLDT, CLDT-LP, CLDT-RK, and CLDT-T. As shown in the figure, the data (circles) show no deviations at the higher temperature example of 96 K, but definite deviations are shown for the lower temperature example of 94 K. For

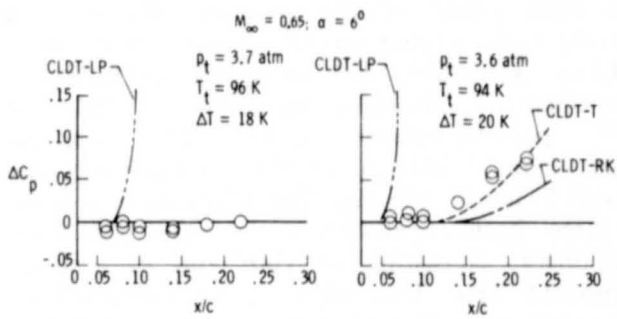

Comparison of data and theories for CAST-10 airfoil.

ORIGINAL PAGE IS
OF POOR QUALITY

the higher temperature, CLDT-LP predicts large effects where none are shown, while CLDT, CLDT-RK, and CLDT-T predict no deviations. For the lower temperatures, CLDT-T shows good agreement and CLDT-RK shows reasonable agreement, while CLDT-LP is unreasonably high and CLDT still predicts no effects at all. Consequently, the data show that CLDT coupled with its CLDT-T modification can be used to successfully predict the onset of self-nucleation, thus allowing more accurate predictions of minimum operating temperatures for the National Transonic Facility.

Robert M. Hall, 2601 505-31-63

Stability of Metallic Alloys for Cryogenic Wind Tunnel Models

An investigation was conducted to examine the various mechanisms that can cause dimensional changes in metal models being tested at full-scale Reynolds number in cryogenic wind tunnels. The Pathfinder I developmental model, designed and fabricated at Langley, is representative of the type of models to be tested at full-scale Reynolds number in the National Transonic Facility (NTF). Small dimensional changes in wind tunnel models become very important when testing at high Reynolds number because of the more stringent requirements on model aerodynamic shape and surface smoothness. Initial problems were encountered with two-dimensional airfoils made of 15-5 PH stainless steel, which warped significantly after being subjected to cryogenic testing in the Langley 0.3-Meter Transonic Cryogenic Tunnel (TCT).

The investigation concentrated on two basic mechanisms that can lead to warpage or dimensional change. These mechanisms are (1) metallurgical structural instability, in which one phase transforms partially or fully into a second phase, which has a different crystal structure and volume, and (2) deformation due to the creation or relief of unbalanced induced or residual stresses as a result of heat treatment, machining, and fabrication processes.

Various materials were evaluated for dimensional stability characteristics. Two of the materials, 15-5 PH and 17-4 PH stainless steel, have been used for 2-dimensional models in the 0.3-m TCT. The other materials, NITRONIC 40, PH 13-8 MO, A286, 300-series stainless, 18-percent Ni maraging, and special 9-percent Ni steel, are either candidates or are presently being used for NTF models. The materials in the second group have better fracture toughness and, for the most part, higher strength properties at cryogenic temperatures. Dimensional stability specimens were designed, fabricated, and cryogenically cycled. Of the materials examined, those judged to be best for use in cryogenic models in view of dimensional stability were PH 13-8 MO, NITRONIC 40, A286, and 18-percent Ni steel. It was also concluded that warpage can be minimized by exposing the model or model component to one or more cryogenic cycles (preferably three) and coordinating verification prior to the final stages of machining. Additionally, cryogenic cycling and coordinate verification after final machining should be done prior to tunnel entry.

Clarence P. Young, Jr., 4508 505-31-63

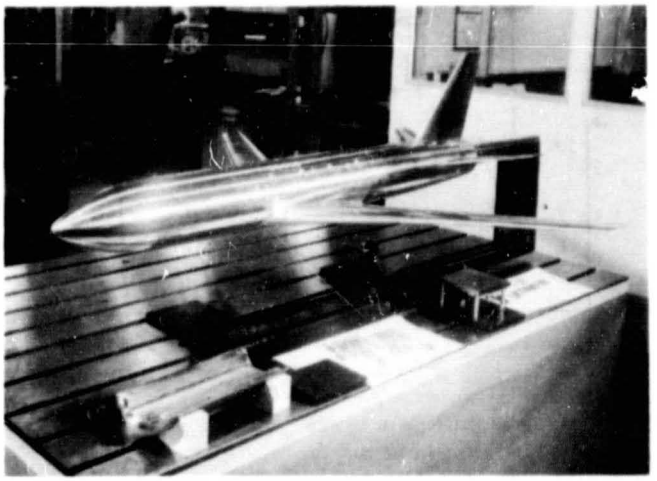

Pathfinder I model.

Full-Potential Solutions for Supersonic Flow Past Wing-Body Configurations

A nonlinear aerodynamic prediction technique based on the full-potential equation written in conservation form has been developed under an ongoing contract with Rockwell International for the treatment of supersonic flows past wing-body configurations. The method employs a novel technique to simulate the flow structure that includes embedded shock waves and mixed cross flow. The body-fitted

ORIGINAL PAGE IS
OF POOR QUALITY

grid system used in every marching plane is generated numerically using an elliptic grid solver. Recent modifications permit solutions for various classes of configurations, including conical and nonconical wing-body configurations.

The computed spanwise pressure distribution is shown for an analytically defined arrow-wing configuration. This configuration is a difficult test case due to the "wake"-separated wing and body near the rear of the configuration (x/ℓ = 0.8). Excellent agreement was observed at low angles of attack (M = 2.36 to 4.63) between the calculation and the data throughout the flow field, including the wake region. Agreement remains good for the case shown (M = 2.96; α = 10^0) except in the wake region, where no wake modeling was employed. These results compare favorably with Euler calculations for this configuration and have demonstrated an order-of-magnitude reduction in computational time.

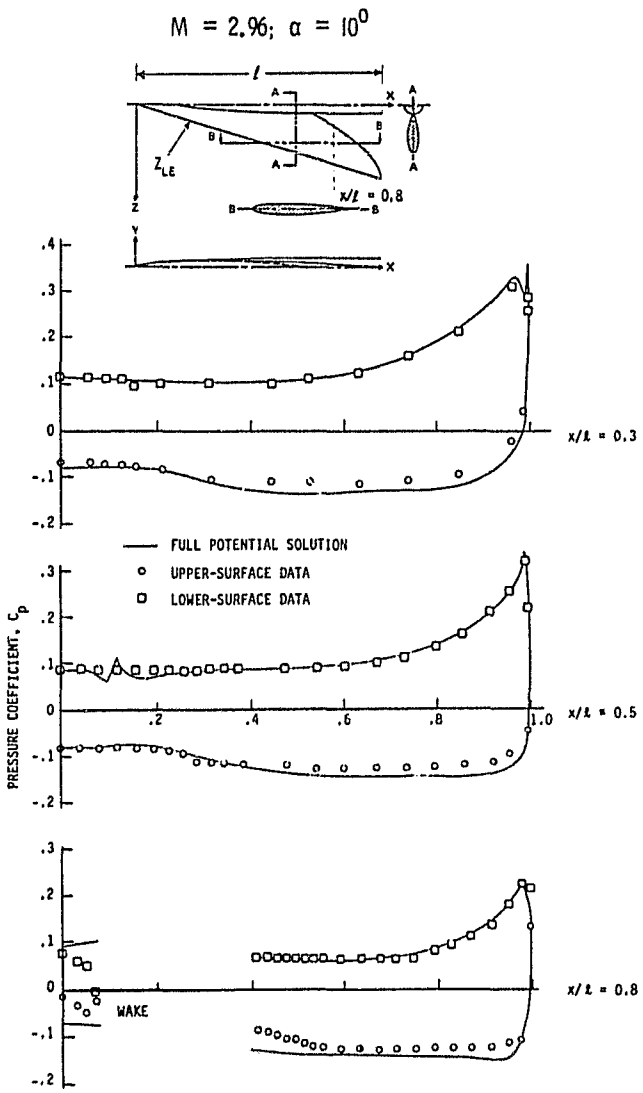

High-angle-of-attack arrow-wing solution.

Kenneth M. Jones, 3294 505-31-73

A Technique for Generating a Mesoscale Terrain Data Base

The speed and memory of the new generation of computers such as the Control Data CYBER 203 allow processing of more detailed numerical weather prediction models with higher resolution. As these models have grown in sophistication, the need for a better defined terrain data base to be used as a lower boundary condition has become acute. Previously, the coarse LFM 190-km terrain grid developed by the National Meteorological Center was used. However, operational mesoscale models with grid spacings of 50 km are now being developed, and to be completely consistent they require terrain data at the same resolution.

To develop a mesoscale terrain data base, high-resolution data were obtained from the Bureau of Mines and Mining in Boulder, Colorado. The data were on a very fine grid, with a data point every 0.5 minute of latitude and longitude. This corresponds to a data density 1600 times greater than that required by the Mesoscale Atmospheric Simulation System model under study at LaRC. In order to sample the data onto the coarse grid of the model and minimize aliasing, the data first had to be smoothed. A very sharp two-dimensional smoothing filter was designed using Tukey's twicing technique. The convolution of a constant 3 × 3 filter and a constant 5 × 5 filter was sharpened using Tukey's technique and resulted in a 19 × 19 filter with a spatial frequency response that drops off quickly in the 0.1 to 0.2 cycles per sampling interval frequency range and is nearly zero at frequencies above 0.2. Application of this filter to the data damps all spatial wavelengths of frequency above 0.2, thereby band-limiting the data so that every other point can be sampled without aliasing. The terrain data base was smoothed and sampled five times in this fashion to produce a terrain data base that has approximately the resolution required by the Mesoscale Atmospheric Simulation System

ORIGINAL PAGE IS
OF POOR QUALITY

model. The final step in the development of this data base was to use bilinear interpolation to register the data onto the model grid.

Patricia Winters Kerr, 2747 505-31-83

An Improved Algorithm for Image Reconstruction

Cubic convolution is a process originally developed in the early 1970's for the reconstruction and resampling of Landsat digital images. Since its development, this process has come to be generally acknowledged as providing a good compromise between computational complexity and reconstruction accuracy, and it is now used in a variety of applications that involve bivariate interpolation. Cubic convolution image reconstruction is actually interpolation implemented by convolving the image samples with a smooth, spatially limited, one-parameter family of functions constructed by joining cubic polynomials in a spline-like fashion. Traditionally, however, the parametric nature of cubic convolution has not been exploited. The one member of this family that was originally proposed remains the standard for comparison and software implementation.

In recent research conducted jointly at Langley and the University of Arizona, the reconstruction properties of the one-parameter family of cubic-convolution interpolation functions were studied and the image degradation associated with reasonable choices of this parameter was analyzed. This research demonstrated analytically that in an image-independent sense there is an optimum value for this parameter, and it is not the standard (default) value commonly used. This important result was subsequently verified with actual image data. In addition, this research demonstrated that in an image-dependent sense, the parameter can be adjusted to optimize cubic convolution to any class of images characterized by a common energy spectrum. This important result has also been verified by numerical simulation with multispectral image data.

Stephen K. Park, 2747 505-31-83

Pseudospectral Navier-Stokes Solver for the CYBER 203

A vectorized code for the Control Data CYBER 203 has been developed to implement a mixed finite-difference and pseudospectral technique for solving the three-dimensional Navier-Stokes equations. The code is intended for use in basic studies of compressible shear flows at high Reynolds number, such as the simulation of the incipient stages of transition to turbulence.

The algorithm implemented employs a three-level operator-splitting technique for solution. The inviscid parts of the equations are solved with a variable-step second-order-accurate Adams-Bashforth method for time advancement and a pseudospectral method for approximating the spatial derivatives in order to obtain the high accuracy required. The second operator invokes an implicit pressure correction and the final solution operator involves a semi-implicit solution of the viscous terms.

The five dependent variables are interleaved one horizontal plane at a time, and their values at the grid points in a plane constitute a typical vector in the calculation. This organization of the data base permits a predictable paging sequence from the virtual system that is minimized by performing all three solution operators in one forward-backward sweep through the data base.

The main computation involves one- and two-dimensional fast Fourier transforms, finite-difference approximation to derivatives, and the solution of a large number of independent tridiagonal systems of equations. For a 32 × 32 × 64 grid, a complete forward-backward pass required 3.2 CPU seconds.

Jules J. Lambiotte, Jr., 4612 505-31-83

Aeroacoustic Computation of Cylinder Wake

The ability to calculate sound generation by a fluid flow from first principles has long been a goal of the aeroacoustics community. As a demonstration of such a capability, computation of noise radiation from a cylindrical body of diameter D normal to a uniform stream of

ORIGINAL PAGE IS
OF POOR QUALITY

velocity U has been accomplished. This flow is known experimentally to produce a highly regular von Karman vortex street in the wake over the wide Reynolds number range from 10^2 to 10^6. The oscillations of the wake result in a narrowband sound (Aeolian tone) production.

The aeroacoustic computation is carried out in two steps. The time-dependent cylinder wake is first calculated by finite-difference techniques. The acoustic radiation is then obtained by integration over the flow field using a modification of the Lighthill theory. Typical results of the noise radiation to a distant observer are shown in the figures. The first graph displays the spectrum of the noise radiated directly above the cylinder. Note that the primary sound is radiated at a frequency f_o given by the Strouhal number ($St = f_oD/U$) of 0.2. This is the characteristic Strouhal number of the time-dependent wake flow and is produced by the fluctuating lift on the cylinder induced as each pair of vortices is shed into the street. The presence of a strong harmonic at $3f_o$ is also observed, in agreement with experimental data. The second graph depicts the noise spectrum directly behind the cylinder. Here, no power at the frequency f_o exists. The primary radiation is at $2f_o$ and its harmonic $4f_o$, again in agreement with experimental data. This is produced by the drag fluctuation induced on the cylinder as each vortex is shed into the wake.

J. C. Hardin, 2617 505-32-03

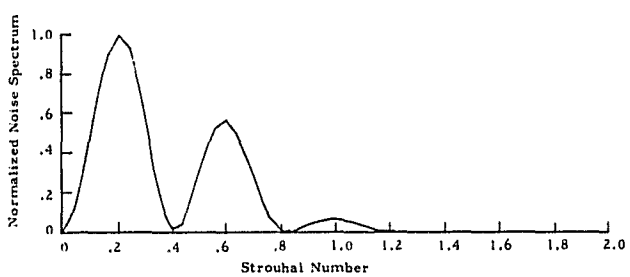

Noise spectrum directly above cylinder.

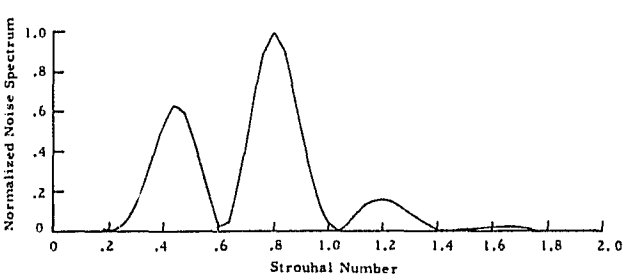

Noise spectrum directly behind cylinder.

Lateral Attenuation of Aircraft Noise

Lateral attenuation is a term used to describe all the atmospheric and ground reflection effects associated with propagating aircraft noise, with the exception of spherical spreading and atmospheric absorption. Lateral attenuation is maximum when aircraft are closest to the ground; that is, during takeoffs and landings. The significance of lateral attenuation lies in the fact that it may be as much as 20 dB and can therefore greatly affect the area enclosed in calculated noise contours. This, in turn, is directly related to the noise exposure of the surrounding airport communities. Lateral attenuation is therefore a critical parameter in all airport/community noise modeling programs, and international agreement on its value when applied to airport noise modeling is highly desirable.

A flight experiment was conducted by Langley in cooperation with the Society of Automotive Engineers using a Boeing 747 to gather lateral attenuation data for a wide-body aircraft. Results of the 747 experiment are shown along with the lateral-attenuation curve recommended by the Ground Reflection Measurement Subcommittee of the SAE, which represents previously available data for turbojet- and turbofan-powered commercial, executive, and military aircraft. The difference in lateral attenuation shown in the figure suggests that the lateral attenuation exhibited by the 747 is less than the average of those aircraft for which data were previously available. This difference must be considered in making airport noise modeling calculations where this type of aircraft operates in significant numbers.

W. L. Willshire, 2645 505-32-03

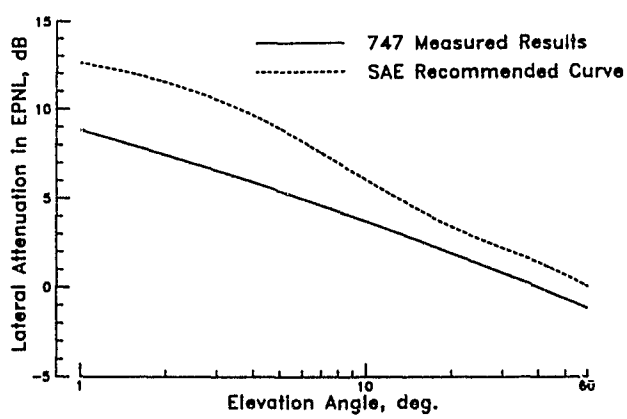

Lateral attenuation of wide-body aircraft.

ORIGINAL PAGE IS
OF POOR QUALITY

Inlet-Radiated Fan Noise Reduction

Scale-model and full-scale static engine tests conducted by various airframe and engine manufacturers have shown that bulk absorber acoustic treatment can result in improved suppression bandwidth and greater suppression magnitude relative to commonly used single-degree-of-freedom treatments. Recently, noise reduction from the inlet of a high-bypass-ratio turbofan engine has been demonstrated in flight for a duct acoustic liner employing a du Pont Kevlar bulk absorber material. The flight was accomplished with an OV-1 aircraft that had been modified by the addition of a Pratt & Whitney JT15D turbofan under its starboard wing. The JT15D engine has been tested extensively under static, wind tunnel, and flight conditions as part of a NASA inter-center program addressing static simulation of flight inlet noise. The present application utilized a softwall inlet liner.

The softwall liner was designed by the Lewis Research Center and was based on a point-reacting method together with an impedance model for bulk absorber material. The liner utilized a sandwich construction consisting of a 22-percent-perforated cover sheet, 11 layers of compressed Kevlar felt, and a solid backing sheet to provide a treatment depth of 0.45 in. The liner was fully circumferential and extended 10.3 in. over the forward portion of the inner surface of the inlet.

Significant inlet-radiated noise reduction was achieved with this acoustic liner. At an approach power setting for the JT15D, a reduction in sound pressure level of up to 10 dB was achieved at the blade-passage-frequency tone at most angles forward of 90°. At angles greater than 90°, aft-radiated fan noise dominated, and, as expected, little if any noise reduction was observed.

John S. Preisser, 3841 505-32-03

Reduction of inlet-radiated fan noise.

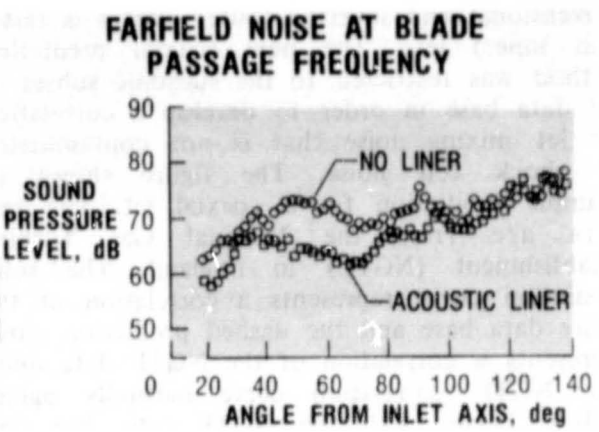

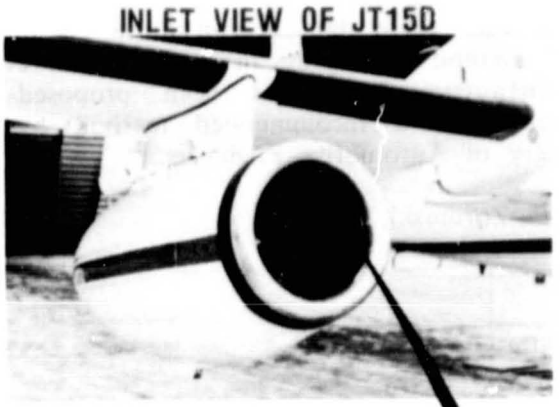

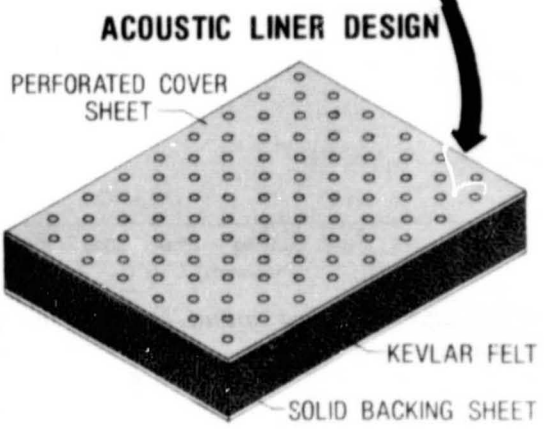

Reduction of inlet-radiated fan noise.

Coaxial Jet Noise Prediction

A new empirical method has been developed for predicting the noise from coaxial jets. The method was developed by correlating jet noise data from the U.S., England, and France. Data from nearly 1000 tests are included in the data base. These tests cover a wide range of jet types and conditions: single and coaxial jets, subsonic and supersonic streams, and

ORIGINAL PAGE IS
OF POOR QUALITY

conventional and inverted (outer stream is faster than inner) jets. The new coaxial prediction method was restricted to the subsonic subset of the data base in order to develop a correlation for jet mixing noise that is not contaminated by shock cell noise. The figure shows an example prediction for a coaxial jet. The test data are from the National Gas Turbine Establishment (NGTE) in England. The solid prediction curve represents a correlation of the entire data base and the dashed prediction curve represents a correlation of the NGTE data only. The NGTE correlation curve naturally agrees slightly better with the NGTE data, but the agreement between the complete correlation curve and these data is still quite good. This new method is already in use by U.S. engine manufacturers and has been proposed for adoption as a recommended method by the Society of Automotive Engineers.

W. E. Zorumski, 2645 505-32-03

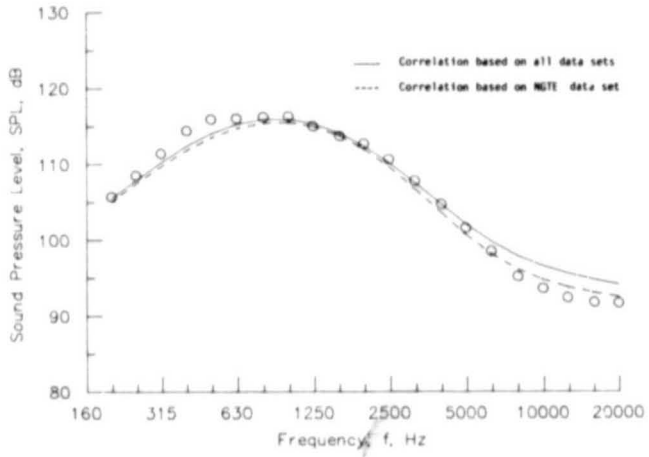

Predicted and measured sound pressure levels for a coaxial jet.

Duct Liner Peripheral Segmentation Effects on Modal Energy

The acoustic energy transmitted through an engine inlet duct is carried by a finite set of modes, each of which is characterized by a unique attenuation rate, radiation efficiency, and directivity pattern. Analytical studies indicate that it is possible to modify the modal distribution of energy by means of abrupt changes in the liner impedance around the circumferential direction (i.e., by peripheral

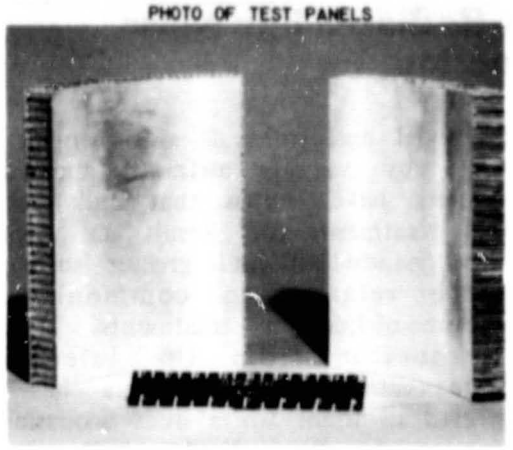

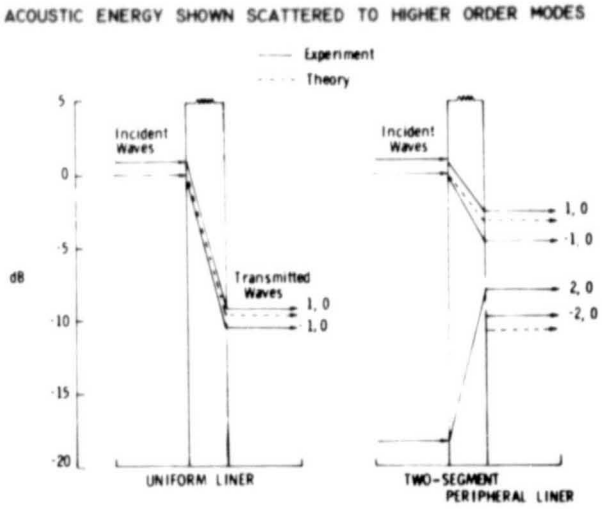

Comparison of theory and experiment for peripherally segmented liner.

ORIGINAL PAGE IS
OF POOR QUALITY

segmentation). In principle, a judicious redistribution of acoustic energy into "appropriate" modes could provide a reduction of perceived noise level in selected regions of the far field.

To validate analytical predictions of modal energy redistribution, an experiment has been conducted at Langley on the Spinning Mode Synthesizer. The experiment propagated a single dominant incident mode through a lined test duct. An acoustic-field mapping rig was used to obtain the modal content of the transmitted acoustic energy. Three different liner configurations were tested: a uniform baseline liner, a six-segment liner whose impedance changed at segment junctures, as shown in the figure, and a uniform liner with a 180° segment blocked with tape to simulate a two-segment hardwall/softwall combination.

The figure shows one example of mode redistribution for the two-segment liner. In this test, two counterrotating modes of circumferential order m = 1 were incident on the test liner. As can be seen, there is significant redistribution of acoustic energy into the m = 2 mode for the two-segment liner. Preliminary calculations suggest good general agreement with theory, as illustrated by the dashed lines.

Tony L. Parrott, 3841 505-32-03

Hot-Film Probes in Supersonic Flow

The convective heat transfer behavior associated with wedge-shaped hot-film anemometry probes has been investigated in the transonic- to low-supersonic-flow regime at high unit Reynolds numbers. These studies have shown that the wedge probe exhibits a uniform, nearly linear response with a Reynolds number based on freestream static temperature conditions over the entire flow regime. This observed behavior permits separation of the fluctuating contributions due to density, velocity, and total temperature and allows for determination of the associated correlations between these variables. This feature represents an important step in providing experimental data for numerical modeling of high-speed turbulent boundary layers and jet plumes. Sensitivity equations have been derived that are appropriate to the observed behavior of the wedge probe.

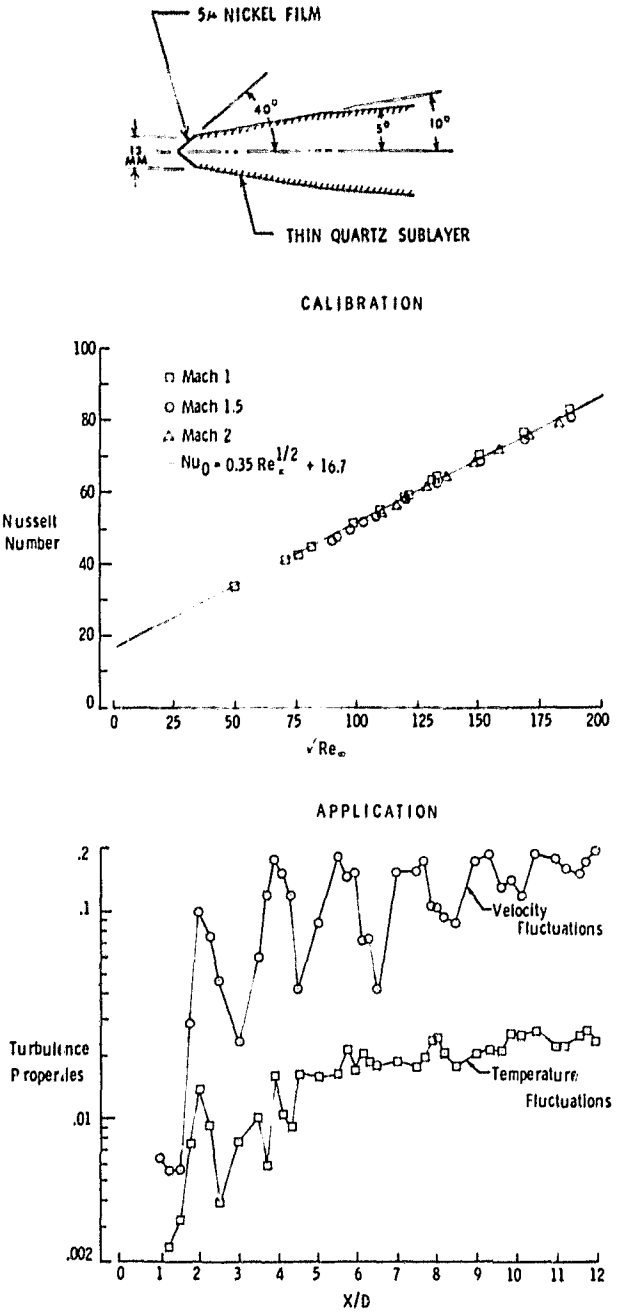

Hot-film anemometry probe.

The wedge probe has been applied to the study of turbulence properties associated with shock-containing supersonic jet plumes. These results revealed that for a mildly underexpanded unheated supersonic jet, velocity fluctuations were an order of magnitude larger than total temperature fluctuations. The figure shows the axial evolution of these parameters along the jet. The modulation of the turbulence by mean flow variations in the shock field can be related to the local oblique shock wave strength. This

ORIGINAL PAGE IS
OF POOR QUALITY

information has been of greater use in the study of mechanisms associated with the broadband shock noise generation.

The wedge probe was found to have a flat frequency response at about 130 kHz, and suffered no degradation in operating performance with long-term use. The wedge probe offers a clear advantage over hot-wire probes and laser velocimetry systems in high-speed flow applications with high unit Reynolds numbers.

J. M. Seiner, 3094 505-32-03

Prediction of Inlet Flow Fields

Recent developments in fighter aircraft design have brought increased awareness of the problem of aircraft-inlet integration. Numerical methods of flow field prediction for complicated wing and body configurations are becoming more and more necessary to aid in efficient wind tunnel testing and to furnish design guidance. To assess current prediction capabilities, two existing computer programs, both inviscid, have been modified and utilized to calculate flow field contours of pertinent flow variables. These data have been compared to wind tunnel data obtained on typical fighter configurations of the early 1970's. The first program is a supersonic code (STEIN) using the three-dimensional Euler equations, with the computational grid fitted between the aircraft surfaces and the bow shock. The second program is a transonic code (WIBCO) utilizing the small-disturbance potential equations and incorporating locally fitted fine-grid systems and approximate body and wing boundary conditions.

Two different configurations are shown along with the local angle-of-attack contours generated by the STEIN code for a side-mounted inlet configuration at $M_\infty = 2.5$ and $\alpha_\infty = 15^\circ$ and by the WIBCO code for a wing-shielded inlet configuration at $M_\infty = 0.9$ and $\alpha_\infty = 15^\circ$. The agreement between theory and experiment shows

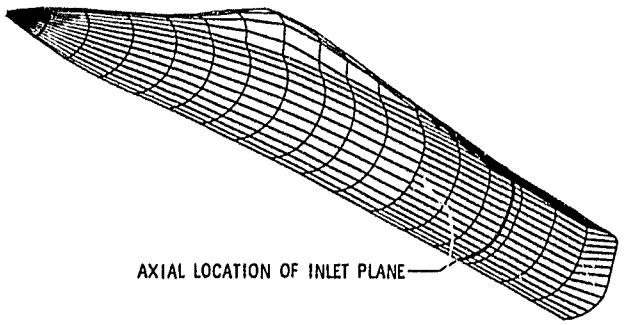

Geometric model of side-mounted configuration.

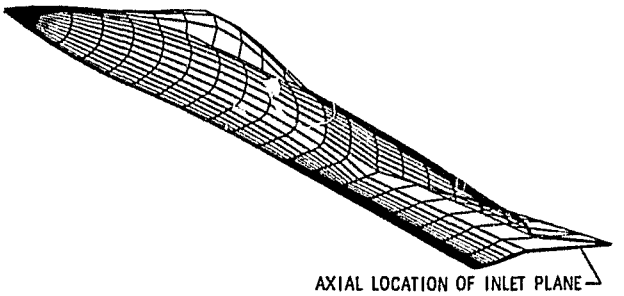

Geometric model of wing-shielded configuration.

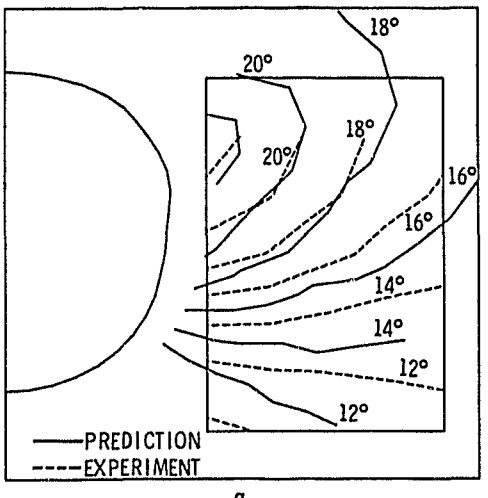

STEIN contours.

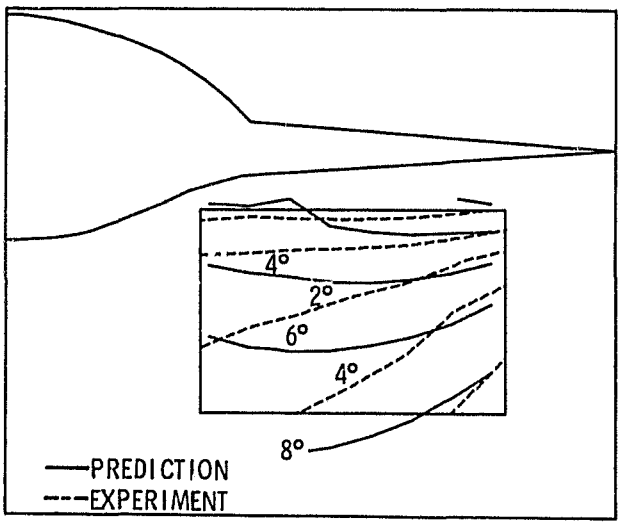

WIBCO contours.

ORIGINAL PAGE IS
OF POOR QUALITY

that both of these codes provide acceptable predictions for planning or design purposes for these types of standard configurations. Further work is needed to include the effects of viscosity and vortex shedding, in particular for aircraft of more exotic design or at more extreme flight conditions.

Steven F. Yaros, 2673 505-32-13

Characterization of Heat Treatment in Aluminum

Recent processing errors by suppliers of high-strength aluminum alloys have resulted in the possible placement of soft aluminum in critical structures such as the Space Shuttle. This research identifies a nondestructive technique with the potential for evaluating structural members in place, thus assuring initial structural viability as well as locating regions of material undergoing annealing resulting from reentry or from processing irregularities. Although previous investigations of ultrasonic velocity indicate its insensitivity to material heat treatment, only second-order elastic constants have been considered. However, a combination of second- and third-order elastic constant measurements offers the potential for characterizing aluminum heat treatment. Measurements of material hardness, conductivity, and ultimate strength in a 2024 aluminum alloy were compared to both stress and thermal ultrasonic constants. Ultrasonic measurements

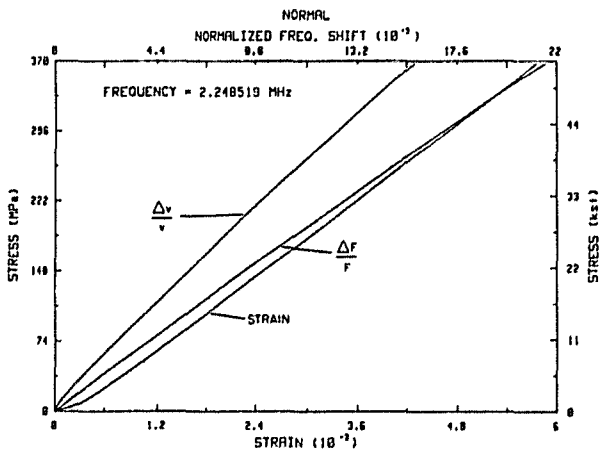

Normal high-strength aluminum threaded rod pulled to failure.

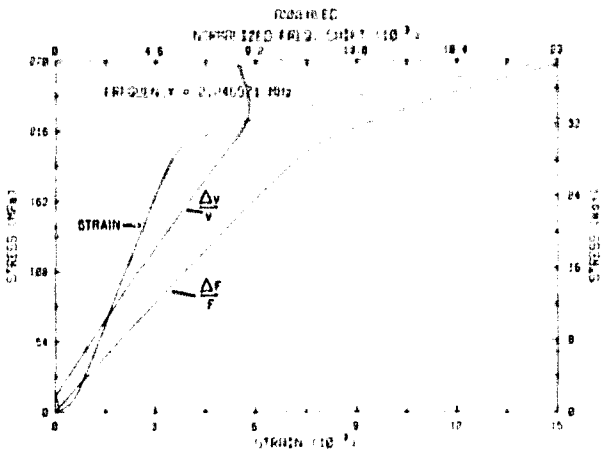

Annealed aluminum threaded and pulled to failure.

were obtained with a pulsed-phase locked-loop ultrasonic spectrometer with resolution of parts in 10^7.

The figures show test results from a normal high-strength aluminum threaded rod and a similar sample annealed at 500°C. Each rod was pulled to failure while measuring stress, local strain, normalized sound velocity, and "natural" frequency (velocity). The largest parameter change was the shear sound velocity stress derivative which showed a 30-percent variation between normal and annealed aluminum.

Joseph S. Heyman, 3418 505-33-23

Relation of Ultrasonic Velocity to Stress State of Materials

Knowledge of the stress state of a material has been a problem of national concern in many areas of application ranging from loads on threaded fasteners to residual stresses in aircraft wings and railroad wheels. The development of LaRC's IR-100 award-winning bolt monitor has made it possible to track changes in the stress state of a material by measuring accompanying changes in the velocity of high-frequency sound waves (ultrasound) propagating through the material. A comprehensive theory of the relationship between such changes in the sound velocity and the stress in a material has recently been developed at Langley utilizing the nonlinear elastic properties of the solid. The theory establishes a quantitative basis for the bolt monitor measurements in terms of

fundamental solid properties and is valid for materials of arbitrary crystalline symmetry. The theory includes for the first time the effect of residual stresses in the material on the bolt monitor measurements. The relationship between the velocity/stress state of the material and fundamental parameters in the equation of state of solids has also been obtained. These relationships provide much of the scientific base and understanding needed for developing further technology leading to absolute measurements of residual stresses in materials.

John H. Cantrell, Jr., 3418 505-33-23

Three-Dimensional Inviscid Analysis of Scramjet Inlet Flow Field

A computer code has been developed to calculate the inviscid flow in the inlet of a supersonic combustion ramjet (scramjet) engine. The three-dimensional Euler equations in conservation form are used to describe the inlet flow field. The governing equations in the physical plane are transformed to a regular computational domain by using an algebraic numerical coordinate transformation that generates a set of boundary-fitted curvilinear coordinates. MacCormack's unsplit explicit finite-difference method is used to solve the transformed equations. This method is highly efficient on the vector-processing computer for which the current code is written.

The code has been used to calculate the flow field in several scramjet inlet configurations, one of which is shown. This particular configuration is also currently being used in experimental studies of scramjet-related problems. In this configuration most of the inlet compression is provided by the sidewalls, which are swept wedge-shaped surfaces. Sidewall sweep provides the potential to operate over a range of Mach numbers even with a fixed-geometry inlet. For this inlet, sidewall sweep ends along line AB. In the present numerical study, results were obtained for sweep angles (Λ) of 30° and 45° over a Mach number range of 3.4 to 6.0 at the face of the inlet.

The sidewall pressure distribution is shown for a 45° sweep angle at Mach 5.0. The

ORIGINAL PAGE IS
OF POOR QUALITY

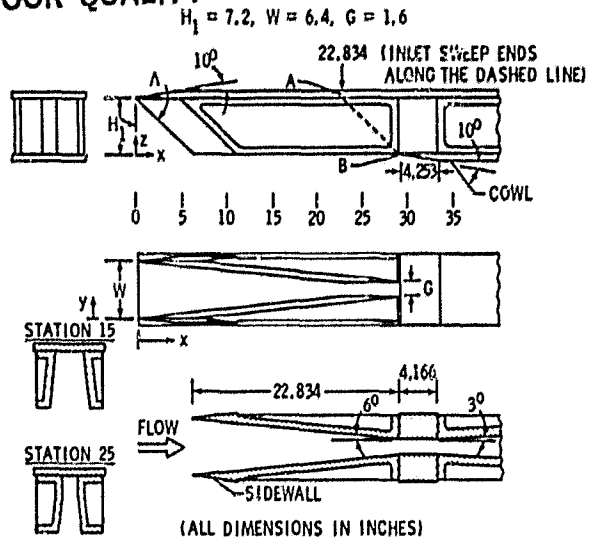

Scramjet inlet geometry.

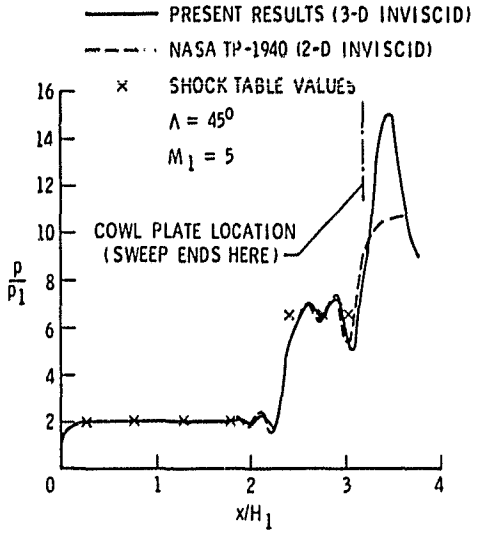

Sidewall pressure distribution.

present results are compared with the pressure distribution obtained from the shock tables and with a two-dimensional analysis. The present results are in very good agreement with the other results up to the point of cowl closure. Beyond this point the present analysis predicts much higher pressure due to the cowl shock, which cannot be accounted for in the two-dimensional analysis.

The preceding calculations were made on the Control Data CYBER 203 vector-processing computer. The code has a compute rate of 1×10^{-5} sec/grid point/time step. A typical solution can be obtained in 10 to 15 minutes

ORIGINAL PAGE IS
OF POOR QUALITY

of computer time, depending on the size of the grid and the number of time steps required for convergence.

Ajay Kumar, 3171 505-32-73

Computation of Ramjet Dump Combustor Flow Field

Increased interest in ramjet propulsion systems with higher performance requirements and tighter constraints on system size and weight has led to the need for improved techniques for analyzing and designing such systems. A critical requirement for achieving high system performance within specified geometric limits is an accurate description of the combustor flow field. Computational techniques offer the potential for analyzing ramjet flow fields, and the techniques are attractive in that they could provide a description of the flow over a wide range of conditions.

A computer program has been developed at LaRC to analyze the subsonic turbulent reacting flow in a ramjet diffuser and dump combustor. The program has recently been compared with a ramjet dump combustor simulation experiment carried out at the Arnold Engineering Development Center to measure parameters that are important in ramjet design. A plot of the computed velocity vector field in the diffuser and dump (step) combustor is shown in the figure. Air is introduced by the diffuser into the combustor downstream of the step, and gaseous hydrogen is injected into the combustor at the step face. Note the predicted flow separation behind the step and the development and growth of a shear layer downstream of the step. Comparisons of the computed and measured mean velocity at two downstream stations (x/D = 1 and x/D = 3) are also given in the figure. The predicted values are in reasonably good agreement with the measured data, indicating a good potential for the analysis of ramjet dump combustor flow fields.

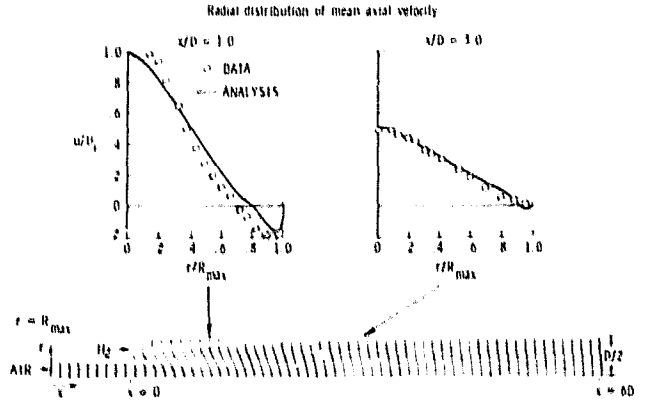

Computed velocity vector field in ramjet dump combustor simulator.

J. Philip Drummond, 3171 505-32-73

Hypersonic Propulsion

A comprehensive research program is in progress to establish the technology required for practical airbreathing engines capable of operating at speeds from Mach 4 to Mach 10. Because of the severe heating encountered at these speeds, an engine with fixed geometry is desirable. In order to accommodate the changes in flow behavior that occur in this speed range and to produce thrust efficiently, operation with both subsonic and supersonic combustion is required. At Mach 4 the key problem is to contain subsonic burning within the engine at a throttle setting that uses all the oxygen available in air. At Mach 10 the problem is to achieve rapid mixing and combustion in the short time available with supersonic flow through the combustor.

Extensive tests of a three-strut inlet-combustor model have been completed at simulated Mach-7 flight conditions. Data include thrust performance, internal pressure distribution, heat transfer, ignition conditions, and flame-out limits for supersonic combustion operation. Performance equal to or exceeding expectations was achieved in all respects. These results indicate that the hydrogen-fueled supersonic combustion ramjet may become a viable propulsion option for future launch vehicles.

Separate tests of a combustor duct have also indicated a promising approach for accomplishing good combustion and thrust performance with both subsonic and supersonic flow. Recent experiments have extended these results to a combined inlet-combustor model at simulated Mach-4 flight conditions. In these tests good combustion and thrust performance were achieved without adverse effects on the

ORIGINAL PAGE IS
OF POOR QUALITY

inlet flow. The engine geometry has potential for good performance at much higher speeds, and tests are planned to evaluate the same engine hardware at simulated Mach-7 flight conditions. Success at both Mach-4 and Mach-7 simulated flight conditions implies that the goal of a fixed-geometry engine for operation over this speed range can be achieved.

H. L. Beach, Jr., 3772 505-32-73

Combustion Diagnostics

Acquisition of meaningful experimental data in the supersonic-velocity/combustion-temperature environments associated with supersonic-combustion ramjets (scramjets) is a major concern. Conventional probe techniques with cooled probes designed to withstand the harsh thermal environment have the inherent disadvantage of significantly altering the very flow they are attempting to measure. In order to enhance the acquisition of combustion data for scramjet environments, a nonintrusive combustion diagnostics program was initiated. After surveying a variety of methods, the technique selected as being the most promising was coherent anti-Stokes Raman spectroscopy, or CARS.

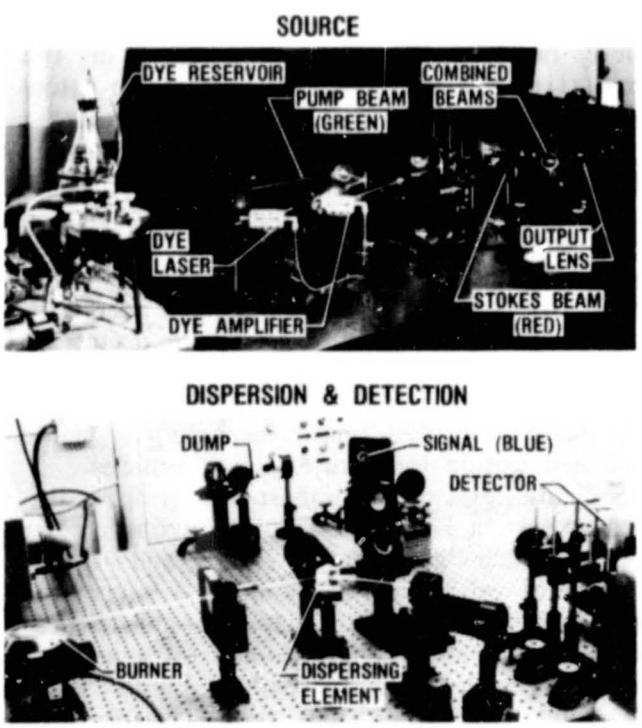

CARS system.

With this technique, two laser beams are focused within the gas or flame being probed. These beams interact with the molecular vibrations of the molecule in such a manner as to produce a third beam that has laser (coherent) properties and contains the spectra of the molecule being investigated. These molecular spectra can then be inverted to yield the temperature of the flame and, with appropriate calibration, the number density of the molecules.

During the past year a CARS system has been constructed and techniques have been developed to measure flame temperature over a flat-flame burner operated at temperatures up to 2100 K. A standard technique, sodium line reversal, was used to determine the reference temperature. At these temperatures, data with a standard deviation of less than ±75 K have been obtained from single 10-nanosecond laser pulses. The spatial resolution of the system is 1 mm^3. A data system is being assembled that will allow the data to be recorded at a 10- to 15-Hz rate, which will allow measurements of fluctuating temperatures in a turbulent flame.

When it is fully developed the CARS system will be used to verify computational fluid dynamics codes modeling supersonic turbulent combustion that is three dimensional with finite-rate chemistry. The CARS system will also be used to investigate the effects of temperature and composition fluctuations on supersonic combustion kinetics.

G. B. Northam, 2803 505-32-73
307-02-01

Superplastic Forming/ Weldbrazing Process Significantly Increases Structural Efficiency

The superplastic behavior of metals, or their ability to undergo elongations of 500 to 1000 percent without necking or fracture, promises to revolutionize the fabrication of future aircraft structures. When heated to 1700°F, titanium can be formed or strained using gas pressure to elongations over 1000 percent, which permits the fabrication of components not possible using conventional forming methods. This phenomenon has been combined with a Langley-developed process designated as weldbrazing (WB) to

ORIGINAL PAGE IS
OF POOR QUALITY

fabricate titanium skin-stiffened compression panels that exhibit a significant increase in structural efficiency.

Superplastic forming (SPF) is used to form a single flat sheet into a mold to fabricate a pan assembly with a single stiffener of the desired configuration. The stiffened pan is attached to a skin or sheet of titanium by resistance spotwelding. Strips of aluminum alloy braze foil are then placed adjacent to the edges of the faying surfaces of the pan and skin. This assembly is heated to the brazing temperature in a vacuum furnace and the braze alloy melts and is drawn into the faying surface gap to join the components and complete the superplastic forming/weldbrazing (SPF/WB) process. Compression panels fabricated by SPF/WB that have unique stringer configurations (such as a beaded web) could not be formed using conventional processes. The buckling strengths of beaded-web and other unique configurations were compared with those of a conventional hat-stiffened panel. The data show that the panels with the complex configurations were 50 to 60 percent more efficient than the specimen with the conventional stringer shape. These improvements in structural efficiency, which are attributed to the increased formability offered by superplastic forming, open the door for innovative design of future lightweight titanium structures.

Thomas T. Bales, 3405 505-33-13

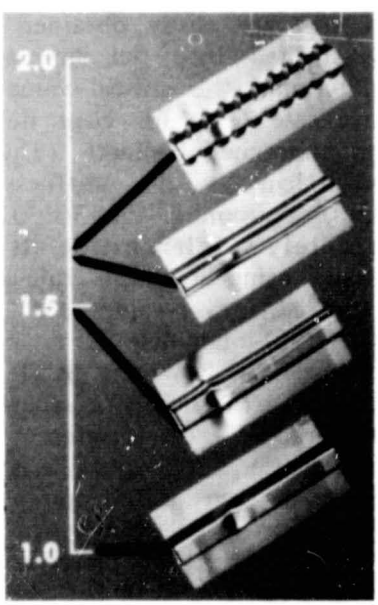

Relative buckling strengths of several configurations.

High Specific Stiffness Developed in Aluminum Matrix Composites

Over the past three decades, improvements in design properties of structural aluminum alloys followed a slow, evolutionary process as ingot chemistries and thermomechanical treatments were refined. The emerging technology of aluminum alloy powder metallurgy promises considerable improvements in material properties for structural applications. By employing cooling rates of 10^{2}°C to 10^{6}°C per second for alloyed powders or by "mechanically alloying" elemental powders, alloying element concentration can be substantially increased and grain sizes in consolidated product forms can be reduced by an order of magnitude from those in conventional ingot metallurgy products. Furthermore, strong, stiff, low-density particles, or whiskers, can be uniformly dispersed in the consolidated powder preforms to produce metal matrix composites with attractive properties.

Under a NASA contract, Lockheed California Company (in conjunction with its subcontractors, the Aluminum Company of America and the International Nickel Company) has been developing 2000-series (Al-Cu-Mg-X-X) powder metallurgy alloys and alloys reinforced with silicon carbide whiskers. As shown in the figure, laboratory-size extrusions exhibit very attractive specific elastic moduli compared to the conventional 2000-series ingot metallurgy alloy, IM 2024-T4 (dashed curve). The four solid curves show that the specific elastic modulus for two powder aluminum alloys, 2124-T4 and 2219-T4, each reinforced with 15

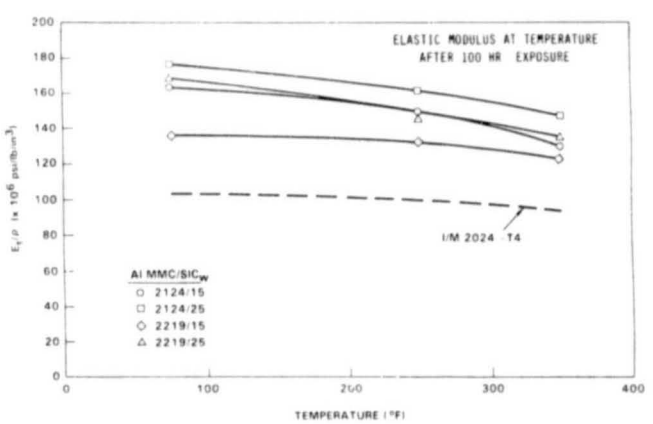

Specific elastic modulus of whisker-reinforced aluminum alloy metal matrix composites (T4 temper).

ORIGINAL PAGE IS
OF POOR QUALITY

and 25 percent silicon carbide whiskers (SiC_W), is 30 to 75 percent higher than the IM 2024 over a temperature range from 75°F to 350°F. Corresponding specific strengths were up to 30 percent higher than those of IM 2024-T4. Further research is needed to enhance ductility in these materials, to develop these properties in other product forms such as sheets and plates, and to scale up to large billets, but the promise of these powder metallurgy aluminum matrix composites appears bright, especially for stiffness-limited aerospace structural applications.

W. B. Lisagor, 3041 505-33-13

Fatigue Lives and Fracture Toughness of Laminated Metals

Laminated metals show promise as damage-tolerant materials. If an adhesive is used to laminate thin sheets of metal, a crack in one sheet does not induce a crack in an adjacent sheet because the adhesive is too weak to transfer enough force to overload the adjacent layers. This is in contrast to brazing the sheets of metal together; the strong braze material can transmit enough force for the crack to travel into the adjacent layer.

The figure shows some results for a titanium alloy (Ti-6Al-4V). The alloy is moderately tough for a metal, and in large solid-plate form it has a comparatively high rate of crack propagation. The first graph compares the life to failure under cyclic loads of a monolithic plate and a laminated plate. After the laminated plate had lasted more than 15 times as long as the monolithic plate, the engineer stopped the test. At that time the crack had grown all across the

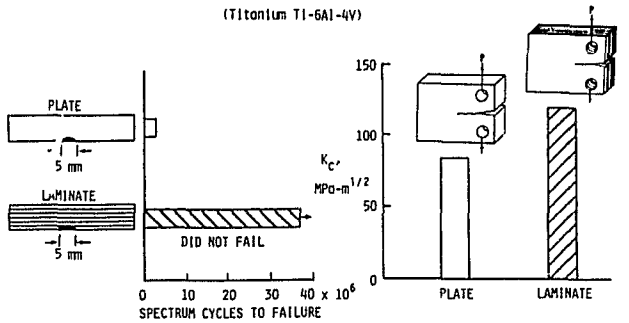

Fatigue lives and fracture toughness of monolithic and laminated metal.

one initially cracked layer, but the remaining layers easily supported the loads. In the monolith, however, the crack grew through the thickness as well as across, leading to the early failure.

The second graph compares the fracture toughness of the monolith and the laminate. With equally long cracks, completely through the thickness in each case, the laminate carries 40 percent more load. Fracture theory suggests that the laminate layers constrain each other so that they are under a plane stress condition, whereas the monolith is under plane strain. The plane stress condition enables the laminate to support greater loads.

W. S. Johnson, 2715 505-33-23

Edge Delamination Test Measures Interlaminar Fracture Toughness

A simple test has been developed at Langley that measures the interlaminar fracture toughness of multilayered fibrous composites. Such toughness is a measure of the resistance of the material to delamination, a common failure mode in composites. This edge delamination test (EDT) involves applying a tensile load to a small 11-ply $(\pm30,\pm30,90,90)_S$ composite coupon until delaminations form at the edges. Coupon stiffness (E_{LAM}) and strain at initial delamination (ϵ_C) are easily obtained from the test and substituted into the simple equation shown to determine the critical value of strain energy release rate (G_C) for edge delamination growth in an unnotched laminate. (The E* term in the equation is the stiffness of the $(\pm30,\pm30,90,90)_S$ coupon if the 30/90 interfaces were completely delaminated. It can be calculated easily using a simple rule-of-mixtures equation and stiffness values of a $(\pm30)_S$ laminate and a $(90)_n$ laminate.)

The figure shows how the EDT can rank the toughness of graphite-fiber-reinforced composites made from different polymer matrices. The brittle 5208 epoxy has very low toughness, whereas the H205 epoxy is much higher. The addition of elastomers to the H205 epoxy to produce F185 material improves toughness even more.

Unlike the widely used double-cantilever-beam test for fracture toughness, the EDT gives failure modes similar to those in tests of

ORIGINAL PAGE IS
OF POOR QUALITY

composite structures. The EDT also has a simpler configuration and simple loading, but, more importantly, it is independent of delamination size. Both tests are being used in NASA's Aircraft Energy Efficiency (ACEE) Program to screen new toughened resin-matrix graphite composites for improved delamination resistance.

T. K. O'Brien, 3011 505-33-33

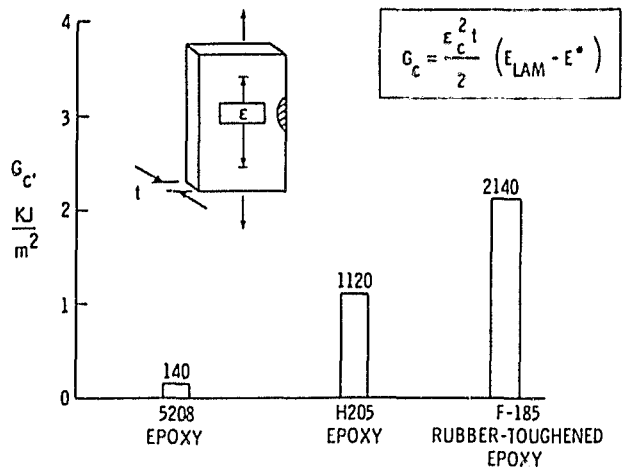

Edge delamination test measures enhanced interlaminar fracture toughness.

Melt-Processable Polyimide

In the past, polyimides have not been processable in the melt form. However, a novel linear aromatic polyimide that retains the typical polyimide thermooxidative stability and is also hot-melt processable has been synthesized and characterized. As shown in the figure, this polymer (HMP-1) exhibited a considerably lower melt viscosity at its midrange processing temperature (300°C) than did either commercially available Torlon (340°C) or a widely used ABS (commercial plastic) resin (200°C). It also exhibited a well-defined decrease in viscosity with increasing temperature, a definite processing advantage.

The measured toughness (G_{Ic}) of the melt-processable polymer was several orders of magnitude greater than that of addition-curing polyimides or elastomer-toughened addition polyimides. The room-temperature lap shear adhesive strength of 6300 psi was quite high compared to conventional polyimide adhesives. The glass transition temperature decreased by only 7°C when the polymer was subjected to a 72-hour water soak and then tested wet. This HMP-1 material also has shown exceptional resistance to common solvents.

Because of its melt-flow properties, high G_{Ic}, moisture and chemical resistance, and thermooxidative stability, this novel polymer exhibits considerable attractiveness as an engineering thermoplastic. In particular, due to its high melt flow, it shows potential as a composite matrix resin and as a hot-melt adhesive.

Harold D. Burks, 3041 505-33-33

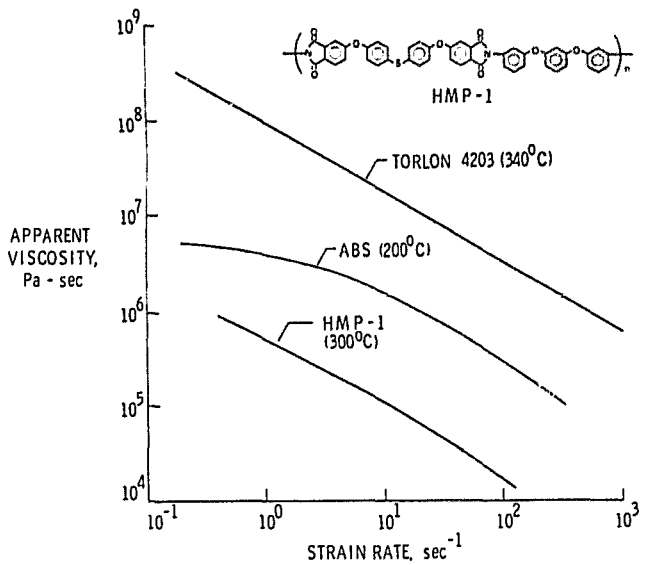

Processability comparisons of melt-processable polyimide (HMP-1) and commercial polymers.

Electrically Conducting Polyimide Film

Because of their low density, thermal stability, and flexibility, polyimide films are currently being considered as materials for large space structures. To dissipate charging in space, the films should possess antistatic properties with an electrical conductivity of at least 10^{-8} to 10^{-10} mho-cm.

Polyimides have a low electrical conductivity, on the order of 10^{-17} mho-cm. Research has shown that the conductivity of the polymer can be increased by as much as 14 orders of magnitude using certain palladium complexes as additives when the metal complexes are

ORIGINAL PAGE IS
OF POOR QUALITY

incorporated into prepolymer solutions. Good solubility of the palladium salt in the polymer is a necessity for achieving conductivity.

Electrical conductivities obtained by the addition of these compounds are more than sufficient for relieving space charging effects. The improved conductivities of these palladium-containing polyimide films have been achieved with only a 4-percent increase in film density, minimal sacrifice in thermal stability, and no loss in film flexibility.

Anne K. St. Clair, 3041 505-33-33

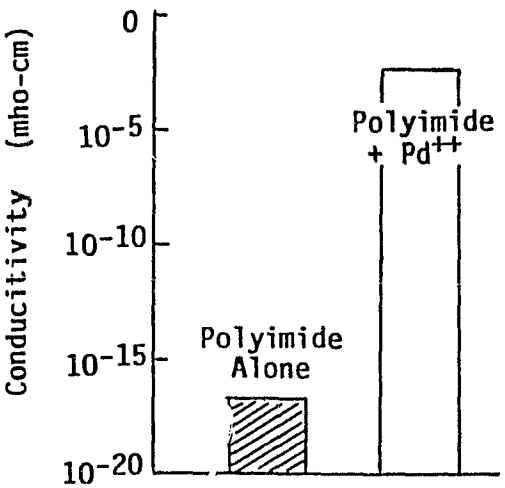

Electrical conductivity of Pd/polyimide film.

Composite Material Characterization

The chemical characterization of cured graphite fiber/polymeric matrix resin composites presents a difficult problem because the composites are both insoluble and opaque. Standard analyses, which depend on the ability to either dissolve the sample or detect transmitted radiation, are impossible. As a result, changes in resin molecular structure, which most likely contribute to any observed change in composite weight or mechanical properties, can only be postulated.

Diffuse Reflectance-Fourier Transform Infrared (DR-FTIR) spectroscopy is being developed in an effort to gain an insight into molecular changes that occur during cure of composite materials, as well as into changes due to environmental exposure. A small portion of the composite is pulverized and irradiated, and diffusely reflected components are detected. Multiple scans are made to improve sensitivity. The result can be a high-quality interpretable IR spectrum containing information identifying which molecules are present in the resin and how they are arranged.

The figure shows a DR-FTIR spectrum of a cured graphite/addition polyimide composite. Bands at 1778, 1724, and 1389 cm^{-1} are due to imide ring vibrations. An attenuated total reflectance (ATR) spectrum, previously the best available technique, is included for comparison. Changes in band intensity, new bands, and frequency shifts have been observed for environmentally aged composites using DR-FTIR. This new information enhances a fundamental understanding of molecular changes within the polymeric resin and, ultimately, of how these changes affect composite performance.

Philip R. Young, 3041 505-33-33

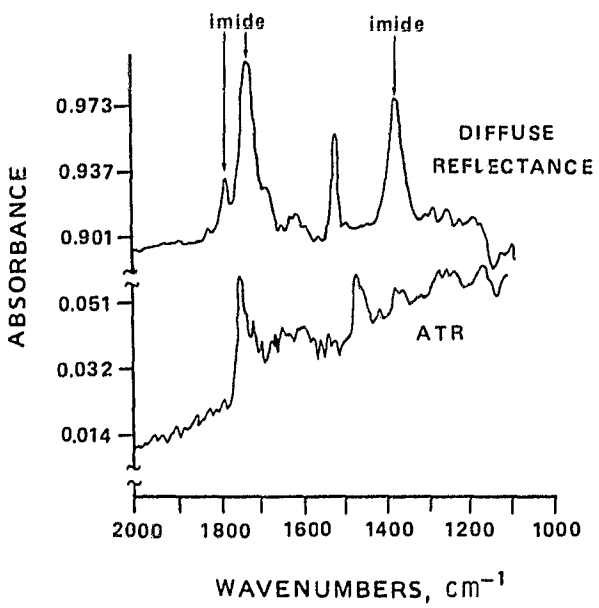

IR spectra of cured composite.

Tests of High-Temperature Composite Joints

A fabrication and test program has been conducted by the Boeing Aerospace Company under contract to Langley to provide a data base for the design of graphite/polyimide composite joints useful for service at elevated

ORIGINAL PAGE IS
OF POOR QUALITY

temperatures. The material and structural joining characteristics were determined with allowable and small-specimen tests. Joint tests were conducted to determine the static and fatigue behavior at elevated temperature of both bonded and bolted attachment concepts for skin splices and rib-skin and spar-skin interfaces. Over 1500 individual laboratory tests were conducted on composite elements and components.

The tests showed that seven types of joints successfully transferred their design loads at 550°F (as high as 10,000 lb/in. for bolted splice joints). The bonded joints used an adhesive formulation based on the Langley-developed high-temperature adhesive LaRC-13. Room-temperature tests of bolted concepts showed that the PMR-15/Celion fiber composite had the same net tension and shearout capabilities at ambient temperature as corresponding graphite/epoxy joints, so that there was no compromise of room-temperature capabilities by using polyimides. The figure shows a schematic of the components of both a bonded and bolted corner joint and a picture of an assembled graphite/polyimide bolted corner joint test specimen.

The test results were a strong factor in influencing the decision to start an in-house applications research program at Boeing Commercial with PMR-15/PI for possible use in Boeing 757 and 767 cowlings and nacelles. The results were also used in an Air Force research study to configure a joint between a brittle ceramic radome and a titanium missle body. The component was successfully tested at 800°F.

Paul A. Cooper, 3787

524-71-03
743-01-03

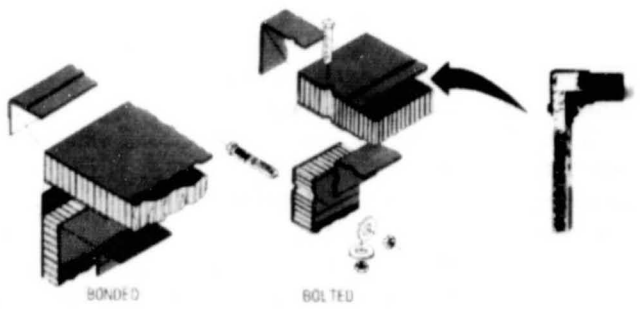

PMR-15 polyimide/graphite fiber composite bonded and bolted joints carry spacecraft design loads at 550°F.

Threshold Impact Energy for Composite Materials

Composite laminates are susceptible to damage when struck by hard objects. The figure summarizes some results from tests and analyses of laminates. The impact energy was the energy of a 1-in.-diameter steel ball as it struck the laminate. The laminate itself was a quasi-isotropic plate (cross-plied laminate) eight plies thick, cut in the form of a disk. The plate was glued over a circular hole in an aluminum backup plate; the hole radius is shown on the abscissa. The results for two epoxy matrices and fibers are shown. The solid lines represent theory, the symbols test results. The two lower slanting lines represent matrix failure. When struck, small radius plates develop high shear stresses between laminate layers because of the high constraint from the support. The HX205 epoxy, because of its higher toughness, withstood the impact somewhat better than the 5208.

Increased toughness, however, can bring about only a limited benefit. The nearly horizontal line represents fiber failures. At somewhat larger support diameters the laminate, while deflecting, develops high membrane stresses, much like a drumhead. The fiber failure mode therefore limits the amount that the damage threshold can be raised by improving matrix toughness. For illustration, 1J is about the amount of energy in a 6-oz box wrench dropped from a height of 2 ft. An equivalent (based on weight) aluminum plate can absorb about 10 times as much energy as the composite. For this reason, a substantial

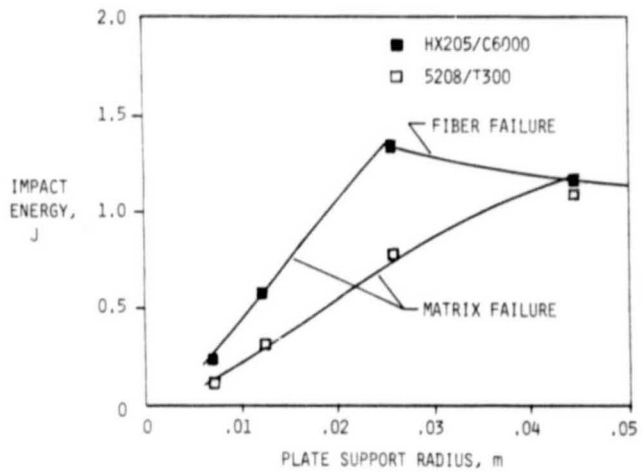

Threshold impact energy for two composites.

ORIGINAL PAGE IS
OF POOR QUALITY

research program is under way at the Langley Research Center to study the behavior of composites under low-velocity impact.

Wolf Elber, 2093 505-33-33

Governing Parameter Identified for Postbuckling of Plates

Normalized load end-shortening results are presented in the figure for the postbuckling in compression of long, simply supported, orthotropic plates. The applied load P is normalized by the buckling load P_{cr} and the end shortening Δ is normalized by the end shortening at buckling Δ_{cr}. Buckling of such orthotropic plates is known to depend on two well-known parameters (shown in the figure) involving various bending stiffnesses (e.g., D_{11}, D_{12}, D_{22}, D_{66}). Postbuckling results were previously obtained using available general-purpose computer programs for each set of dimensions and material properties. The present analysis identifies the fact that for compressive postbuckling the results depend on the buckling parameters plus the one new parameter $(A_{22}D_{11}/A_{11}D_{22})$, where the A_{ij} are the various membrane stiffnesses. These results are general in that, with just a few more sets of curves for other values of the D_{12} parameter, they apply to the complete range of dimensions for many classes of layups of laminated composites.

The slope of the load end-shortening curve is a measure of the overall plate stiffness. The figure shows that prior to buckling, the curve is a straight line of slope 1. After buckling this line may change slope depending on the values of the parameters chosen, and the slope of the curves decreases with increase in loading. These results were obtained by converting the two-dimensional equations of plate theory into one-dimensional equations by assuming trigonometric functions in one direction. These equations are then solved numerically so that results may be obtained at low cost for any set of dimensions or directly for design in a weight optimization study. Agreement between theoretical results and experimental results has been obtained for isotropic plates and for composites.

Manuel Stein, 2813 505-33-33

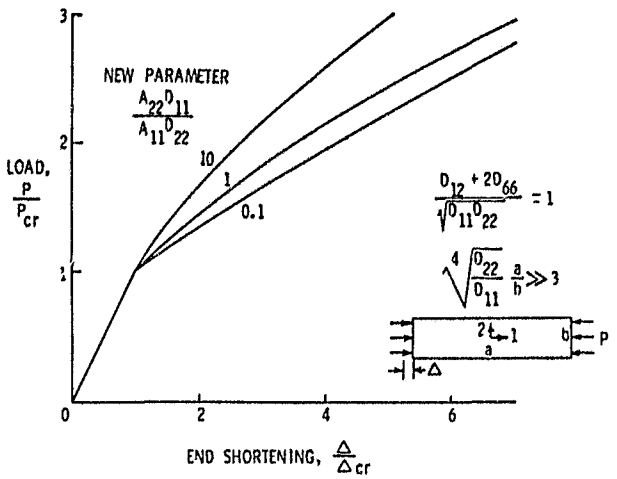

Characteristic curves for postbuckling of plates.

Aerodynamic Panel Method SOUSSA for Steady and Unsteady Flow

In order to analyze time-dependent aeroelastic problems of aircraft, such as flutter, gust response, and active-controls behavior, as well as steady and quasi-steady problems such as performance, static and dynamic stability, and structural loads and deformations, it is necessary to calculate the distribution of pressure over the aircraft. For this purpose a general aerodynamic panel method called SOUSSA (steady oscillatory and unsteady subsonic and supersonic aerodynamics) has been developed. The method is based on linearized potential flow and is applicable to general shapes, such as complete aircraft having arbitrary shapes, motions, and deformations. An early version of a computer program, SOUSSA P1.1, implementing this method has been validated by comparison with experimental pressure data and with results from the more limited lifting-surface theory.

The figure shows some results of one such application. The wing, which was tested in the Langley Transonic Dynamics Tunnel, is a sharp-edge clipped delta wing oscillating in pitch. The Mach number is 0.4, and reduced frequency based on root semichord is 0.66. The surface paneling array used in the SOUSSA calculations contained 10 panels per chord and 10 panels per semispan on upper and lower surfaces. The real and imaginary (in-phase and out-of-phase) components of calculated and

ORIGINAL PAGE IS
OF POOR QUALITY

measured surface pressures are compared in the figure at the 0.33 semispan station, and the overall good agreement shown is typical for other span stations and other frequencies.

E. Carson Yates, Jr., 2661 505-33-53

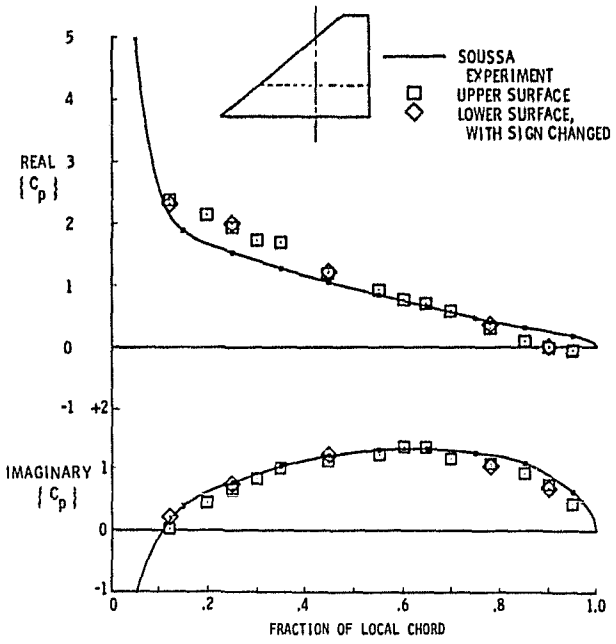

Surface pressures on clipped delta wing.

Transonic Analysis of Flexible Wings

A method for including the effects of elasticity in the analysis of steady transonic wings has been developed. The method iterates between a nonlinear aerodynamic calculation and a linear structural analysis. The aerodynamic calculations are obtained using the full potential code, FL022 (developed by Jameson and Caughey at New York University), while the structural analysis is performed external to FL022 with a method that was developed at Langley. Since the structural analysis may be used without the assumptions of slender-beam theory, this is a significant improvement upon previously published methods. The aerodynamic solution is gradually converged throughout the aerodynamic/structural iteration process; thus the cost of a flexible-wing analysis is usually less than 50 percent greater than the cost of analyzing a rigid wing.

The importance of including elastic effects in the analysis of flexible wings is shown in the figure. Computed lifting pressures (ΔC_p) on the DAST (Drones for Aerodynamic and Structural Testing) ARW-2 (Aeroelastic Research Wing) with and without the effects of elasticity are shown at the design cruise Mach number (0.80) and dynamic pressure (126.4 psf) with a wing root angle of attack of 1.36°. Allowing the wing to deform under load results in a large reduction of lift (C_L) and significant changes in shock strength and location.

Woodrow Whitlow, Jr. 2661 505-33-53

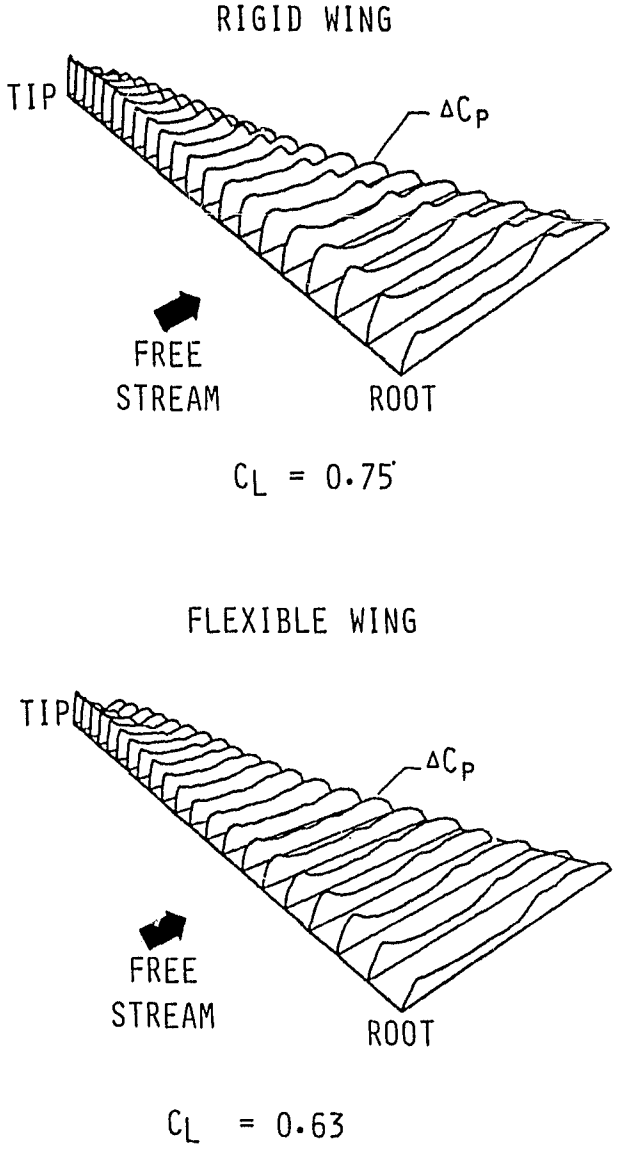

Lifting pressures on ARW-2.

ORIGINAL PAGE IS
OF POOR QUALITY

Two-Degree-of-Freedom Flutter Mount System

A new mount system concept for obtaining wind tunnel flutter research data has been developed and demonstrated in the Transonic Dynamics Tunnel (TDT). The mount system is shown with a wing model attached. It is expected that this system will be extremely useful in flutter research studies because it provides a means of testing structurally simple but aerodynamically representative configurations. This feature will be particularly useful in evaluating analytical methods because differences between theory and experiment will be due solely to aerodynamic effects since the structure can be mathematically modeled very accurately. The new system is relatively simple and consists of a splitter plate attached by a system of beams to an existing turntable in the tunnel wall. The beam system provides much greater stiffness in the fore and aft direction than in the vertical (plunge) direction. Because each beam has fixed-fixed end conditions, the splitter plate is constrained so that neither roll nor yaw motion is possible; in other words, only pitch and plunge motions are allowed. Two characteristics of the mount system are particularly noteworthy. First, it can carry large lift loads at high angles of attack; that is, the system is very strong, but is flexible enough to produce flutter at reasonable test conditions. Second, it has very small and constant structural damping.

The usefulness and versatility of the new mount system has been demonstrated during wind tunnel tests. In the example shown, flutter boundaries at zero lift are compared for two wings with the same planform but with different airfoil sections, namely a symmetric conventional 64A010 and a symmetric 10-percent-thick supercritical. These data show that the supercritical airfoil has a more pronounced transonic "dip". Also shown is a data plot illustrating the effects of angle of attack on flutter. These results are for the conventional-airfoil model. The Mach number is constant. As the angle of attack is increased from zero degrees, the flutter dynamic pressure at first decreases linearly. When the angle of attack reaches 7^{o} a rather abrupt decrease in flutter dynamic pressure occurs. The flutter dynamic pressures at the higher angles of attack are considerably below that at zero degrees. Based on observations of this type of behavior in previous studies, this abrupt decrease is believed to be caused by the transition from classical flutter to stall flutter.

Moses G. Farmer, 2661 505-33-53

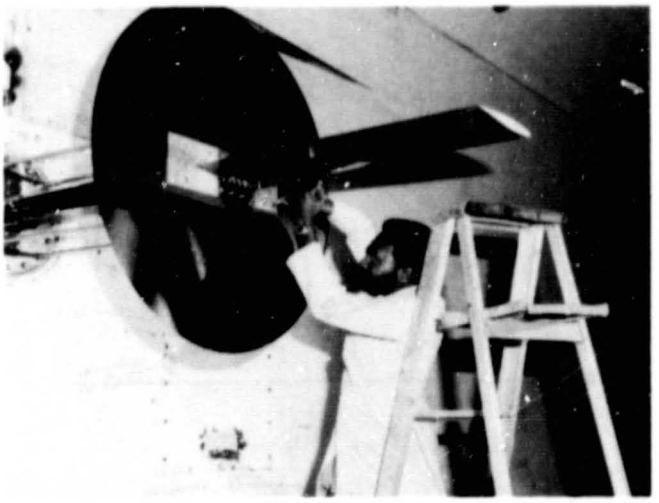

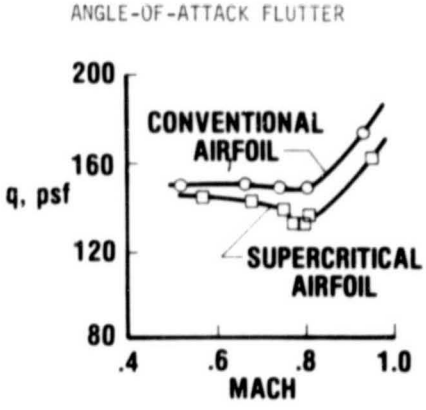

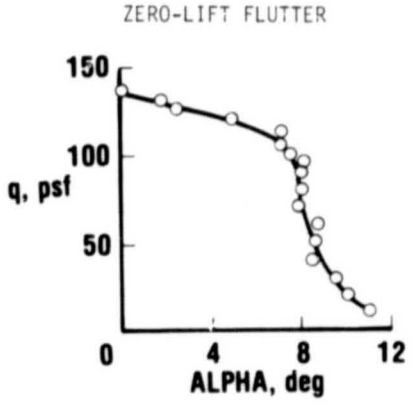

New two-degree-of-freedom flutter mount system demonstrated in TDT.

ORIGINAL PAGE IS
OF POOR QUALITY

Angle-of-Attack Effect on Transonic Flutter

Flutter tests of the TF-8A supercritical wing in the Transonic Dynamics Tunnel (TDT) have investigated the effect of wing root angle of attack, α_0, on flutter. Near the design Mach number of 0.98 the flutter boundary was found to curl backwards for angles of attack above zero and for Mach numbers between 0.95 and 1.0. A study was conducted at Langley to see if a recently developed two-dimensional transonic finite-difference computer code would predict this phenomenon. A sketch is shown of a two-dimensional airfoil section (MBB A-3) mounted on a pitch spring. This simple model is analogous to the effect of washout of angle of attack at the tip of a loaded wing in which the nosedown pitching moment, C_M, twists the section from its "root" angle, α_0, to a more negative angle, α. When the flutter speed index is plotted versus Mach number for fixed angles of attack of $\alpha = 0^\circ$ and 1° a significant transonic dip is seen, but there is no evidence of the curl-back seen in the TF-8A results. When the effect of static twisting is included and the boundary is plotted for "root" angles, a curl-back develops between 2° and 4°. The curl-back is due to the static twisting of the airfoil under the combined influences of Mach number and dynamic pressure. The higher angles obtained near the bottom of the transonic dip induce transonic effects that produce the curl-back of the flutter boundary.

John W. Edwards, 2661 505-33-53

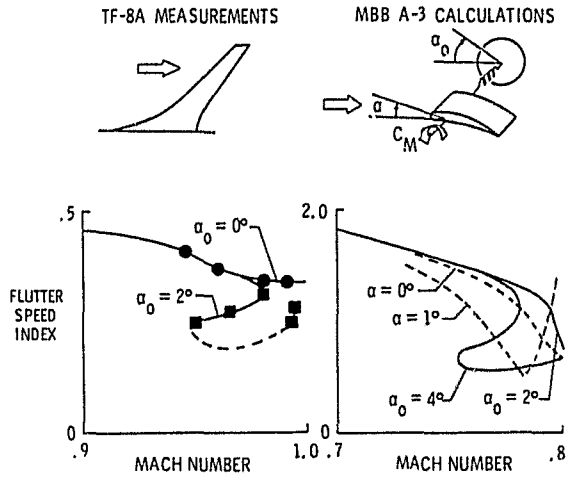

Measured and calculated transonic flutter speeds.

Components of Singular-Perturbation Solution to Trajectory Problems

Singular-perturbation theory offers a framework for the solution of complex trajectory optimization problems. This framework provides a systematic approach for separating the high-order numerical problem of finding optimal trajectories into a series of smaller subproblems that can be solved on board an aircraft in real time. The solutions to the individual subproblems are then combined to approximate the solution to the original trajectory optimization problem.

The chart shows an example altitude time history of a fuel-optimal trajectory for a transport aircraft. The curve labeled C represents the so-called outer-layer subproblem solution and corresponds to a constant-altitude cruise for the aircraft. The curve labeled B represents the first boundary layer subproblem solution. It converges toward the cruise solution, but does not meet the initial condition on altitude. The curve labeled A represents the second boundary layer subproblem solution, which meets the initial condition on altitude and converges to the first boundary layer solution.

This hierarchical approach to solving trajectory optimization problems is being applied to computations of fuel-optimal trajectories for transports and time-optimal trajectories for fighters. The techniques under development allow real time on-board control of optimal trajectories using feedback control laws.

Douglas B. Price, 4681 505-34-03

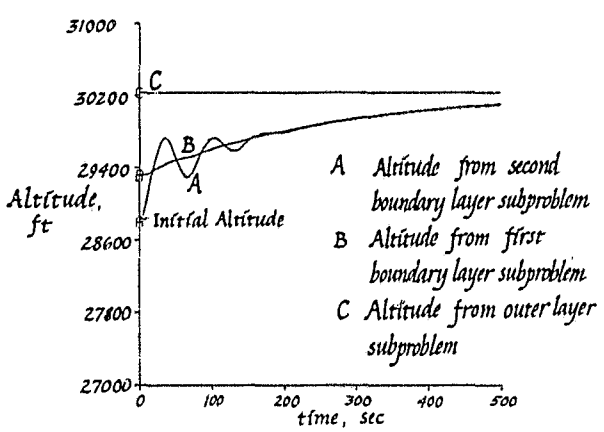

Fuel-optimal trajectories for transport aircraft.

ORIGINAL PAGE IS
OF POOR QUALITY

Sensor Redundancy Management

To achieve desired performance and economic improvements in the coming generation of aircraft, flight control systems will rely on integrated avionics concepts. Langley Research Center has developed sensor redundancy management concepts in which the multiple flight-control sensors of a typical modern commercial aircraft have been replaced with a skewed array of strapdown inertial sensors. Redundant computers are used to perform flight control and air data and navigation processing. To meet mission reliability requirements for the inertial sensors, failure detection, and isolation algorithms have been developed to account for a wide range of sensor uncertainties and failure modes with minimum false alarms. Since reliability is enhanced with physical separation of sensors, methods of exact compensation for structural modes and lever arm acceleration have been included in variable dynamic-threshold functions that test for sensor failure. Multiple-channel detection methods, which encompass flight control, display, and navigation systems, have been implemented to ensure minimum time to detection of sensor anomalies affecting these channels. Fault-down processes further enhance the integrity of the system output since failure-corrupted solutions may be reset with valid sensor data.

A methodology has been developed and applied for quantitatively assessing the reliability of sensor redundancy management concepts using Markov modeling techniques. This methodology optimizes system performance through analysis of the effects of sensor failure rate, threshold level, failure detection coverage, correct failure isolation, damage caused by environmental effects, and mission time on system reliability. The redundant strapdown inertial measurement unit being used to validate the theoretical work uses two-degree-of-freedom gyros and accelerometers. The failure detection and isolation algorithms enable the unit to survive two gyro and two accelerometer failures to provide dual fail-operational performance.

Frederick R. Morrell, 3291 505-34-13

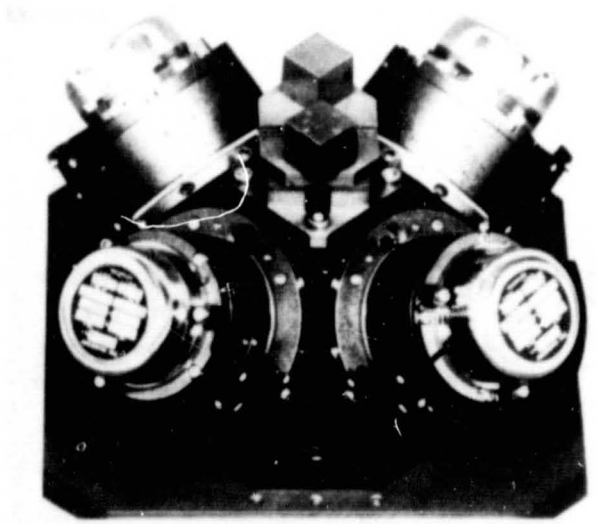

Semi-octahedron sensor mounting.

Multifunction Keyboard Developed Using Yellow LEDs

The Crew Station Technology R&T base program, in conjunction with the Air Force, has developed an experimental multifunction keyboard (MFK) with programmable legend switches using bright yellow light-emitting-diode (LED) alphanumeric displays. The MFK is designed to declutter vehicle cockpits by

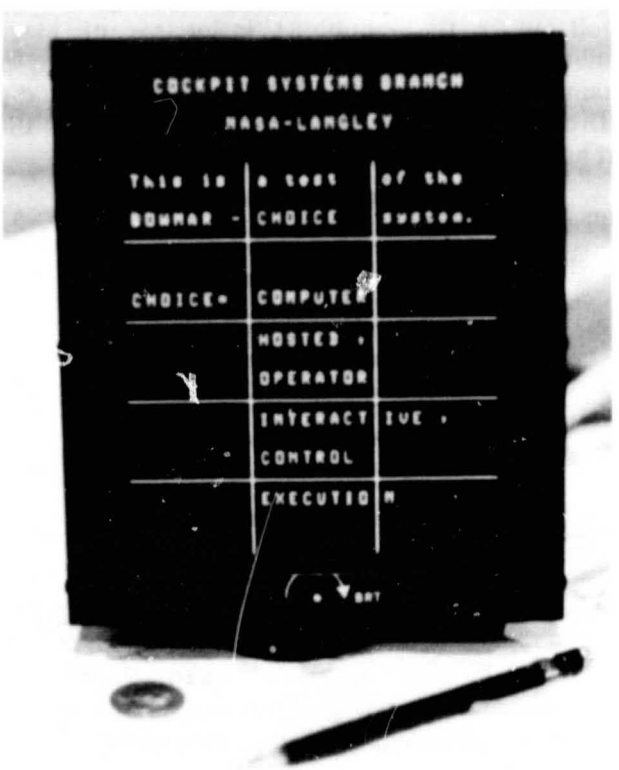

Multifunction keyboard.

reducing the number of dedicated switches/controls and replacing them with a programmable-legend multifunction panel, as shown in the figure.

The MFK provides a 3 × 5 array of programmable-legend switches for accepting pilot/crew inputs and a scratch pad for displaying vehicle computer outputs. Each key or switch has an alphanumeric display of two rows of eight characters. Tactile switch feedback is provided by each switch. Each switch is front-panel replaceable. The MFK displays can be dimmed with a manual control for night viewing.

The MFK is based on an eight-bit microprocessor that provides the capability for generating legend displays on a self-contained basis or through a host processor via data link or bus inputs. The experimental MFK has the potential to be used simultaneously as a controller for navigation, communications, and systems management, thereby replacing numerous single-purpose switches and controls. Laboratory and simulator evaluations of the MFK are being planned.

James B. Robertson, 3856 505-34-23

Liquid-Crystal Display Used in Integrated Control Panel

The Crew Station Technology R&T base program has been engaged in the development of flat-panel display technology for application in cockpits of future aircraft or aerospace vehicles. One of these development efforts has produced a large-area (5 × 7 in.) liquid crystal display with good uniformity and contrast for application in a candidate cockpit device known as the Integrated Control Panel (ICP).

The ICP is being developed jointly by NASA and the Navy. It is designed to declutter vehicle cockpits by reducing the number of dedicated switches/controls and replacing them with a programmable-legend multifunction panel. The ICP contains a set of mode switches, a scratch pad for receiving messages from the aircraft, and a set of multifunction switches with programmable legends for inputting data and commands to the vehicle.

The liquid-crystal display (LCD) used in the ICP is the basis for the scratch-pad display and the display for programmable legends in a 5 × 6 array. The LCD uses a dichroic-dye/liquid-crystal mixture as the display medium and a zinc oxide varistor layer to produce the electro-optical threshold needed for X-Y matrix addressing of the display. The LCD used in the ICP has a resolution of 36 lines/in. and a 4:1 contrast ratio, and is readable in bright sunlight.

James B. Robertson, 3856 505-34-23

Simulator Evaluation of New Vertical VSI

In response to an FAA request, tests have been conducted in Langley Research Center's General Aviation Simulator. Pilot scanning data were collected while pilots performed an ILS (Instrument Landing System) flying task with both the conventional vertical-speed indicator (VSI) and the new vertical bar graph vertical-speed indicator (VVSI). Six subjects participated in these tests. To investigate the effects of workload, the pilots were given four levels of a mental loading task. The purpose of this task was to deliberately overload the pilot to produce differences in performance that would then be attributable to the display.

Analysis of the results showed that during the approach phase of an ILS maneuver the entropy rate measure of pilot scanning was greater for the VVSI than for the conventional VSI. Entropy rate can be thought of as a measure of randomness or an indication of spare scanning time. The interpretation of the data is that the mental workload of the conventional VSI is greater than that of the VVSI by an amount approximately equal to performing the mental loading task every 20 seconds.

The dwell time histograms of the two vertical-speed indicators show that the ratio of short looks to long looks was greater when the pilots were using the VVSI than when they were using the conventional VSI. This indicates that the pilots were able to extract the information more quickly with the VVSI than with the conventional VSI. Although this difference is small, it does mean that in instances of time criticality, the VVSI would be a better instrument to use. This agrees with the previous result, suggesting that there would be a lower mental workload with the VVSI. This

ORIGINAL PAGE IS
OF POOR QUALITY

testing technique and the data analysis of scanning behavior are effective in evaluating subtle differences in panel arrangement and instrument design.

Randall L. Harris, Sr., 3917 505-35-43

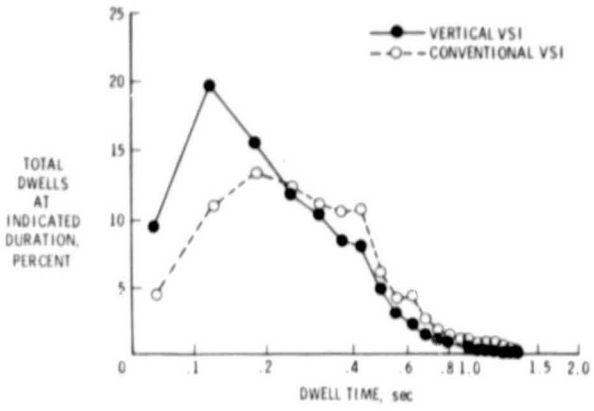

Dwell time histogram.

Exploratory Research on Advanced Regional Transport Aircraft Configurations

As part of a general research program to provide fundamental aerodynamic information on advanced regional transport aircraft configurations, wind tunnel tests are currently being conducted in the Langley 30- by 60-Foot Tunnel and associated facilities on several promising configuration concepts. The experimental work is directed at configurations offering improved performance and safety with emphasis on aerodynamics, stall/spin resistance, and engine-out operations. The experimental work is closely coordinated with feasibility studies and analytical and computational methods conducted in house and under a grant with the University of Kansas.

The first in a series of static and wind tunnel tests of a three-surface twin-engine design has recently been completed in this program. Tests included studies of several configuration layouts for the canard and engine locations, including the effects of power. Particular emphasis was given to the stability and control characteristics at stall. Potential problem areas, such as pitch-up, were identified at moderate angles of attack within the range of expected operation. Configuration modifications, including such items as wing-fuselage fairings and wing leading-edge devices, were investigated to alleviate such stability problems. These results are being used to plan further wind tunnel studies needed to develop a mature data base. Such a data base will be used to define the most promising configuration concepts for more in-depth study using large-scale model tests, dynamic-model flight tests, and piloted simulation studies.

William A. Newsom, 2184 505-41-13

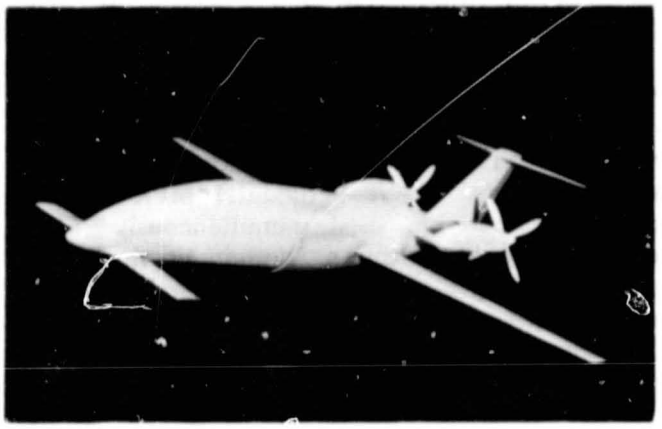

Advanced regional transport configuration.

Natural Laminar Flow

Recent flight experiments have shown that modern airframe construction techniques can provide production surface conditions compatible with natural-laminar-flow (NLF) requirements. These experiments were conducted on 10 different aircraft, including both propeller- and turbojet-powered configurations, with airframes constructed of either aluminum or composites.

The experimental methods included use of sublimating chemicals for visualization of boundary layer transition, as illustrated in the figure, which shows the extent of NLF on the Bellanca Skyrocket. Recent Langley-developed refinements to this method using thick coatings of the properly selected chemicals permit flight experiments to be conducted without "bagging" the wing for protection of the chemicals during the off-condition climb and descent portions of the flight. The chemical pattern transition data can then be recorded on the ground after the flight. Other experimental methods included use of hot-film and acoustic techniques for transition detection.

ORIGINAL PAGE IS
OF POOR QUALITY

Boundary layer transition on the lifting surfaces evaluated was observed to occur downstream of the analytically estimated minimum pressure locations for each airfoil at its particular flight conditions. Transition Reynolds numbers as large as 11 million were obtained at chord Reynolds numbers of 28 million. In all cases conservative agreement was observed between the empirically predicted allowable and the actual measured waviness on the surfaces tested. Significant regions of laminar flow were also observed in propeller slipstreams. The effects of laminar flow on airplane aerodynamics were measured by comparing free- and fixed-transition test results. It is estimated that the laminar flow measured would increase the cruise range by about 25 percent.

B. J. Holmes, 3611 505-41-13

Laminar flow on Bellanca Skyrocket.

An Aerodynamic Design Program for General-Aviation Propellers

A combined effort by the Bionetics Corporation and NASA Langley has resulted in the development of an aerodynamic propeller design program that can accommodate either supercritical airfoil designs or circulation-controlled supercritical airfoil designs. The circulation-controlled supercritical design uses the Coanda effect by blowing at the trailing edge of the propeller to vary the effective pitch, thus providing propulsion efficiencies comparable with those of conventional variable-pitch propellers without the attendant mechanical complexities of the variable-pitch hub. A cross-sectional view of a candidate circulation-controlled propeller implementation is shown, and details of the blowing slot and the blunt-based trailing edge are given.

The design program can accommodate minimum-loss fixed- or variable-pitch supercritical propellers and circulation-controlled propellers with a single plenum extending to 0.7 radius or 1.0 radius. The propeller design program is written in BASIC so that only a minimal computer investment is required to use the program for designing any type of propeller. This choice in programming language was made to enhance the utilization of this design tool within the general-aviation community. The program description and a users' guide are currently being developed for submission to COSMIC for further distribution.

Wayne H. Bryant, 3404 505-41-63

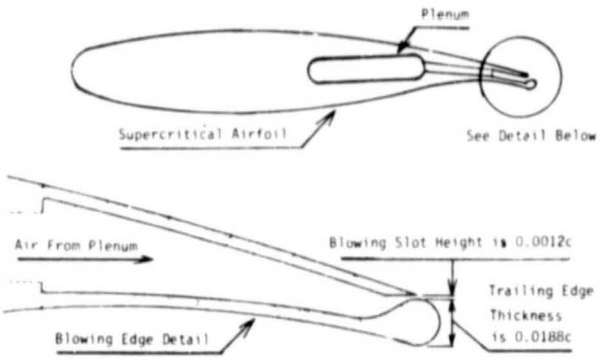

Circulation control propeller system.

Parametric Tip Effects Determined for Conformable-Rotor Applications

Reducing helicopter vibratory loads while improving performance is the goal of the Aeroelastically Conformable Rotor (ACR) concept. The current ACR design methodology incorporates reduced blade torsional stiffness and planform geometry to achieve its goals. To obtain maximum benefits from the ACR concept it is important that the effects of geometry changes on loads and performance be determined. Consequently, wind tunnel tests of a model rotor representing a modern utility

ORIGINAL PAGE IS
OF POOR QUALITY

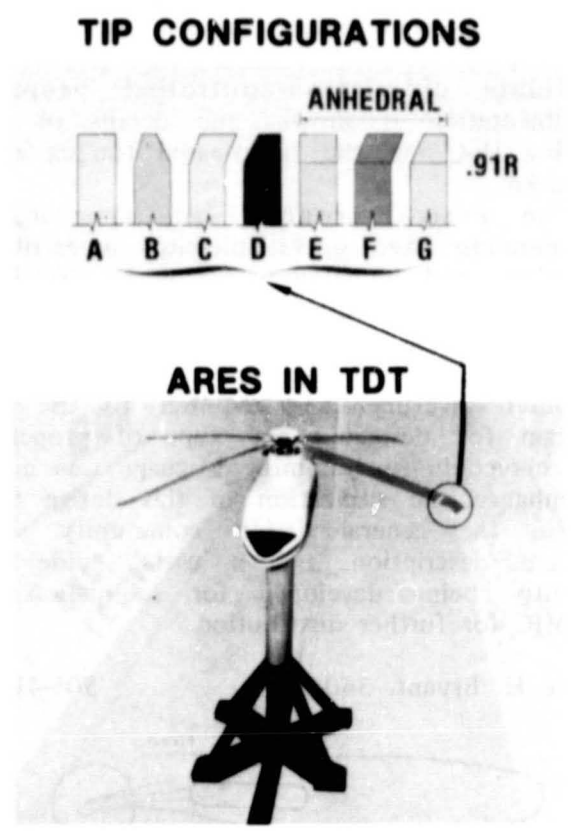

Parametric tip effects determined for conformable-rotor applications.

class helicopter were conducted using the Aeroelastic Rotor Experimental System (ARES) in the Langley Transonic Dynamics Tunnel to parametrically evaluate seven blade tip designs. The tips incorporated a systematic variation in geometric parameters such as sweep, taper, and anhedral to evaluate the effect of these parameters and their combinations on blade torsional response, rotor performance, and vibratory loads.

Each rotor configuration was tested at scaled flight conditions representative of the utility class helicopter. Flight parameters of interest included advance ratio (μ = 0.35), rotor tip Mach number (M_T = 0.65), and rotor lift parameter (C_L/σ = 0.08). The changes in tip geometry produced marked variations in rotor performance and vibratory loads. Incorporation of sweep, taper, and anhedral in rotor tip geometry significantly reduced vibratory loading and power required, as compared to a conventional tip shape. Sweep and taper without anhedral also improved loads and performance. This systematic determination of key parametric effects provides important data for future conformable-rotor development.

W. R. Mantay, 2661 505-42-13

F-16XL Piloted Simulation

For several years Langley has been involved in a cooperative program with General Dynamics to study the high-angle-of-attack flight characteristics of the F-16XL airplane design. This research is part of the Military Stall/Spin Research Program at Langley. As shown in the figure, the F-16XL incorporates an advanced cranked arrow wing to provide improved supersonic performance. This current study is providing an early look at some of the high-angle-of-attack stability and control problems inherent in advanced fighter designs. A piloted simulation of the F-16XL was recently completed using the Langley Differential Maneuvering Simulator to investigate the high-angle-of-attack flight characteristics and to define the automatic flight control laws needed for such an airplane design. The piloted simulation was conducted in parallel with the contractor's efforts to define the airplane flight control system, and these simulation results provided important design information that was

ORIGINAL PAGE IS
OF POOR QUALITY

used to arrive at the final control system now being used in the F-16XL airplane. Both NASA and contractor test pilots participated in the simulation study. The airplane is now involved in full-scale flight tests at Edwards Air Force Base.

Results of the F-16XL high-angle-of-attack simulation effort provided a set of automatic flight control laws that will be highly effective in providing the F-16XL airplane and similar designs with crisp, positive angle-of-attack control, the maximum available rolling performance, and a high level of resistance to loss of control and spinning.

Marilyn E. Ogburn, 2184 505-43-13

First F-16XL airplane in flight.

Rotary Balance Tests of High-Performance Military Aircraft Configurations

Current fighters exhibit long slender fuselage forebodies that have been shown to strongly influence high-angle-of-attack aerodynamic stability. Recently completed tests of a series of different forebody designs on the F-15 configuration showed that several designs provided strong positive static stability at high angles of attack. Since previous experience had shown that the forebody design also strongly influences aerodynamic damping at high angles of attack, a series of rotary balance tests were conducted in the Langley Spin Tunnel to measure the spin aerodynamics on several of the forebody designs.

Results of these rotary balance tests showed that the forebody designs that provided the largest stabilizing influence on static stability also produced highly unstable values of aerodynamic damping. These same results were found during earlier flight tests at NASA Ames/Dryden, where stall/spin flight tests were conducted using a remotely piloted vehicle incorporating the forebody designs of interest. This research program is providing unique aerodynamic data that are necessary in the design of high-performance military configurations.

James S. Bowman, Jr., 2521 505-43-13

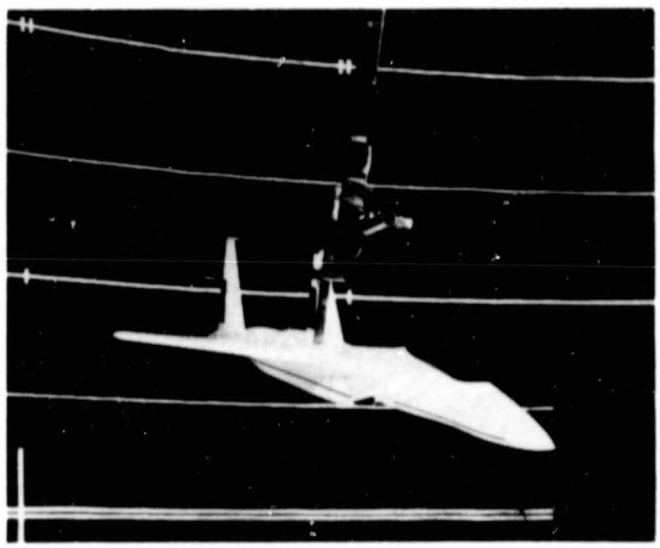

Rotary balance tests of 1/12-scale model of F-15.

Missile Aeropropulsion Integration Research

An experimental research program has been conducted over the last 5 years in which several Langley researchers from the Supersonic Aerodynamics Branch have developed a technology base on the effects of aerodynamics and propulsion integration for a new generation of tactical airbreathing missiles. This research allowed the Navy and its contractors to develop a Sparrow-sized airbreathing missile configuration with stability, control, and performance characteristics for extended range and improved end-game maneuvers.

The Naval Weapons Center in China Lake, California is involved in a 1984 flight

ORIGINAL PAGE IS
OF POOR QUALITY

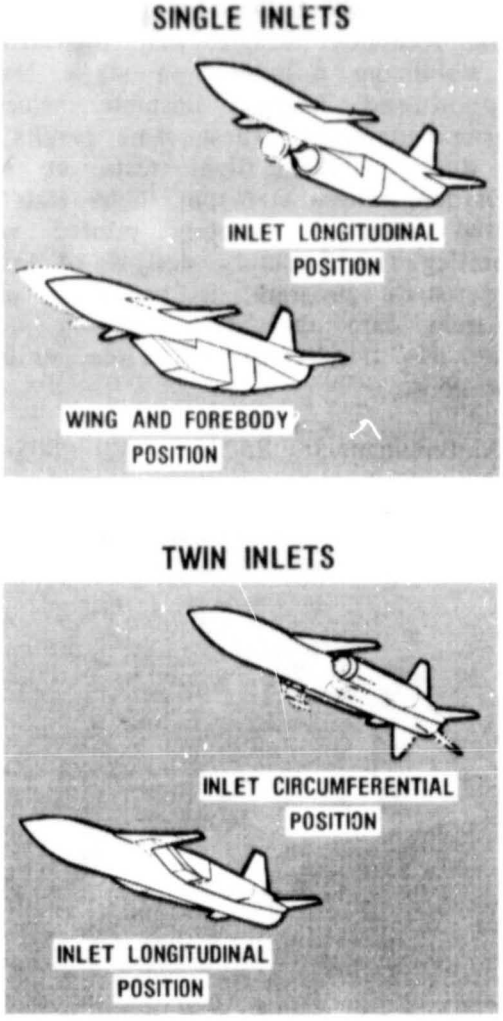

Development of ACIM configuration.

demonstration program to verify the technology for airbreathing maneuvering missiles. This flight program has been designated the Advanced Common Intercept Missile (ACIM) Program. As the developers of the basic aerodynamic technology, the NASA researchers have been requested to participate in the development of the flight vehicle and have conducted tests to evaluate the aerodynamics of the ACIM configuration for autopilot design.

James L. Dillon, 3181 505-43-23

Active Flutter Suppression of Wings With External Stores

The carriage of external wing-mounted stores by modern fighter airplanes can result in flutter speeds that are well within the operational envelope of the clean (no stores) airplane. To determine the effectiveness of active flutter suppression systems (FSS) to increase flutter speeds in these instances a flutter model of the F-16 airplane equipped with an FSS was tested for several different combinations of external stores in the Langley Transonic Dynamics Tunnel. The 1/4-scale full-span model was flown on a cable suspension system that simulated free-flight conditions. The FSS operated by sensing wing and/or store dynamic response with an accelerometer and feeding back this signal through a computer-implemented control law to drive aerodynamic control surfaces (in this case, flaperons on each wing) in such a way as to reduce the response and thus suppress the impending flutter instability.

Testing proceeded in the following manner. The flutter boundary was first determined without the aid of a FSS. The FSS was then engaged and the model tested at conditions well above the unaugmented flutter boundary without encountering flutter. Although no attempt was made to determine the maximum increase in velocity or dynamic pressure (q) obtainable, increases in dynamic pressure in excess of 100 percent were demonstrated at 0.80 Mach. Another significant result was obtained when the model was flown above the flutter boundary with the control surface on one wing disabled, simulating a failed actuator. Although the damping was reduced for this

ORIGINAL PAGE IS
OF POOR QUALITY

case, the original control law was still effective in preventing flutter up to the flight conditions tested for the fully effective actuator case.

F. W. Cazier, Jr., 2661 505-43-33

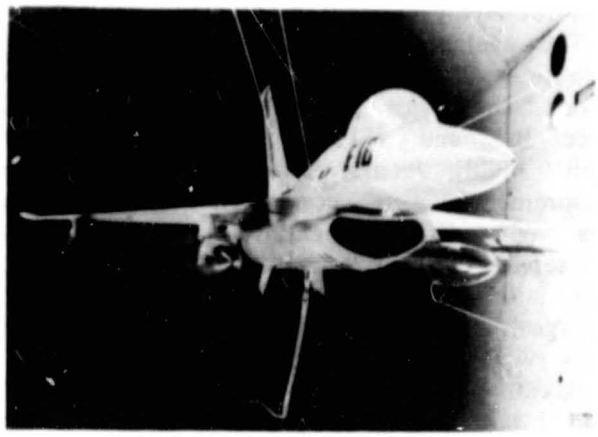

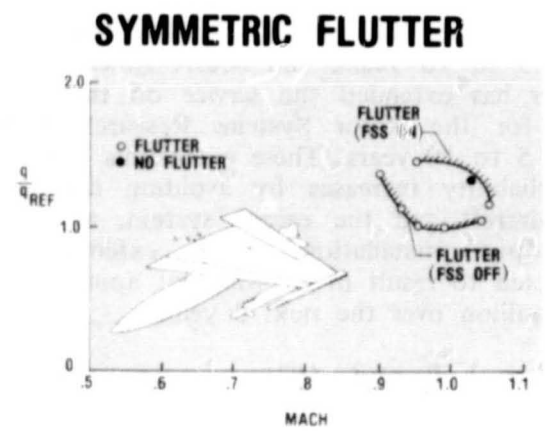

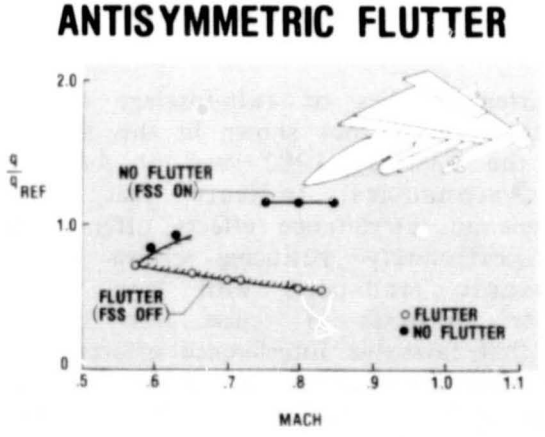

F-16 flutter suppression systems evaluated in TDT.

Miniature Solid-Propellant Rocket Motor

A high-performance light-weight low-cost miniature solid-propellant rocket motor was developed in conjunction with an ongoing stall/spin recovery research program involving Department of Defense subscale aircraft models. The first use will be on the AV8B advanced Harrier V/STOL aircraft model to size a full-scale rocket motor for flight spin test purposes. The miniature motor utilizes the latest in high-temperature composite material technology and all-bonded construction to achieve minimum total weight. The motor case is fiberglass epoxy tubing, the tube end closures with mounting tabs are injection-molded silica phenolic, the nozzle is molded-in-place graphite, and the igniter is a subminiature electrically initiated squib. The motor produces a constant thrust level of up to 5 oz for 4 seconds and is 1/2 in. in diameter, up to 2 in. long and weighs up to 12 g. Lower thrust levels and shorter burn times are achieved through substituting other propellants of smaller diameter and shorter length, with corresponding reductions in overall motor length and total weight.

M. H. Lucy, 4621 505-43-33

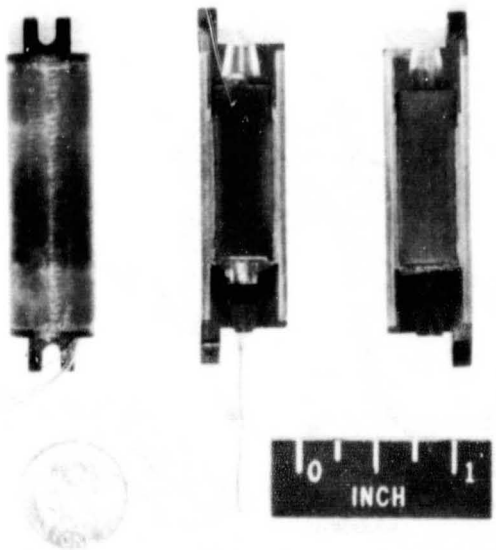

Miniature solid-propellant rocket motors.

ORIGINAL PAGE IS
OF POOR QUALITY

Service Life Evaluation of Rigid Explosive Transfer Lines

A service life evaluation program has been conducted on rigid explosive transfer lines, which are used extensively in military and NASA aircraft, in an effort to increase system reliability and reduce costs. Explosive transfer lines, used to initiate aircraft emergency escape functions, have limited service lives due to high-reliability requirements of man-rated systems. As illustrated, explosive transfer lines utilize a cord containing a small load (2.5 grains/ft, or 0.53 g/m) of very stable explosive materials. An explosive shock input to the booster tip causes a shock wave to propagate through the cord and explode an identical tip on the opposite end. The transfer lines are assembled like high-pressure plumbing to fully contain the explosive products and communicate this shock wave to each escape system function, as in the Army helicopter system shown.

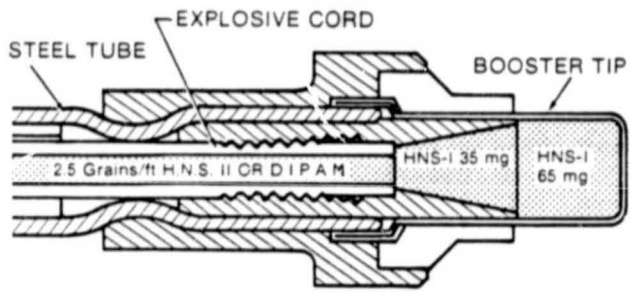

Rigid explosive transfer line.

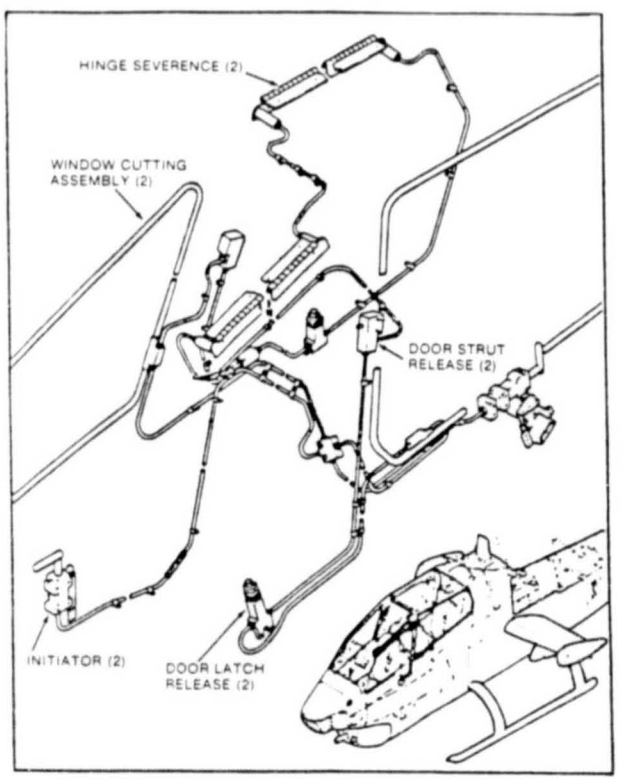

Army AH-1S canopy removal system.

The evaluation program was conducted on more than 700 lines removed from five military aircraft: the Army AH-1G and AH-1S, the Air Force B-1 and F-111, and the Navy F-14. Twelve highly accurate functional and chemical measurements were conducted on groups of lines having different ages, full-rated service, and full service with a repeat thermal qualification (the major environment influencing these lines). The results indicated no detectable change with age, service, or repeat thermal qualification.

Based on this technology, the Army has decided to leave their explosive transfer lines in their aircraft fleet and remove samples for evaluation on an annual basis. The Air Force has extended the service of B-1 transfer lines from 3 to 10 years, and NASA Ames Research Center has extended the service on the transfer lines for the Rotor Systems Research Aircraft from 5 to 10 years. These extensions will result in reliability increases by avoiding damage to the aircraft and the escape system, as well as improper installation. These extensions are projected to result in a savings of approximately $10 million over the next 3 years.

Laurence J. Bement, 4621 505-42-39

Multibody Aerodynamic Interference at Supersonic Speeds

Current studies of twin-fuselage supersonic aircraft, such as that shown in this illustration from the February 1982 issue of Astronautics and Aeronautics, indicate that favorable aerodynamic interference effects offer a means of significantly reducing cruise drag for supersonic transports with large passenger capacity. Analyses of cruise flow conditions show that favorable interference effects between two bodies can decrease wave drag from that of a single body of equal volume. While studies of fully integrated configurations are proceeding, detailed evaluations of existing analytical tools are leading to improvements in the overall design methodology.

ORIGINAL PAGE IS
OF POOR QUALITY

Aerodynamic interference effects have been studied for isolated twin bodies at Mach 2.7. The combined experimental and analytical study was conducted for two slender bodies of revolution with a variety of lateral-longitudinal spacing. Proper spacing was expected to locate the nose shock of each body on the aft surface of the other body; this could result in an increase in pressure on the back of both bodies and a net decrease in wave drag.

Results indicate that this interference can be predicted within 2 percent by existing numerical methods. For example, in the test, total drag of two bodies was decreased to about 80 percent of that for a single body of equal volume. Such correlation with theory for simple bodies allows further analyses of complete configurations with confidence.

Samuel M. Dollyhigh, 4576 505-43-53

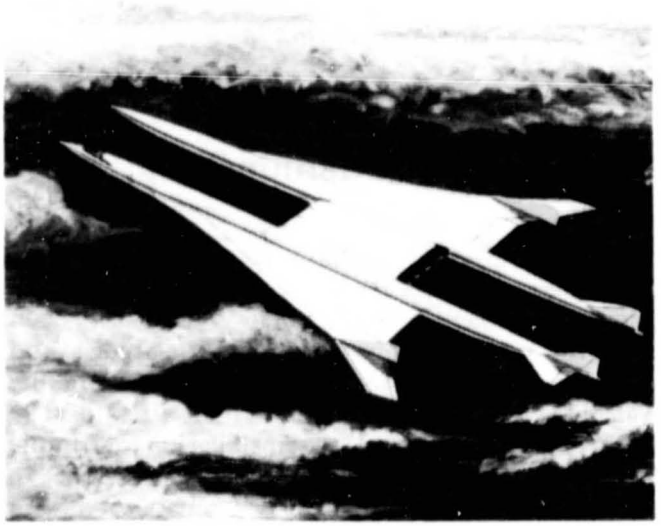

Twin-fuselage supersonic aircraft.

High-Pressure-Ratio Nozzle Static Test Apparatus

Researchers at Langley are currently conducting studies of advanced concepts for hypersonic aircraft. These concepts could require a combination of two- and three-dimensional nozzles. These nozzles would operate at a pressure ratio approaching 300 during cruise conditions, which is significantly higher than can be achieved in static test facilities with the flow exhausting to the atmosphere. In order to obtain experimental data needed to establish performance and verify numerical methods, the Langley Nozzle Test Chamber has been modified to obtain high nozzle pressure ratios and to measure nozzle thrust.

This nozzle static test system utilizes an existing test chamber connected to vacuum spheres, with a 600-psia air supply installed in such a way as to allow use of nozzle test procedures and hardware developed for use in the Langley 16-Foot Transonic Wind Tunnel. The nozzle exhaust flow discharges into a 60-ft-diameter vacuum sphere through a flow diffuser, and a separate control exists to exhaust the test chamber into a 41-ft-diameter sphere. The result is a versatile test system allowing a wide range of nozzle pressure ratios. Very high pressure ratios are achieved by opening the valves to both spheres to maintain a low test chamber pressure. By discharging only to the 60-ft-diameter sphere, a lower pressure ratio can be set. By closing both spheres the nozzle can be exhausted to atmosphere, overlapping the low-pressure-ratio capability of existing static test facilities.

This system is now operational and calibration runs have been made to determine its operating characteristics. Nozzle pressure ratios of from about 9 to 400 have been obtained with a nozzle total pressure of 100 lb/in.^{2}. Experimental programs utilizing this test system will include both internal static pressure and six-component force balance measurements.

J. Wayne Keyes, 3294 505-43-83

Long-Endurance Solar-Powered Airplane

Application of recently developed solar-energy balance, aerodynamics, and airplane-sizing algorithms has produced preliminary design concepts for remotely piloted, solar-powered airplanes for long-endurance high-altitude flight. This class of aircraft is proposed as an alternative to orbiting satellites or manned aircraft for regional applications in communications, mapping, reconaissance, and phenomenological monitoring. They offer frequent or continuous monitoring from altitudes up to 100,000 feet with endurance limited only by systems reliability. By contrast, endurance of manned aircraft is limited by

ORIGINAL PAGE IS
OF POOR QUALITY

human factors, and satellites suffer either loss of resolution due to high orbit or intermittent coverage due to low orbit.

Results from in-house studies have identified enabling technologies that are essential to future development of this class of aircraft. The most critical technology is energy storage; specific energy of at least 100 W-hr/lb will be required to store excess solar energy during daylight for subsequent night flight. The design algorithms have so far led to high-aspect-ratio mono-wing concepts. Other configuration concepts, such as guyed or joined wings, also show promise for these applications.

In cooperation with the U.S. Department of Agriculture, NASA has contracted with Lockheed Missiles and Space Co. for a preliminary design of a solar-powered unmanned airplane to fly in the vicinity of the San Joaquin Valley in California. The proposed 1-year mission requires hourly daytime monitoring of crop conditions to enable near-real-time crop management.

James W. Youngblood, 3666 505-43-93

Measurement of Spanwise Gradient of Atmospheric Turbulence

An instrumentation system developed at NASA Langley for accurately measuring atmospheric turbulence to wavelengths of at least 30,000 ft. has been adapted to provide the capability to measure the spanwise gradient of atmospheric turbulence. The photograph shows the installation on the sampling airplane, a B-57B Canberra. In addition to a gust boom on the fuselage, rigid booms have been mounted 60 ft apart at the wing tips. Balsa flow vane sensors mounted near the end of the booms provide time histories of flow angle fluctuations, which are a direct measure of the atmospheric turbulence or gust velocity. Quartz pressure sensors are used to sense the airspeed fluctuations or longitudinal gust velocity. Aircraft motions are sensed by an inertial platform and rate gyros, and these data are applied as corrections to the basic flow measurements. Spanwise turbulence gradient measurements were obtained from 11 flights made near thunderstorms in the Denver area in July 1982 as part of the Joint Airport Weather Studies (JAWS) Program.

H. N. Murrow, 3527 505-44-23

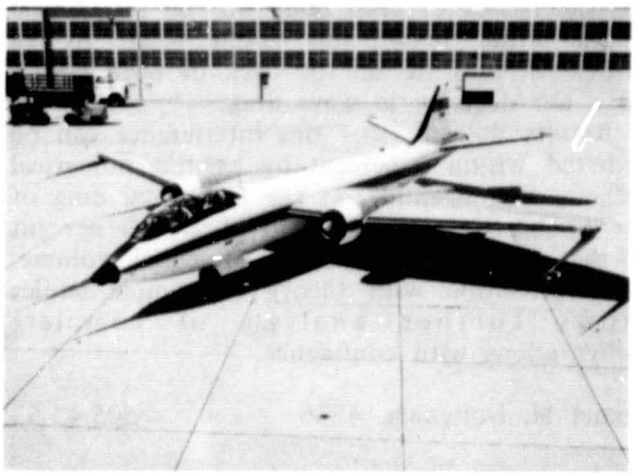

Gust booms mounted on B-57B.

Free-Body Air Cushion Test

The NASA air cushion landing system test vehicle (ACLSTV) equipped with a four-compartment experimental ACLS, has been used for preliminary ground stability studies and exploration of various steering and braking concepts for hovercraft and other aircraft. The stability studies led to the installation of simple but very effective pressure relief doors, one in the cushion or cavity area and smaller ones in the forward and side trunks, which have resulted in completely stable operations in all regimes tested thus far. The most effective steering concept has proven to be a lightly loaded free-rolling nonsteerable wheel and tire assembly installed in the cushion cavity area. The air rudders on the ACLSTV can then be used to change both vehicle heading and direction of motion with great precision on a variety of operational surfaces. This concept is also effective in countering the effects of crosswinds or runway slopes.

The free-body test vehicle has also been used in corroborative studies of an analytical computer model developed under contract by Foster-Miller Associates, Inc., for a smaller, more generalized ACLS model. Considerable modification to the original model was

ORIGINAL PAGE IS
OF POOR QUALITY

necessary, but quite good agreement has been obtained recently between analytical and ACLSTV test results.

R. H. Daugherty, 2796 505-44-33

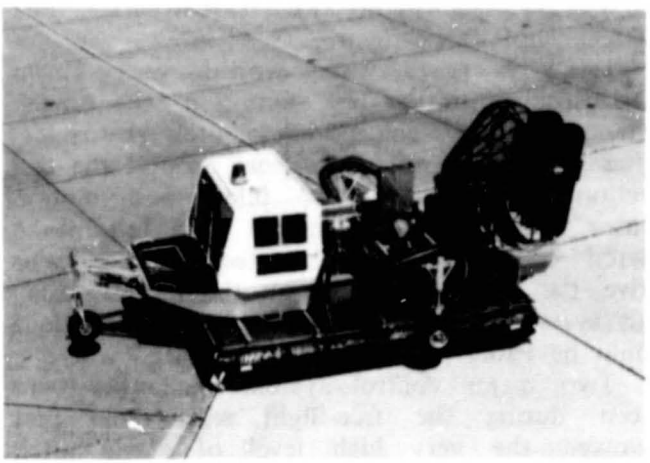

Air cushion landing system test vehicle.

Navajo Active-Main-Gear Experimental Results

An experimental program employing a modified main landing gear from a Piper Navajo airplane has been conducted at the LaRC Aircraft Landing Dynamics Facility. Results obtained from a landing test of active and passive versions of the gear are shown in the figure. The normal forces applied through the center of gravity of the test apparatus are shown plotted as a function of time for touchdown impact, traverse of 1.25-in.-amplitude step bumps, and natural bumps with an amplitude of 1.25 in. The touchdown (zero second) ground speed was 80 knots and the sink rate was 5.5 ft/sec. During touchdown impact the active gear was 9 percent more effective than the passive gear in reducing the decelerating force (negative force), and during rebound the active gear reduced the accelerating force by 36 percent. During traverse of the two step bumps, which were spaced to provide an encounter frequency of 2 Hz, the active gear was effective in reducing the decelerating force by 31 percent for the first bump and 23 percent for the second bump. However, when the test apparatus was accelerating towards the surface during rebound from each of the step bumps, the active gear resulted in increases in accelerating forces of 35 percent and 62 percent for the two bumps. This reduced performance of the active gear may be attributed to inadequate response of the control system, since at lower ground speeds the active gear was much more effective. During traverse of the natural bumps, which had considerably lower slopes than the step bumps, the active gear was very effective in reducing both the decelerating and accelerating forces, as shown by the reductions of 62 percent and 54 percent, respectively.

John R. McGehee, 2796 505-45-23

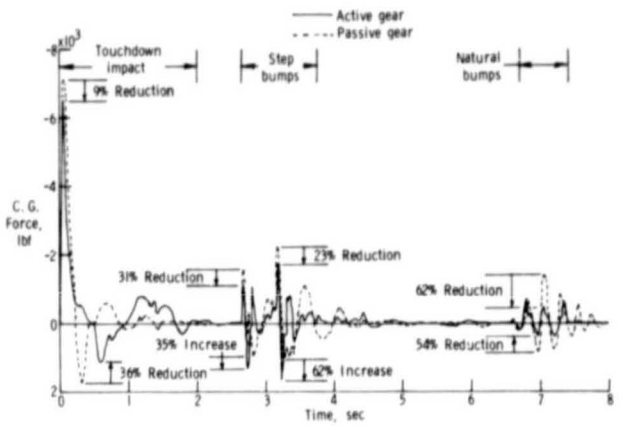

Experimental results for Navajo active main gear.

RIM Provides Major Advancement in Engineering Data Management Technology

Recent years have witnessed a virtual explosion in data associated with the design and development of complex engineering projects, but only limited facilities exist to manage such data. A major advancement in needed capability to manage engineering data has been developed through a joint NASA/industry project denoted Integrated Programs for Aerospace Vehicle Design (IPAD). This capability is a Relational Information Management (RIM) software system based on relational algebra concepts. The basic idea of RIM is that it stores tables of data and relationships among tables. Through this approach it provides a high degree of flexibility in defining and storing data, is easy to use, and handles a wide variety of data

ORIGINAL PAGE IS
OF POOR QUALITY

types typical of engineering needs. It is written in FORTRAN and has convenient features to support interactive users as well as to interface with applications programs. In 1981 an earlier version provided critically needed capability for management of data associated with Langley investigation of the integrity of Shuttle tiles. Since that time over 200 copies of RIM have been distributed for use in a broad spectrum of engineering, manufacturing, and business applications by both aerospace and nonaerospace groups. One planned use by Harza Engineering of Chicago is for RIM to manage construction information over the 10-year development life of a $5-billion dam project in South America.

The NASA/IPAD development of RIM was completed in early 1982. Several commercial ventures have been initiated to provide further enhancements, maintenance, and support for the continually expanding number of RIM users. The RIM system has been implemented on most mainframe computers and minicomputers and one firm is marketing a version of RIM for microcomputers. RIM is a good example of NASA's research efforts providing needed technology for both the aerospace and nonaerospace community.

R. E. Fulton, 2887 505-54-13

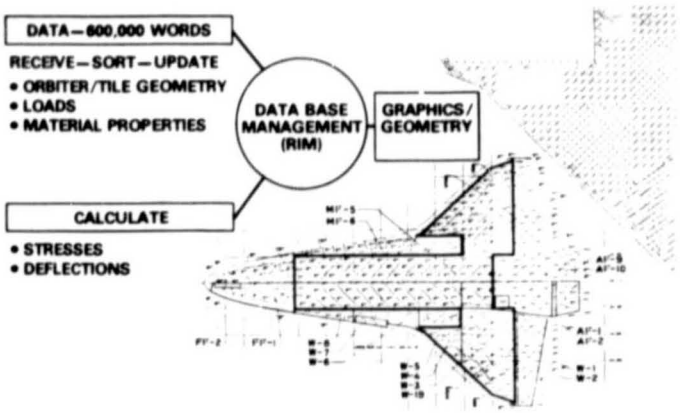

IPAD/RIM application to Shuttle tile analysis.

X-29A Free-Flight Tests

As part of a broad research program to study the high-angle-of-attack flight characteristics of the Forward-Swept Wing Demonstrator (X-29A), free-flight tests of a 0.16-scale model were recently conducted in the Langley 30- by 60-Foot Wind Tunnel. The primary purpose of the tests was to study stability and control characteristics up to the stall and to make an initial assessment of control system requirements for high-angle-of-attack flight.

In the tests the model was flown unconstrained in the test section of the tunnel. The model was controlled remotely by pilots situated at appropriate positions around the test section. Inputs from the pilots and motion sensor signals from the model were fed into a digital computer that generated commands to drive the control surfaces on the model. Using this system, the effects of control law variations could be easily and efficiently assessed.

Two major control system challenges were faced during the free-flight tests. The first involved the very high level of static pitch instability designed into the airplane to minimize trim drag during transonic maneuvering. The level of instability is nearly an order of magnitude higher than those of current fighters, such as the F-16, that incorporated this concept. The second challenge faced was the susceptibility of the configuration to very large amplitude undamped roll oscillations caused by loss of roll damping at high angles of attack. During the tests, control laws were developed to address both of these areas of concern and to provide satisfactory flying characteristics throughout the angle-of-attack range of the tests. With this control system, the model was flown to angles of attack as high as 40^{o}.

Daniel G. Murri, 2184 533-02-83

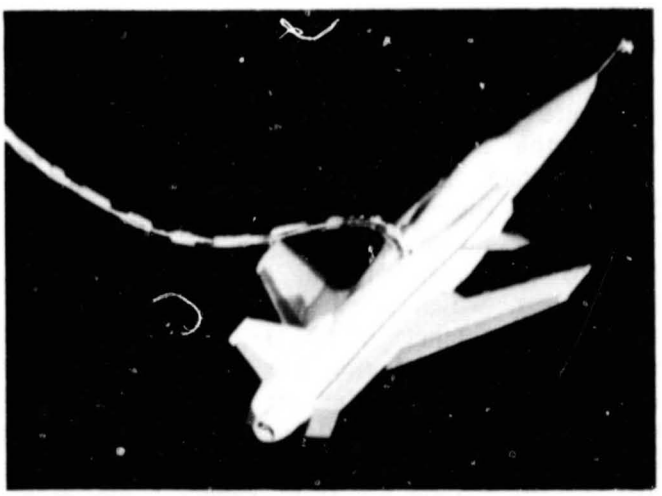

X-29A model in free-flight tests.

ORIGINAL PAGE IS
OF POOR QUALITY

Laminar-Flow-Control Technology

Under a grant with Virginia Polytechnic Institute and State University, low-speed tunnel tests were made of boundary layer suction through an electron-beam-perforated titanium surface. Measured parameters include disturbance levels, transition Reynolds numbers, and inflow/outflow tolerance as a function of suction hole Reynolds numbers. Results indicate that existing design criteria are conservative. It was shown that suction concentrated in the weakly amplified disturbance region near the leading edge was more effective in stabilizing boundary layer velocity fluctuations in two-dimensional flow. This technique differs from the original approach of applying suction farther downstream in the maximum disturbance growth region. Theoretical stability calculations using linearized "triple-deck" theory predict this result and the experiment data.

Under a contract with the Douglas Aircraft Company, fabrication techniques were developed for routinely building laminar flow control (LFC) suction panels (with perforated titanium skins) that could be gloved onto typical aircraft wing structure. Resulting chordwise waviness on the panel surface is typically less than 0.001 in. from peak to peak. This waviness achievement is well within established LFC criteria and is a major accomplishment towards helping to establish the feasibility of LFC for commercial transports.

Other progress in LFC development includes the initialization of exploratory testing with the slotted swept-airfoil model in the Langley 8-Foot Transonic Pressure Tunnel.

Richard D. Wagner, 2045 534-01-13

Cloud/Ice Crystal Effects on Laminar-Flow-Control Aircraft

Cloud detection observations previously obtained in the Global Atmospheric Sampling Program (GASP) have been analyzed to estimate the effect of atmospheric ambient ice crystals on the aerodynamic performance of aircraft utilizing laminar flow control (LFC) to reduce drag. Theory and limited operational experience to date predict that the drag improvements with LFC will be degraded by an amount that can be correlated with the size and number density of the particles encountered in flight. Analysis of the GASP data collected at the operational altitudes for commercial aircraft (7.6 to 13.7 km) has provided the first published estimates of probabilities for cloud and particle concentration encounter on a worldwide scale, along with their variability with season, latitude, altitude, and vertical distance from the tropopause. An example of the type of result obtained is given by the figure, which shows the probability (ordinate) of encountering clouds more than a given portion of the time (abscissa) for three altitude bands on a worldwide basis. The example (vertical dashed line) shows that the probability of being in clouds more than 20 percent of the time in the 8.7- to 10.2-km-altitude band (28.5 to 33.5 kft) is approximately 12 percent, in the 10.2- to 11.7-km (33.5 to 38.5 kft) band it is approximately 9 percent, and in the 11.7- to 13.3-km (38.5 to 43.5 kft) band it is approximately 5 percent.

Analyses of the data indicate that poleward of 25° latitude, flight in the uppermost altitude range, i.e., 11.7 to 13.7 km (38.5 to 45 kft), is definitely superior for cloud avoidance, whereas at lower latitudes, flight in the 10- to 11.7-km (33 to 38.5 kft) range appears best. An algorithm for estimating the probability of

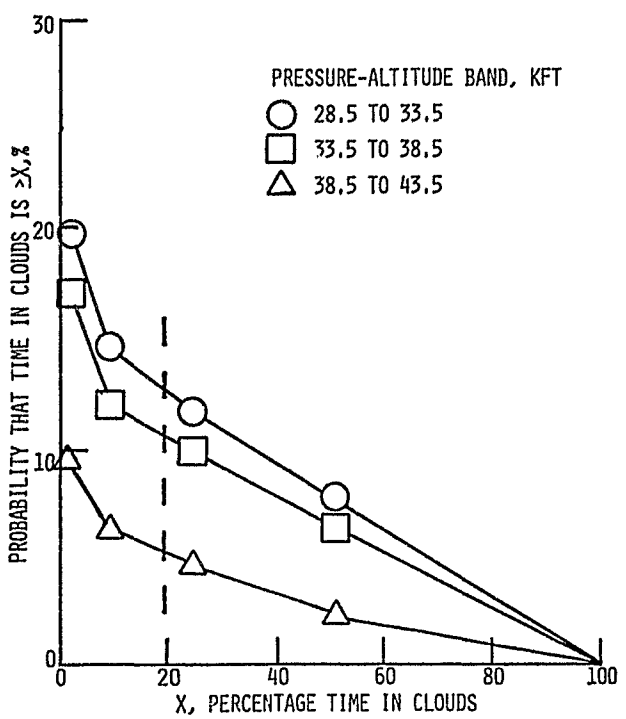

Probabilities of cloud encounter.

LFC loss within clouds and "clear air" was developed by combining the GASP data with Knollenberg probe particle spectrometer data obtained in USAF cloud research programs. The results indicate that in "clear air" LFC should be degraded about 1 percent of the time overall; however, LFC effectiveness is always degraded in clouds and cirrus haze by at least 26 percent, with greater than 50-percent degradation occurring about 1 percent of the time. The analysis effort is being conducted by Langley and Lewis researchers, with support by Control Data Corporation, as part of the Aircraft Energy Efficiency (ACEE) Program.

Richard E. Davis, 3761 534-01-13

Energy-Efficient Transport

A number of research activities directed toward improving aircraft energy efficiency have been pursued under contract to LaRC this year. Flight evaluation of winglets applied to a McDonnell Douglas DC-10-10 has been completed by the McDonnell Douglas Corporation. At high-speed cruise conditions, the best winglet configuration tested produced about a 3-percent reduction in fuel burned. At low-speed high-lift conditions, a drag reduction of about 5 percent was obtained. However, a leading-edge device on the winglet was required to achieve this gain. Additional wind tunnel tests will be conducted in order to define a suitable winglet with a simple, deployable leading-edge device.

Lockheed-California Company has conducted a study to determine the benefits and associated development costs in applying advanced technologies in the design of a new wing for a new derivative wide-body trijet that would be entering service around 1990. The advanced technologies that were considered included: (1) high-aspect-ratio supercritical wing technology, (2) advanced high-lift systems, (3) pitch active-control systems, (4) all-electric systems, (5) advanced engines, (6) airframe/propulsion integration, (7) graphite/epoxy composites, (8) advanced aluminum alloys, (9) titanium alloys, and (10) silicon-carbide/aluminum composites. By combining the benefits of these technologies, a reduction in block fuel of about 40 percent was identified as compared to a current-technology transport. The major technology contributors to the 40-percent reduction in fuel burned were the high-aspect-ratio supercritical wing, the pitch active-control system, advanced engines, and graphite/epoxy structure.

Flight tests of a pitch active stability augmentation system on the Lockheed L-1011 have been completed. The tests demonstrated that good handling qualities could be achieved for a near neutrally stable configuration. Production applications of this technology would provide a 2- to 3-percent reduction in fuel use.

A hybrid laminar-flow-control (HLFC) concept has been analyzed by the Boeing Commercial Airplane Company to establish its range of applicability and potential benefits/penalties. An HLFC wing was designed with suction ahead of the front spar only and natural laminar flow over the wing box. It was determined that laminar flow could be maintained over 60 percent of the chord of a 25° swept-back wing at a Reynolds number of 35×10^{6}. The reduced drag would result in about 8 percent less block fuel for a Boeing 757 class airplane on a 4000-km mission.

Ray V. Hood, 2396 534-02-13

Trim Drag for Supercritical Wings

In order to balance the lift generated by its wing and maintain sufficient longitudinal stability, a transport airplane usually requires a horizontal tail. The addition of the horizontal tail results in an increase in the total airplane drag, called trim drag. Recently an experimental investigation was undertaken to determine if aerodynamically advanced supercritical wings incur higher trim drag values at cruise conditions than do current wide-body aircraft wings. Significantly higher trim drag would lessen the performance benefits to be gained from the supercritical wings. The investigation was conducted in the Langley 8-Foot Transonic Pressure Tunnel and was designed to measure relative trim drag increments between a high-aspect-ratio supercritical wing and a wide-body aircraft wing. Five different horizontal tail configurations were tested with each wing. The three low-tail configurations and two T-tail configurations were designed to

ORIGINAL PAGE IS
OF POOR QUALITY

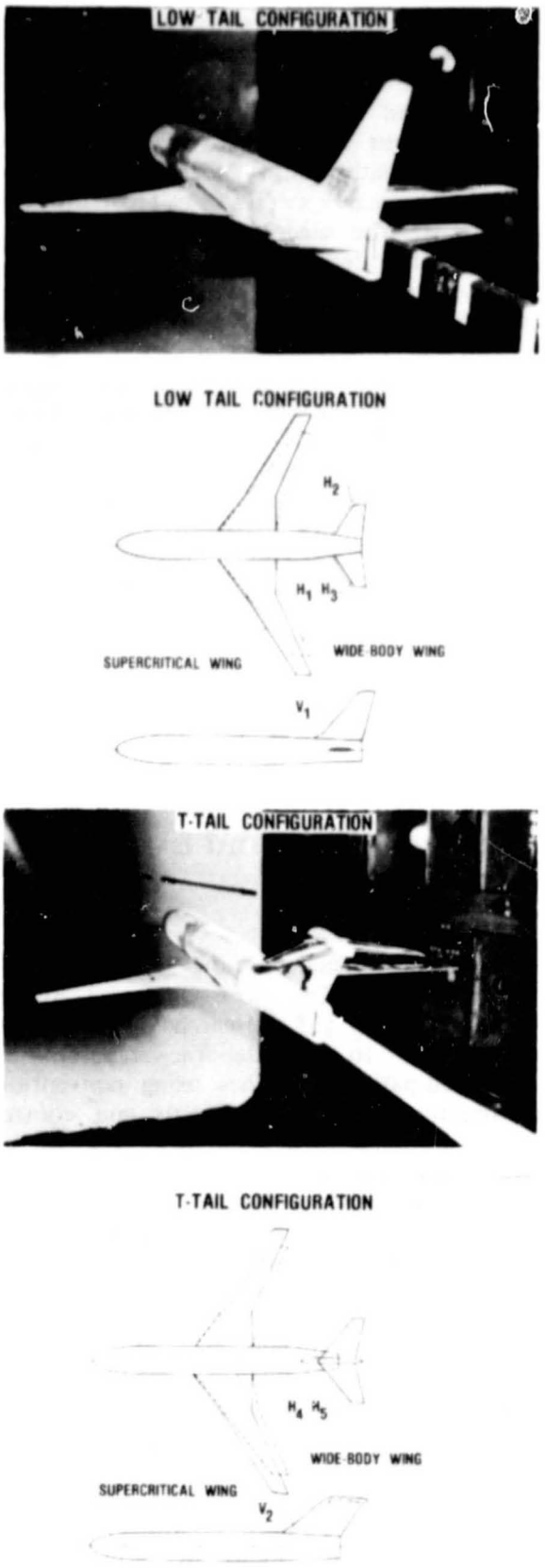

Energy-Efficient Transport (EET) horizontal tails investigation.

measure the effects of horizontal tail size, location, and camber on the trim drag increments for the two wings.

Data at a cruise Mach number of 0.82 indicate that the supercritical wing does not have significantly higher trim drag than the wide-body wing. Both wings experienced reductions in trim drag for the small tails when the longitudinal stability was relaxed slightly. The cambered tails had higher trim drag increments than the symmetrical tails for both wings, and the T-tail configurations had lower trim drag increments than the low-tail configurations. The performance of the supercritical wing was 11 percent better (lift-to-drag ratio) than the wide-body wing with the best low-tail and T-tail configurations.

Peter F. Jacobs, 2601 534-02-13

Composite Components for Commercial Aircraft

Composite components developed under the NASA Aircraft Energy Efficiency (ACEE) Program are being widely accepted in airline service. Five shipsets of Boeing 727 composite elevators have accumulated more than 33,000 flight hours since entering airline service in mid-1980. Thirteen McDonnell Douglas DC-10 rudders have accumulated more than 192,000 flight hours in service with six airlines since 1976. The high-time rudder has accumulated more than 22,000 flight hours. The Lockheed L-1011 composite aileron received FAA certification in September 1981, and four shipsets have accumulated more than 3600 flight hours with two airlines since entering service in early 1982. The first FAA certification of composite primary structure for commercial transport aircraft was issued August 23, 1982, for the Boeing 737 composite horizontal stabilizer. Boeing plans to install five shipsets on aircraft in production prior to delivery to airlines in 1983. Approximately 3300 lb of composite components on the new 757 and 767 aircraft use technology developed through the NASA ACEE secondary-component programs.

Douglas Aircraft Company has improved the design of the DC-10 composite vertical stabilizer after a premature failure during ground tests. It was determined that an unexpected load concentration occurred at a cut-out for an

ORIGINAL PAGE IS
OF POOR QUALITY

access hole in the rear spar web of the stabilizer. A second, structurally modified stabilizer will be ground tested during 1983 to meet FAA certification requirements and to evaluate ultimate load, fatigue lifetime, and damage tolerance capability. Flight check-out will occur in 1984.

The L-1011 composite fin was tested to 120 percent of design ultimate load during test-to-failure following an extensive ground test on static and fatigue loading. Cover and spar segments for the composite fin have successfully completed 14 years of a planned 20-year simulated service life exposure to flight conditions, including cyclic loads, moisture, and temperature.

Herman L. Bohon, 3081 534-03-13

DC-10 vertical stabilizer.

MLS Curved-Path Autoland Control Laws

The new Microwave Landing System (MLS) will provide extended approach and landing control in the terminal area. The extended volumetric coverage and high accuracy of the MLS allow precision aircraft guidance on curved approach paths for noise abatement and obstacle clearance. Approaches from a wide range of initial headings and with shorter finals will also provide new capabilities for more efficient air traffic control, thereby reducing terminal area congestion and improving safety. The Boeing Commercial Airplane Company, under contract with Langley Research Center, has developed and verified, in noise- and error-free simulation, new flexible MLS guidance and control algorithms that have the capability of capturing the extended runway centerline from a wide range of initial approach intercept angles and positions without the need to manually program the approach path, enter MLS/runway data, or execute complex navigation/guidance computations. The algorithms include automatic approach path definition to allow automatic landing approach control with last-minute path changes by ATC. The algorithms developed include (1) a simple wide-angle localizer capture law that computes steering commands directly from MLS azimuth with or without distance measuring equipment (DME) using azimuth and azimuth rate in place of DME range, and (2) a localizer capture law that automatically defines and flies a logical path to the localizer centerline from virtually any engage point within the MLS azimuth coverage. These control laws eliminate the undesirable transient maneuvers caused by switching from area navigation to more accurate MLS guidance.

Richard M. Hueschen, 3635 534-04-13

MLS Service Test and Evaluation Program

The Langley Visual Motion Simulator (VMS) and the Advanced Transport Operating Systems (ATOPS) Boeing 737 research airplane have been modified to provide the capability of flying curved-path approaches using conventional flight director cockpit instruments and controls. This was done as a part of the FAA's Service Test and Evaluation Program (STEP) for the new Microwave Landing System (MLS). Modified flight director algorithms provide commands for complete three-dimensional area navigation, including descending turns of up to 180°. In addition to the standard flight director cockpit displays, there are annunciators for the new modes and a digital display on which the pilot can select either distance along path to touchdown, height above touchdown, or ground speed as computed from MLS data.

NASA and FAA test pilots participated in evaluation and modification of the system both in the VMS and in flight. In addition, these pilots flew numerous simulator approaches to aid in selection of candidate curved-path approaches for the data collection phase of the

ORIGINAL PAGE IS
OF POOR QUALITY

program, which will be flown at Wallops Flight Center. The suitability of the final path selections was subsequently verified by 737 flight tests. The VMS was also used to train several airline pilots in procedures for flying curved approaches. These pilots will aid in compiling a statistical data base that will be used by the FAA for setting obstacle clearance criteria and designing MLS approaches and missed approaches at different airports. At the conclusion of the program these pilots will have flown at least 42 approaches, six each on seven variations of the four basic types shown in the figure.

William F. White, 2541 534-04-13

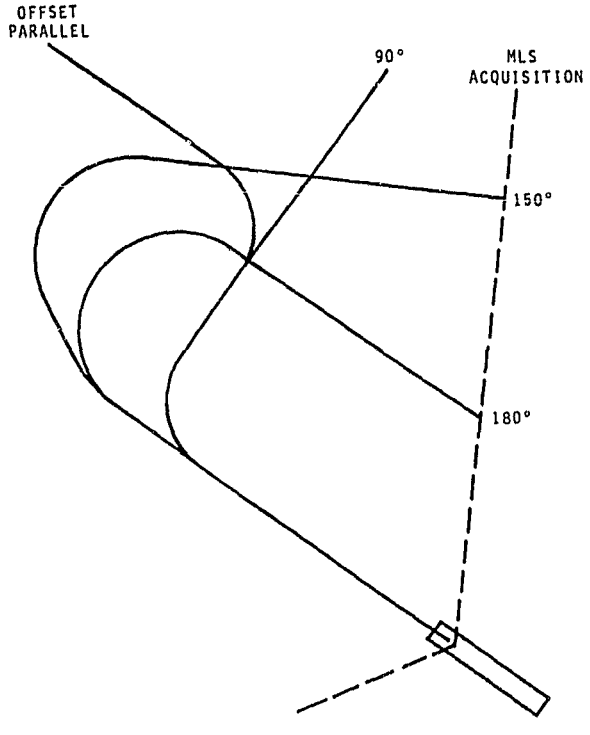

MLS complex approach test profiles.

Coordinated Elevator and Thrust Control

Autopilot design has classically evolved by adding new control laws for each new function, which results in performance compromises and a high level of complexity. In the longitudinal axis the lack of elevator and throttle control coordination results in undesirable activity of these controls and in flight path/speed coupling errors. Other problems include inadequate stability in some portions of the flight envelope, command capture overshoot, and control transients when switching autopilot modes. The Boeing Commercial Airplane Company, under contract with Langley Research Center, has designed and verified, in piloted simulation, an integrated elevator/thrust control system called Total Energy Control System (TECS). The system provides coordinated control for all longitudinal modes of the autopilot/autothrottle and the flight management system using a common generalized flight path and speed control algorithm. The system design philosophy uses thrust to control the total energy of the aircraft and elevators to control the distribution of that energy between flight path and speed objectives. TECS provides full-time thrust and elevator coordination to eliminate speed deviations caused by flight path maneuvering and flight path deviations caused by speed changes. This coordination also eliminates capture overshoots and mode-switching transients. Further, the integrated approach simplifies both the hardware and software requirements over a conventional flight control system. TECS is expected to result in large savings for future airplanes in the areas of engineering development, flight tests and certification, hardware and software acquisition costs, improved performance, and reduced maintenance requirements.

Richard M. Hueschen, 3635 534-04-13

Wind Turbulence Models for Piloted Simulation

Application of ground-based simulation of piloted aircraft flight has increased dramatically in recent years because of the availability of more sophisticated simulation capabilities, widening requirements for handling and ride quality research, and the increased costs associated with flight testing. One important aspect of ground-based flight simulation is the introduction of disturbances representing atmospheric turbulence, which has been shown to significantly affect the results of handling and ride quality studies, pilot work load investigations, and achieved pilot performance results. The Douglas Aircraft Company, under contract to Langley's Advanced Transport

ORIGINAL PAGE IS
OF POOR QUALITY

Operating Systems (ATOPS) Program Office, has performed a study to evaluate state-of-the-art turbulent-gust-modeling techniques used in flight simulations of large transport aircraft, with the eventual goal of identifying the most suitable turbulence model for motion-based simulation of transport aircraft.

As part of the study, a functioning computer code was produced for six prominent turbulence-generation models. A description of the formulation and implementation of each model was developed, along with example gust time histories, probability distributions, power density spectra, and tabulated statistical properties. Furthermore, each model was evaluated based on calculated statistical properties, which provided a direct comparison among the different models and with statistical properties of actual atmospheric turbulence. It was found that some models, as presently implemented, simulate noticeably lower turbulent energies than would be expected from previous research findings.

Roland L. Bowles, 3917 534-04-13

Fuel-Efficient Descent Guidance for Today's Cockpit

The Federal Aviation Administration has developed an automated time-based metering form of air traffic control, called Local Flow Management/Profile Descent, which is designed to improve the efficiency of terminal area enroute operations. The concept is based upon delivering enroute traffic to a metering fix (typically 30 to 40 n. mi. from the airport) at a specified altitude, airspeed, and time such that the aircraft are properly sequenced and spaced for approach and landing. Flight tests have demonstrated that this task can be accomplished in an airplane with an integrated flight management system. However, in airplanes not so equipped, the pilot must rely on various "rules of thumb" to plan the descent. In an effort to provide the pilot with some open-loop time-constrained descent guidance, a fuel-conservative descent guidance algorithm was developed at Langley for hand-held calculator applications. The algorithm was implemented on a hand-held programmable calculator with certain key functions, as shown in the figure. This algorithm allows the pilot to fly an idle-thrust clean-configured (landing gear up, flaps and spoilers retracted) descent, arriving at the metering fix at the prespecified conditions. The calculator algorithm is currently being tested to determine its accuracy and feasibility in an airline operational environment.

Dan D. Vicroy, 3621 534-04-13

Hand-held descent-planning calculator.

Evaluation of a Total-Energy Rate Sensor

A sensor has been developed that measures the rate of change of aircraft total energy with respect to the airstream. This device consists of a cylindrical probe containing a small orifice located on the downstream side of the cylinder,

ORIGINAL PAGE IS
OF POOR QUALITY

an in-line pneumatic-noise filter, and a pressure-sensing altitude-rate transducer that provides an electrical signal proportional to the time rate of change in pressure. The pressure measurement is a function of both static pressure and dynamic pressure and has been shown to be a measure of total energy (potential plus kinetic).

Initial aircraft tests were made on a de Havilland DHC-6 Twin Otter. For the boom-mounted configuration excellent time history comparisons were obtained between calculated and measured values of specific total energy rate.

The Twin Otter flights demonstrated the sensor measuring capability with the probe located in the free airstream. Recently a flight evaluation was made with the probes located on the fuselage of a Boeing 737. For this evaluation two probes were mounted on opposite sides of the airplane and the outputs were combined to make one measurement. Comparisons between sensor-measured specific total energy rate and calculated values under conditions of several aircraft maneuvers showed sufficiently good results to warrant application studies. These tests confirmed that the sensor responds to energy changes due to wind shear, and thus has application in automatic control systems designed to alleviate adverse effects of wind shear. A time history comparison between measured and calculated data for a landing (plotted as a specific total energy rate $\dot{H}$) is shown in the figure.

Aaron J. Ostroff, 3209 534-04-13

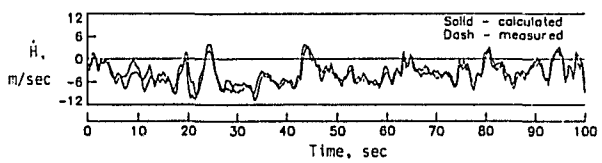

Time history of specific total energy rate.

Pilot Modeling Promises Savings in R&D Dollars

For the past few decades LaRC and similar research institutions in the U.S. have engaged in research to acquire an understanding of the principles and strategies by which a pilot controls an airplane and to apply this knowledge to improving design of displays and control systems. Recent efforts at LaRC have turned to integrating knowledge already acquired into a computerized model of piloting behavior. The goal of the development is to construct a research tool that will generate predictive data describing pilot performance and behavior in new or untested systems in such a manner that they would be virtually indistinguishable from data obtained in hardware-type simulator and flight research. Unlike much of the pilot modeling work to date, this work requires that the model be able to mimic the actual behavioral and thought processes of a pilot. The model includes representations of the pilot's eyes, hands, and feet and aspects of his thought processes. As a minimum, the model will store previous research results and eliminate much of the need for running standard conditions in piloted simulator and flight testing, thus reducing the cost of obtaining valid research results.

The model is currently being applied to NASA's Advanced Transport Operating Systems (Boeing 737) approach and landing operations and has mimicked pilot scanning behavior in acquiring information from the instrument panel, pilot evaluation and use of that information to make decisions related to control of the airplane, and the resulting control activities. Analysis of model results and comparisons to simulator data indicate that it does provide a realistic representation of pilot behavior and has the ability to provide useful measures of pilot workload and changes in piloting behavior due to system changes.

Marvin C. Waller, 3917 534-04-13

Structure-Borne Noise in Advanced Turboprop Aircraft

Passenger acceptance of new aircraft, especially the planned advanced high-speed turboprop, is highly dependent on the capability to predict and control interior noise levels. To date, the airborne component of this noise has been most extensively studied. There are indications, however, that structure-borne noise could also be of importance. An extensive interior noise measurement program has been conducted on a de Haviland DHC-6 Twin Otter

ORIGINAL PAGE IS
OF POOR QUALITY

airplane to develop improved methodologies for quantifying airborne and structure-borne interior noise components.

The test program consisted of a sequence of exterior noise measurements (engine mount, wing, and panel vibration) and interior noise measurements in the forward, aft, and passenger compartments during engine ground runup at different power levels. For each step in the sequence, additional layers of sound insulation (foam with lead septum) were applied to the fuselage, bulkheads, and finally to the wing surface to reduce the airborne components of the noise and hence uncover the structure-borne noise components. The most extensive treatment is indicated in the photograph. In addition to engine runup tests, acoustic and vibration data were obtained for a pure acoustic (loudspeaker) source and a pure vibratory (shaker) source. Measurements were also obtained using advanced techniques and a noise source separation device recently developed at Langley. Results have indicated that structure-borne noise is a very important component of the interior noise level of propeller aircraft, particularly at low frequencies, and should be considered in the design of future propeller aircraft.

William H. Mayes, 3561 535-03-13

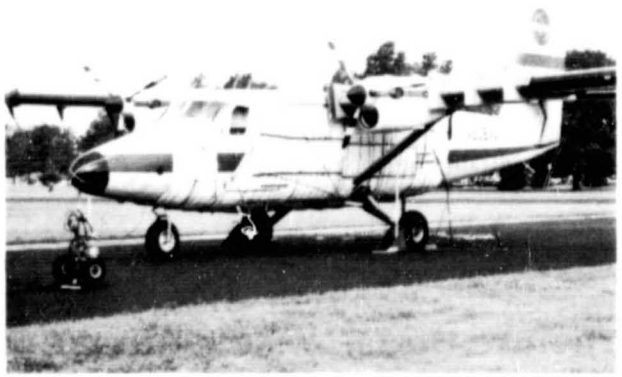

Twin Otter interior noise tests.

A Relational Information System

A core system has been developed at Langley for the evolution of a number of computer-aided design applications. One of the main challenges in computer-aided design systems is the efficient handling of many different types and formats of data that must be communicated between many computer programs and engineers. Past approaches have been to develop a single-purpose information system. For the present computer-aided design application, this single-purpose approach lacks adaptability to present data communication needs and future data management requirements.

Based on the evaluation of current data management systems, a relational information system called ARIS was developed. It uses state-of-the-art internal data structuring for quick segmental and random data access. The external architecture was designed specifically as an integration system for independent computer programs that comprise a computer-aided design system.

Although ARIS is not yet fully operational on the Aerospace Vehicle Interactive Design (AVID) system for which it was developed, it is being used in other areas. It is currently being

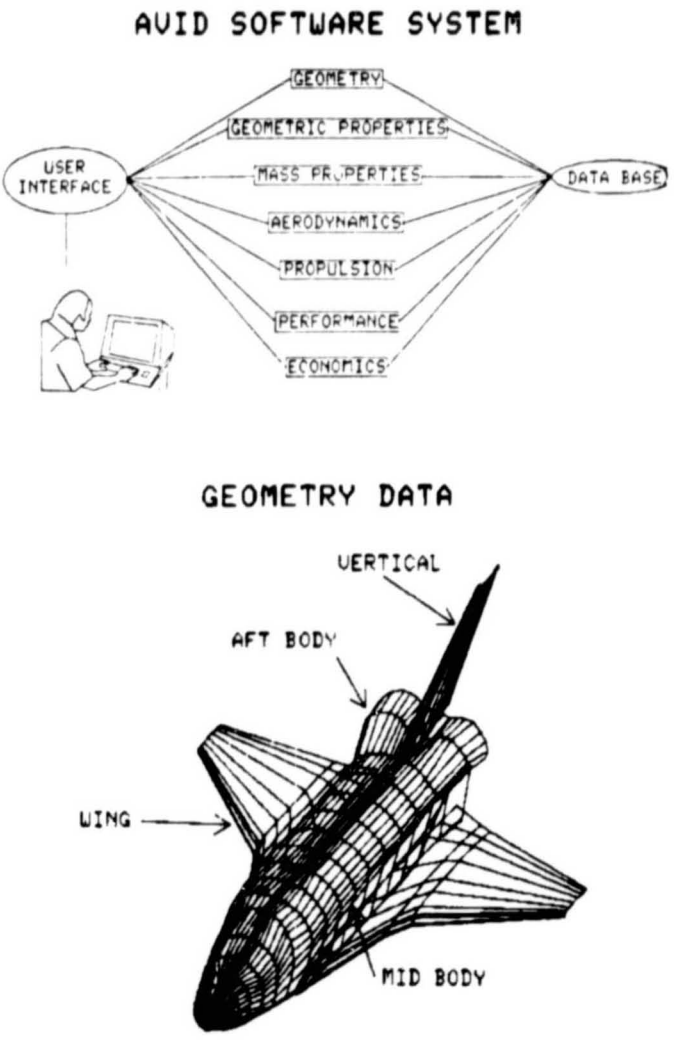

Some present ARIS applications.

ORIGINAL PAGE IS
OF POOR QUALITY

used for data creation, manipulation, and retrieval; for analysis of current and projected payload missions for the Space Shuttle; and as a data base of aerospace vehicle component masses for developing mass estimation techniques.

Alan W. Wilhite, 3911 506-51-13

Application of a Tip Fin Controller for Improved Yaw Control

One of the major development problems in controlling the Space Shuttle Orbiter was to provide yaw control during entry while the Orbiter is transitioning from a high-angle-of-attack low-dynamic-pressure regime to a low-angle-of-attack high-dynamic-pressure regime (Mach 15 to 1.5). Since for most of this time the rudder is ineffective, aerodynamic yaw control is provided by the aileron with additional yaw control provided by the yaw reaction control system (RCS). This method of control causes concern because: (1) the aileron yaw characteristics are very dependent upon elevator position; (2) there are uncertainties in extrapolating the aileron characteristics determined in wind tunnel tests to flight conditions; and (3) the RCS must be designed to operate under high-dynamic-pressure conditions. In response to these concerns, a configuration modification has been developed at Langley that would add small wing tip fin controllers and remove the vertical tail. Wind tunnel data on this configuration from Mach 0.3 to 4.63 show that the tip fin controller is a very effective yaw control device with essentially no roll interaction in the supersonic flight regime. In addition, a six-degree-of-freedom analysis shows that the reaction control system could be deactivated much sooner than is currently possible.

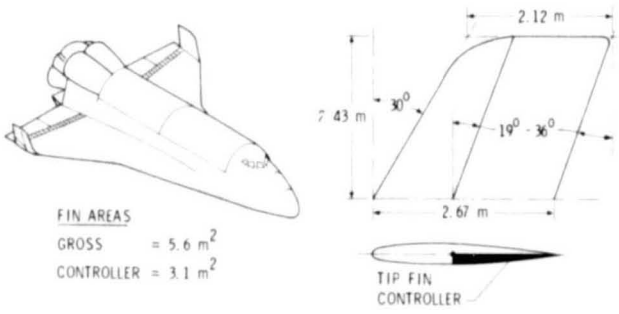

Shuttle tip-fin-controlled configuration.

Richard W. Powell, 3911 506-51-13

Leeward Flow Characteristics on Aeromaneuver Vehicles

Measurements on spherically blunted, $13^{o}/7^{o}$ on-axis, and bent (nose bent upwards 7^{o}) biconics at Mach 6 and 10 in air have illustrated the complexity of the leeward flow on these simple-appearing configurations at large angles of attack. Several interesting flow characteristics occur when the angle of attack exceeds the fore-cone half-angle. One is an embedded shock within the shock layer on the leeward side. This shock originates just downstream of the sphere-cone junction and is attributed to the flow expanding around the spherical nose to a supersonic condition and recompressing because of the cone section. Another is the formation of counter rotating longitudinal vortices due to flow separation. These vortices also originate just downstream of the sphere-cone junction and their attachment

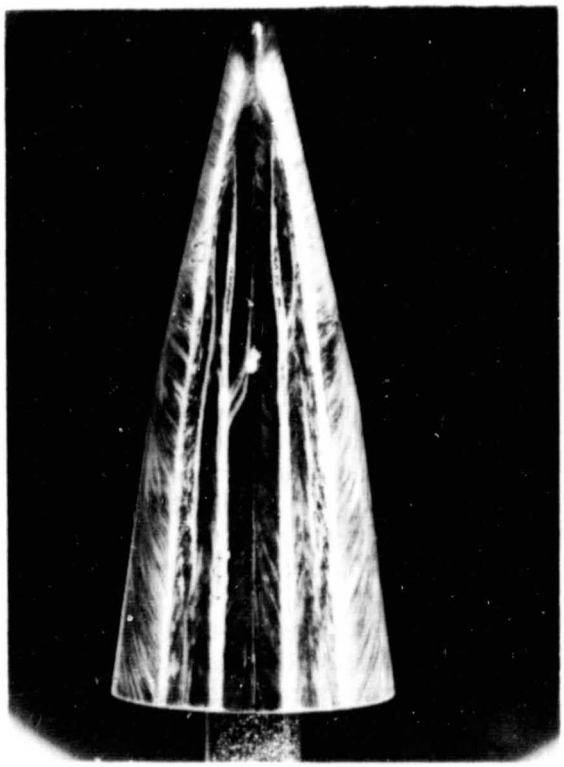

Biconics flow characteristics.

ORIGINAL PAGE IS
OF POOR QUALITY

line falls on the most leeward ray of the biconics. Secondary separation and attachment lines occur, as observed form oil flow patterns, implying that the primary vortex sheet splits with part of it rolling up into one or more secondary vortices. Force and moment tests imply that these vortices are symmetrical for angles of attack up to 20°, but that they become asymmetric at higher angles of attack, thereby resulting in side forces. The complex, viscous-dominated leeward flow region has been successfully modeled using a steady three-dimensional viscous-flow-field code that solves the parabolized Navier-Stokes equations for angles of attack up to 20°.

Charles G. Miller, 3031 506-51-23

Shuttle Flight Heating Analysis With Surface Catalytic Efficiency

The technology base for future aerospace vehicle design can be augmented by analyzing the Shuttle flight data with the existing ground test data base and computational techniques. One area of interest is the reduction of nonequilibrium heating over the Shuttle's lower surface by using a glassy tile coating called RCG (reaction-cured glass). The RCG coating and similar types of materials have exhibited reasonably low but scattered values of catalytic recombination rates for atomic oxygen and nitrogen from ground-based experiments at the Shuttle operational wall temperatures. Carefully chosen catalytic recombination rates are used in the computational analysis of the flight heating data. A nonequilibrium two-dimensional viscous-shock-layer code, which contains five air species and six reactions, has been modified to include finite catalytic recombination rates in the boundary condition. The convective laminar heating on the Shuttle windward centerline is calculated using the "equivalent axisymmetric body" concept for several STS-2 flight conditions ranging from 92 to 48 km in altitude (or from 200 to 1215 sec in entry time).

The results indicate an overall agreement with the flight heating data along the Shuttle length when appropriately chosen catalytic recombination rates for oxygen ($k_{w,0}$ = 100 to 200 cm/sec) are used. Comparison at a body location of x/L = 0.025 (near the nose) is shown for the altitude range considered. Also shown is the calculated result assuming the equilibrium condition. The difference between the equilibrium and nonequilibrium result demonstrates the significant heating reduction realized.

Judy L. Shinn, 3786 506-51-33

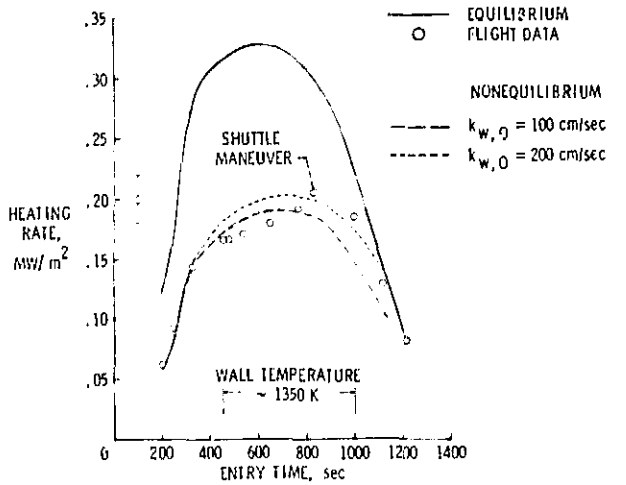

Shuttle heating rate time history.

Shuttle Reaction Control System Evaluation

An evaluation of the Space Transportation System (STS) Reaction Control System (RCS) effectiveness was made using flight measurement data from STS 1, 2, and 3. The evaluation made use of statistical estimation methods to determine the STS vehicle response to a known RCS input. The effectiveness is the ratio of the response to the input.

The Shuttle RCS system consists of yaw jets for lateral control and pitch jets for longitudinal control. The yaw jets were analyzed over the speed range from Mach 2 to Mach 26. They were found to be approximately 100 percent effective in terms of side force produced and from 85 to 90 percent effective in terms of the yawing moment produced. However, the rolling moment effectiveness varied significantly over the speed range and differed significantly from preflight aerodynamic data book predictions. An alternative and independent method involving the integration of upper-wing-surface pressure measurements (illustrated in the figure) was

ORIGINAL PAGE IS
OF POOR QUALITY

devised to verify these differences. Preliminary results indicate that this method is indeed a viable way of computing rolling moment effectiveness.

The RCS pitch jets were analyzed only in the vicinity of Mach 26. This was due to the limited number of jet firings available for analysis. Pitch jet firings are restricted to the high-altitude regions and are turned off at Mach 26, the region in which useable flight data becomes available. The pitch jet effectiveness at Mach 26 was significantly different from preflight predictions. It was found that up-firing jets were 15 percent more effective than down-firing jets.

Harold R. Compton, 3984 506-51-33

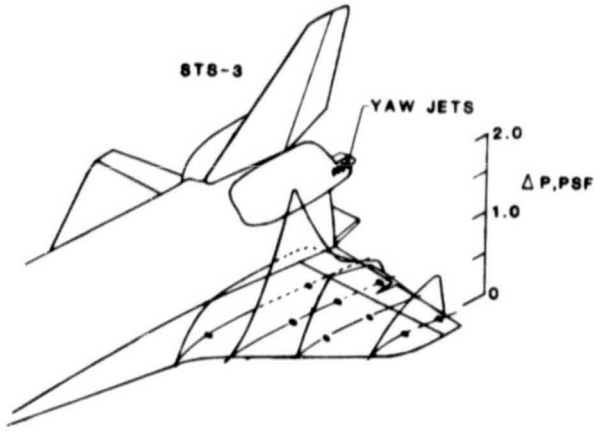

Schematic of RCS-induced pressure gradients on leeward surface of Shuttle wing.

Effect of Microcracks on the Thermal Expansion of Graphite/Epoxy

Microcracks in resin/matrix composites are small fractures in the matrix material that extend parallel to the fiber direction. They occur when the internal stresses exceed the transverse strength of an individual lamina. The two primary causes of microcracks are mechanical loading and thermal cycling. Permanent changes in the thermal expansion and/or permanent residual strains can result from this type of damage. These changes in material behavior may be critical for structures requiring a high degree of dimensional stability.

An experimental and analytical investigation is being conducted to quantitatively correlate the change in the coefficient of thermal expansion (CTE) with microcrack density. As a first effort, specimens from two quasi-isotropic graphite/epoxy laminate configurations were mechanically loaded to produce varying amounts of microcracking in plies perpendicular to the load direction. The amount of microcracking was characterized by computing an average crack density in the damaged plies. The average CTE over the temperature range 25°C to 150°C was then measured using a moiré interferometry technique. A finite-element analysis was also developed to predict the effect of microcracks on the CTE. Results showed that microcracks reduce the CTE, and the amount of reduction is a function of both the microcrack density and the laminate stacking sequence. The analytical predictions were verified by experimental data.

David E. Bowles, 2143 506-53-23

Large-Area Repair of Graphite/Polyimide Composites

The capability to repair large areas of graphite/polyimide (Gr/PI) structures was recently developed at Langley. Previously, repair of Gr/PI structures using adhesive bonding processes had been limited to small areas due to entrapment of gases in the bondline. A technique was developed for replacing damaged plies of Gr/PI with Gr/PI prepreg and curing in place using standard cure parameters. NDE (nondestructive evaluation) C-scan photographs and photomicrographs of the bondline are shown for a 10- by 10-in. Gr/PI panel fabricated with the cure-in-place technique, an adhesively bonded panel, and a 20-ply control panel. Ten plies of prepreg were cured onto a 10-ply precured panel to fabricate the cure-in-place panel. Two 10-ply precured panels were bonded together using a PI adhesive to fabricate the adhesively bonded panel. Twenty plies of prepreg were laid up and cured to fabricate the control panel. The C-scans shown were obtained using the same transducer and sensitivity setting on the ultrasonic equipment. Dark areas indicate porosity or debonds. The dark areas indicated at the thermocouple locations are expected and are due to surface irregularities that result from the thermocouple being placed at the edge of the panel. However,

ORIGINAL PAGE IS
OF POOR QUALITY
ORIGINAL PAGE IS
OF POOR QUALITY

the dark areas in the adhesively bonded panel are due to voids caused by entrapment of gases in the bondline, as evidenced by the photomicrographs.

Mechanical property results were obtained from short-beam-shear and flexure specimens machined from cure-in-place and control panels. Tests were conducted at -250°F, room temperature, 400°F, 500°F, and 600°F. The data indicated that the strengths of the cure-in-place panels equalled or exceeded the control panel strengths throughout the temperature range. Rockwell International is applying the cure-in-place technique to repair damaged laminates, skin-stringer panels, and honeycomb core panel specimens.

Jerry W. Deaton, 2848 506-53-23

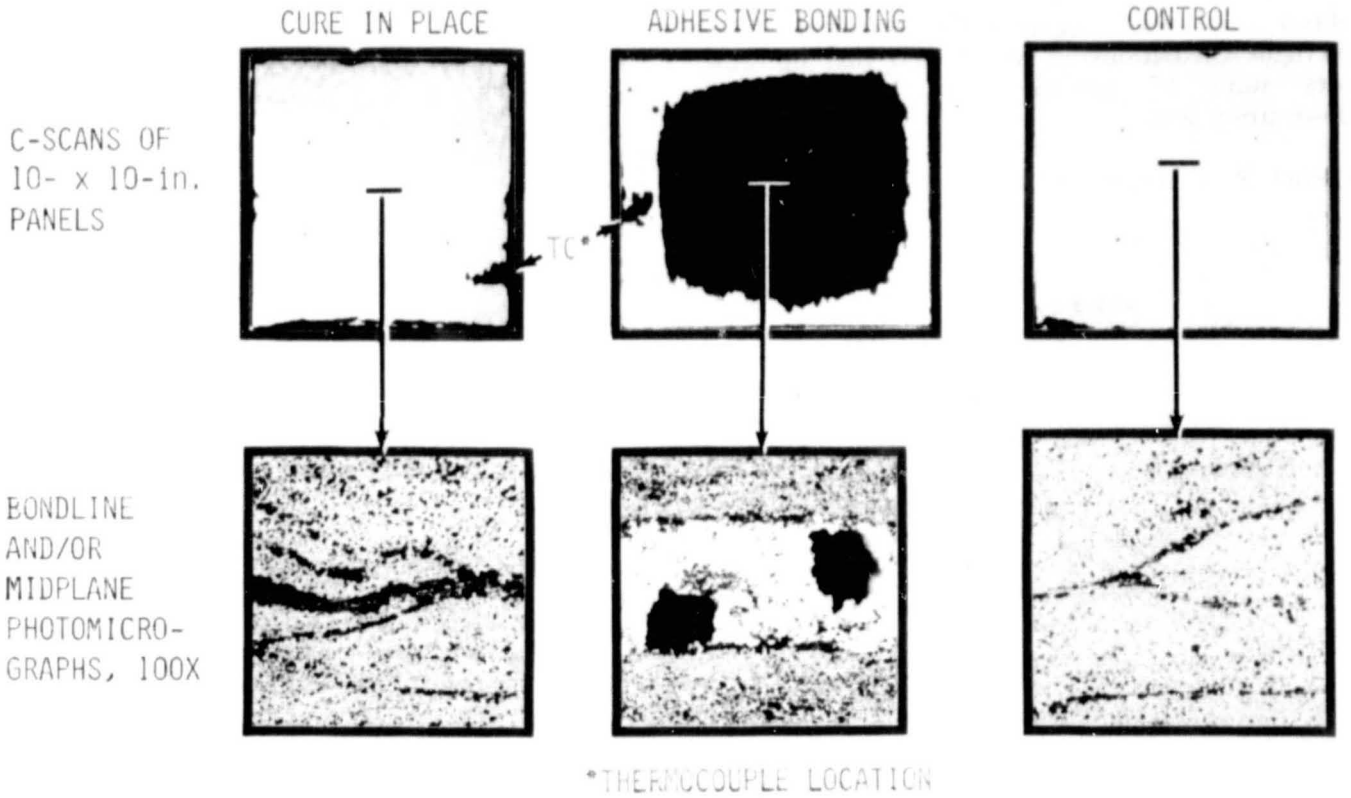

Large-area repair of graphite/polyimide.

Advanced Insulation/Structural Concept for Shuttle Orbiter

The high-energy noise field outside the Langley 8-Foot High-Temperature Structures Tunnel is similar in frequency content and intensity to that surrounding the Space Shuttle during ascent, and it has therefore been useful in acoustic testing of an advanced insulation/structural concept for the Shuttle. The concept is a product of the Composites for Advanced Space Transportation Systems (CASTS) Program, which has shown that significant reductions in mass can be realized by using high-temperature graphite/polyimide composite structure that is bonded directly to the ceramic reusable surface insulation (RSI) without a strain isolation pad. The 20- x 40-in. test panel, which is representative of a section of the Shuttle body flap, has been positioned near the exit of the wind tunnel, where it is exposed to an overall sound pressure level of approximately 154 dB each time the tunnel is operated.

To date the panel has been exposed to 38 minutes of tunnel noise at an overall sound pressure level (OASPL) of approximately 154 dB (which simulates the total aerodynamic acoustic load for 100 Shuttle missions) and an

ORIGINAL PAGE IS
OF POOR QUALITY

additional 3 minutes at 161 dB OASPL, with no evidence of structural degredation. The panel response peaks at approximately 260 and 470 Hz, which corresponds favorably with the predicted fundamental frequency of 297 Hz, producing acceleration forces of approximately 100 g's near the center of the panel. Recently the panel was repositioned to increase the noise exposure to 161 dB OASPL to simulate the higher decibel levels experienced during liftoff. Ultimately the panel will be repositioned to increase the intensity to 165 dB OASPL, which corresponds to the design level.

Richard W. Tyson, 3158 506-53-33

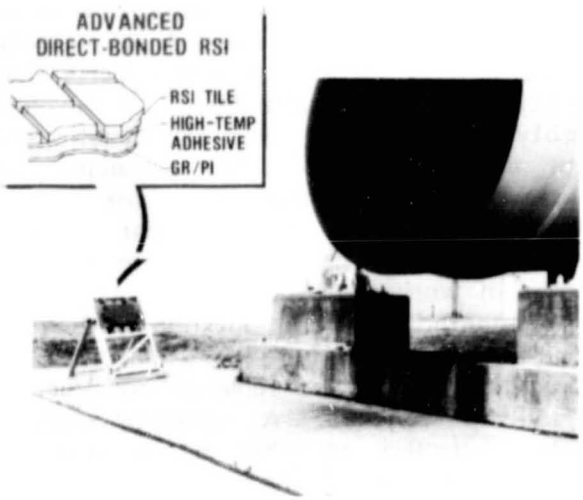

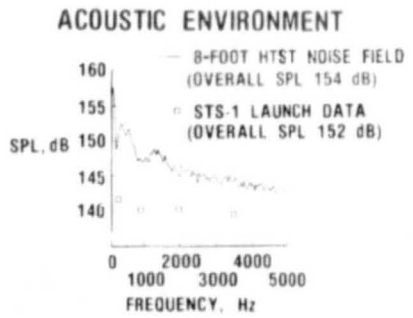

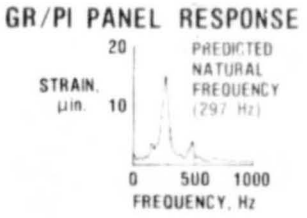

Graphite/polyimide panel survives simulated Shuttle ascent acoustics.

Random Dynamic Tests of Undensified Reusable Surface Insulation Shuttle Tiles

A test program to validate the adequacy of undensified tiles in the Orbiter wing and midfuselage region under random dynamic ascent loads was completed at Langley. The tests were conducted on thermal protection system laboratory specimens that passed the proof test and thus would have remained undensified on the vehicle. The tests were performed to insure the integrity of undensified thermal protection system tiles remaining in the wing and midfuselage region prior to the first flight. The complex program simulated substructure deformation loads, steady tensile and moment loads typical of aerogradient conditions, and random dynamic substructure motions for two load conditions during ascent, shock ahead of the tile and shock on the tile.

A total of 17 specimens were tested. All specimens survived an equivalent of 72 ascent missions and exhibited residual static strength greater than their original proof loads. These results indicate that the undensified tiles had sufficient strength to withstand ascent loads during the first flight and were used by NASA as a part of the certification of the thermal protection system.

Paul A. Cooper, 3787 506-53-33

ITD Method Surpasses FFT for Free-Response Data Analysis

For experimental modal identification, classical analog sine testing procedures are being replaced by digital processing techniques that show considerable speed and accuracy advantages. These digital techniques all strive to correctly decompose measured dynamic responses into the individual contributions of many structural modes of vibration that are excited simultaneously.

In most of these techniques the fast Fourier transform (FFT) is used to estimate the frequency spectrum of each response. Although the FFT can be computed rapidly and produces results that are sufficiently accurate in many cases, two inherent characteristics of the

ORIGINAL PAGE IS
OF POOR QUALITY

procedure limit the performance that can be achieved. The first is the inability to resolve frequency components spaced in hertz closer than the reciprocal of the available data length in seconds. The other is a distortion known as "leakage" that results from the mathematical effects of limiting data records to a finite time interval. Although the leakage effects can be attenuated using "windows" that taper the data within the record, a penalty of reduced resolution is always incurred. These two limitations of the FFT are particularly significant when short data records, such as structural transient responses, are analyzed.

A modal identification algorithm for free-response data analysis, the Ibrahim time domain (ITD) method (developed jointly by Langley and Old Dominion University), completely avoids use of the FFT. A comparison of FFT spectra with typical ITD results for a 3-mode simulation is shown. The unwindowed result, approach #1, shows the best FFT resolution possible with 1 second of data (1 Hz) and illustrates that low-amplitude modes (e.g., 25 Hz) become masked by the leakage effects of high-amplitude modes. The exponentially windowed FFT result, approach #2, shows that the leakage oscillations can be eliminated, but with considerably reduced resolution. Using the ITD algorithm, on the other hand, modal parameters (natural frequencies, damping factors, and mode shapes) are identified directly from the time domain data. The spectrum constructed using the ITD-identified parameters for this example, shown as approach #3, is indistinguishable from the true spectrum.

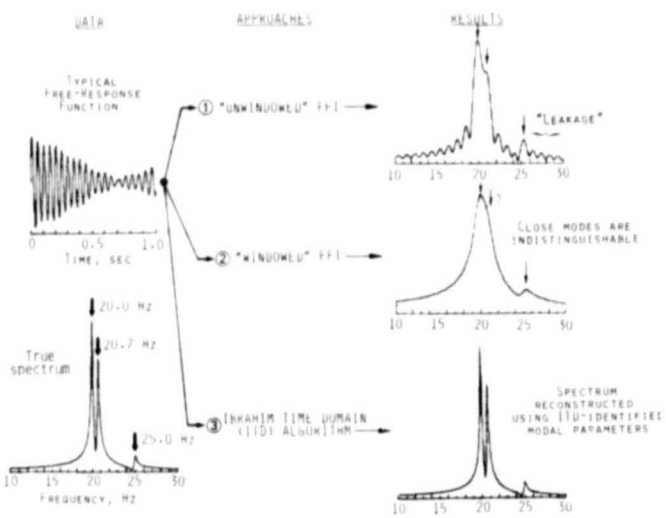

Comparison of FFT and ITD results for typical free response.

Richard S. Pappa, 3196 506-53-43

Astronaut/Mobile Work Station Space Construction Experiment

The establishment of a permanent United States manned space station and other large space structures requires the development of novel on-orbit construction methods. The Langley Research Center has devised, developed, and demonstrated in a simulated zero-gravity environment a mobile work station concept that enhances astronaut capabilities for manual assembly of erectabie truss structure. The concept uses an assembly line technique for rapid assembly of the truss components by two astronauts in an EVA (extravehicular activity) mode of operation. The astronauts are attached to a pair of work platforms that can be moved to an appropriate work location within a bounded work area. The work platforms are also used to transport and replenish construction material as required. A conveyor-equipped remotely controlled assembly jig is used to support the structure being assembled and to clear the work area as segments of the truss are completed. The method permits the assembly of a continuous beam of any practical length and can also be adapted to area-type structures such as platforms. The concept permits the use of doubly tapered, tubular struts that can be nested one inside the other like ice cream cones

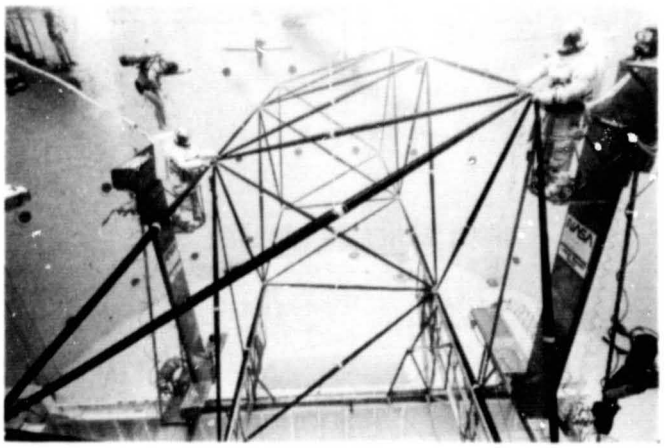

Simulated zero-gravity test of mobile work station concept.

ORIGINAL PAGE IS
OF POOR QUALITY

for compact packaging, thus enabling efficient transportation of material to orbit in the Space Shuttle.

Simulated zero-gravity (neutral buoyancy in water) assembly tests were conducted in which a 38-strut tetrahedral truss beam was assembled by two space-suited test subjects. The truss was assembled in approximately 33-1/2 minutes. This result, when adjusted to remove the effects of water drag, yields an average assembly rate for space assembly of approximately 38 seconds per strut for a structure of comparable size.

Walter L. Heard, Jr., 2608 506-53-43

Improved Solution Method for Transient Thermal Analysis

A research program has achieved a significant reduction in the effort required to predict transient temperature fields in high-speed vehicle structures typified by the Shuttle Orbiter. A set of implicit algorithms denoted GEARIB, developed at the University of Illinois, has been installed in the SPAR finite-element thermal-analysis program. The desirable features of the GEARIB techniques are the ability to utilize large time steps and to adaptively vary the step size throughout the temperature history. This is in contrast to older methods that utilize fixed (and often small) time steps.

An activity involving Shuttle thermal modeling provided a demonstration of the GEARIB techniques. Analyses were performed to trace the 3500-sec temperature history in a section of the Orbiter wing. Two models were considered: a two-dimensional section through the wing depth and a one-dimensional plug through the center of the 2-D model. Calculations for each model were carried out using two state-of-the-art integration methods, explicit Euler and implicit backward differences, as well as GEARIB. The explicit algorithm is burdened by the need to take small time steps (i.e., 0.1 sec) to avoid numerical instability. The implicit backward differences algorithm is typical of its class in that larger but fixed time steps are utilized. The fixed step size is input by the user, and the 1.0-sec step was determined by accuracy considerations.

By adaptively changing its time step to as much as 218 seconds, the GEARIB algorithms obtained solutions with significantly less computer time than was required by the two other methods. The use of GEARIB significantly enhances the ability of thermal analysts to compute temperatures in detailed mathematical models of complex airframe and spacecraft structures.

Howard M. Adelman, 3451 506-53-53

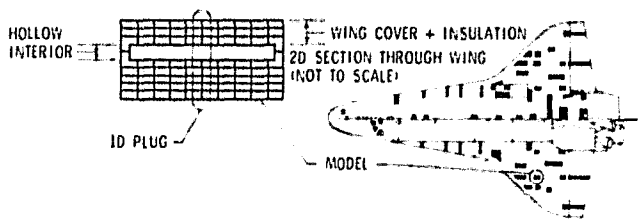

SOLUTION TIMES* FOR 3500-s TEMPERATURE HISTORY

MODEL	1D PLUG		2D SECTION	
METHOD	TIME STEP	SOLUTION TIME	TIME STEP	SOLUTION TIME
EULER-EXPLICIT	0.1	1723	0.1	3205
BACKWARD DIFFERENCES-IMPLICIT FIXED TIME STEP	1.0	256	1.0	1145
GEARIB-IMPLICIT VARIABLE TIME STEP	0.85-218	63	0.1-225	245

*ALL TIMES IN SECONDS

Transient thermal analysis time reduced by improved solution method.

Cove Heating Characteristics for Separated Flow on Wing

The pressure differential across a wing provides the mechanism by which hot gases from the windward wing surface can be ingested through the wing-elevon juncture past seals to the unprotected internal structure. Experimental investigations in the Langley 8-Foot High Temperature Structures Tunnel have identified some characteristics of the wing-elevon cove aerothermal environment. Results indicate that the level of heating within the cove is dependent upon flow conditions on the wing at the cove entrance, as shown in the figure.

In these plots the heating rates are normalized to the laminar attached flow value at the cove entrance ($\dot{q}/\dot{q}_{REF}$). When laminar-flow separation occurs near the cove entrance, wing heating rates (open symbols) under the separated boundary layer decrease sharply from equivalent attached-flow values, and cove heating rates (filled symbols) diminish from the cove entrance by an order of magnitude. Increasing the elevon deflection angle

ORIGINAL PAGE IS
OF POOR QUALITY

extends the length of flow separation, and, as shown by the rising wing heating rates, the separated laminar boundary layer transitions to turbulent flow ahead of the cove entrance. Consequently, cove heating rates are an order of magnitude greater than for purely laminar flow separation at the same cove seal leak gap. However, if the leak gap increases sufficiently for the same elevon deflection, boundary layer suction can force the separated boundary layer to reattach, in which event cove heating rates approximate the level of heating for laminar-flow separation. As indicated, the agreement between test data and calculated values is good. These results give credence to the analytical techniques for predicting structural heating and also suggest that a hot structure that provides for through flow is a viable concept.

William D. Deveikis, 2325 506-53-63

TEST APPARATUS IN 8-ft HTST

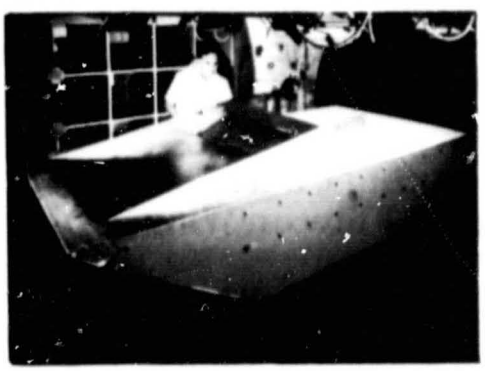

CROSS SECTION

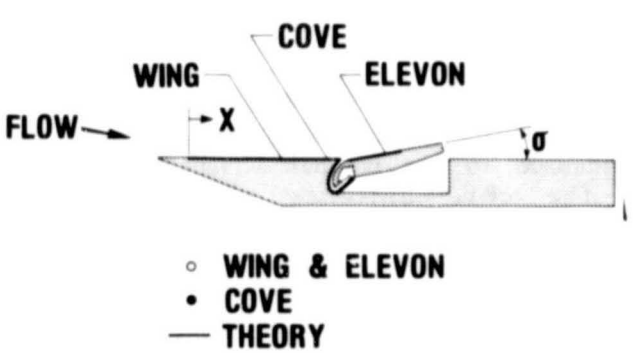

LAMINAR SEPARATED

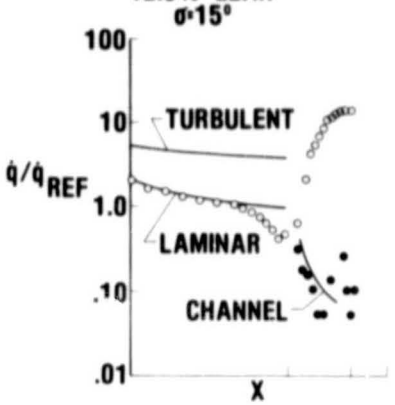

LAMINAR SEPARATED WITH TRANSITION

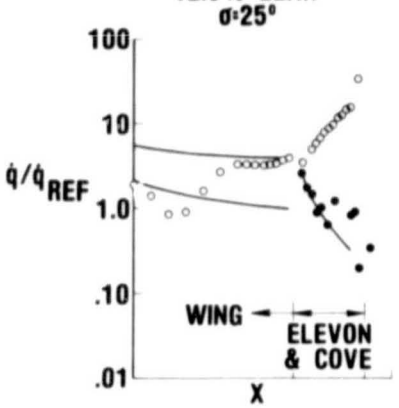

LAMINAR ATTACHED

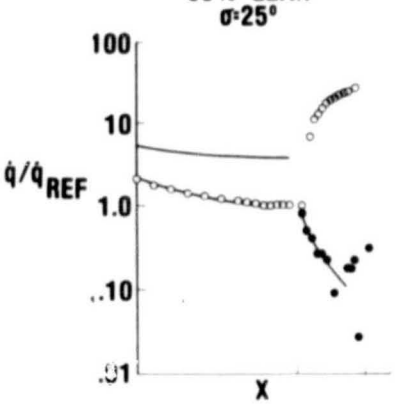

Heating characteristics of unsealed wing-elevon cove at M = 6.8 for separated flow on wing.

ORIGINAL PAGE IS
OF POOR QUALITY

Fiber Optic Wavelength Division Multiplexing Demonstrated

Wavelength division multiplexing (WDM), the concept of putting more than one wavelength into a fiber optics system, has recently been demonstrated as a potential space station expandable-data-bus concept. A system was designed, built, and demonstrated at Langley with single-mode AlGaAs semiconductor laser transmitters operating at 820, 830, 840, and 850 nm. The four wavelengths were optically multiplexed in a biconical tapered coupler and then separated in a four-channel interference filter optical demultiplexer, all designed and built at Langley. The figure illustrates the isolation of the four different laser spectra by the response of the interference filter demultiplexer. This first demonstration of a narrow 10-nm four-channel WDM system was very successful, with all four different wavelength channels running simultaneously at a digital data rate of 20 megabits and a bit error rate of less than 10^{-9}.

Herbert D. Hendricks, 3418 506-54-63

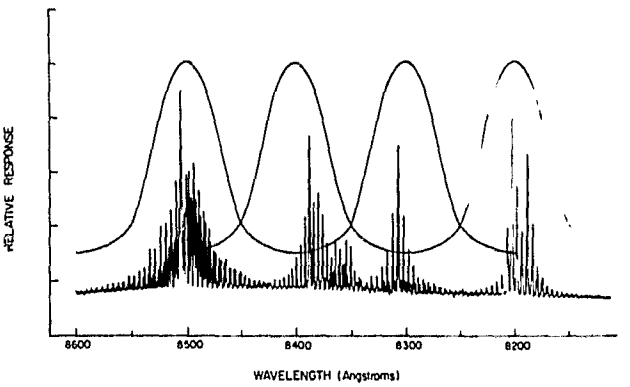

Semiconductor laser output spectra and interference filter response.

Decoupling Control Theory for Large Space-Based Antennas

A technique has been developed utilizing decoupling theory to control the rigid-body attitudes and the flexible-mode amplitudes of a large flexible antenna system. The technique provides a stable and robust control system that has been validated by computer simulations for a model of a 122-m-diameter hoop column antenna system. Decoupling theory permits control of one or more modes without affecting the other modes in the model. Procedures are applied utilizing various locations on the mast and hoop for control moment gyros and/or reaction control jets.

Results of the decoupling technique compare favorably with the standard linear quadratic regulator (LQR) optimal control method. Of the two methods, the LQR method is the more complicated because of the iterative process required to achieve desired performance. The decoupling method provides a simple closed-form solution and produces the exact closed-loop dynamics specified for the system. Procedures have also been developed for analyzing the effects of noise in the sensors and control actuators. Analysis shows that for nominal values of noise, the performance requirements for a geosynchronous Earth orbit mission are achievable.

H. A. Hamer, 4591 506-54-73

Thermodynamic Limits of Radiant-Energy Conversion

Langley Research Center, in conjunction with Christopher Newport College, has developed a theory for predicting the efficiency of the conversion of solar radiation by threshold devices directly into storable chemical or electrical energy for both space and terrestrial applications. Threshold devices encompass a wide range, including photovoltaic, biological photosynthetic, photochemical, and photoelectrochemical systems. All of these devices have in common two important features: (1) they produce storable energy; and (2) they have a characteristic energy absorption spectrum. An analysis based on the first and second laws of thermodynamics leads to a determination of the limiting or ultimate efficiency for any conversion system having a characteristic threshold energy and an operating temperature. The results of this analysis for the Sun as a source of radiation and for a series of receiver temperatures is shown in the figure.

The maximum efficiency for any threshold device is 44 percent; this requires a theoretical operating temperature of 0 K and a threshold energy of 1.1 eV. This threshold energy

ORIGINAL PAGE IS
OF POOR QUALITY

coincides with the energy bandgap for silicon. For comparison purposes, the limiting efficiency for a gallium-arsenide solar cell is 41 percent and for a cadmium-sulfide cell 22 percent at this same temperature. As the operating temperature of a threshold device increases, its limiting solar conversion efficiency decreases.

Although the efficiency curves specifically refer to the conversion of solar radiation, with a simple modification they can also be used to find the limits to the conversion efficiency for threshold devices and radiation from a blackbody at any temperature. In addition, they can be utilized to find the maximum conversion efficiency for devices that have both a threshold and a cut-off energy (i.e., an absorption band), which is often the case for photochemical reactions and solar-pumped lasers. This analysis furnishes the key to understanding energy conversion processes, and the results provide the basis for evaluating solar-energy conversion devices proposed for space and terrestrial applications.

Charles E. Byvik, 3781 506-55-13

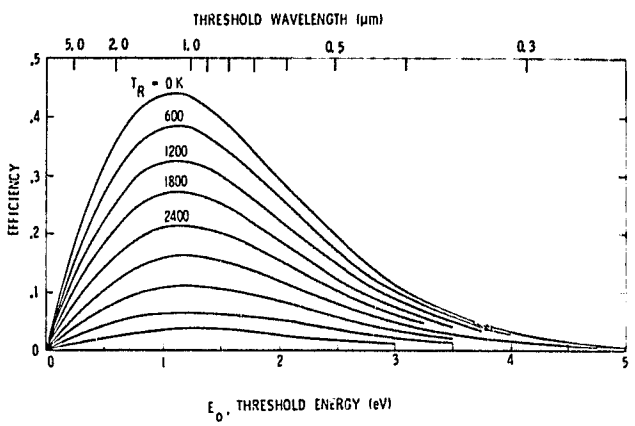

Limiting efficiency for conversion of solar radiation by a photosensitive device.

Wide-Temperature-Range Ion Implant Bubble Devices

Ion implant bubble device technology has been advanced in its ability for wide-temperature-range operation. Device operation over the range from -20°C to +95°C was experimentally demonstrated with bubble chips fabricated from standard CaGe material suitable for 8-μm-period data site spacing. The devices were designed and fabricated as part of a joint DOD/NASA research contract with Bell Laboratories to simultaneously improve device density, temperature range, and packaging quality for onboard memory applications. Typical device operation at field rotation rates up to 100 kHz exhibited a margin greater than 20 oe. However, minor loop margins exceeded 30 oe over the entire span of temperature. This indicates that intrinsic bubble stability and propagation with this particular combination of bubble garnet material, device component design, and processing appear to be outstanding.

Ion implant technology offers an order-of-magnitude improvement in density over conventional permalloy at comparable yield and cost. This device demonstration not only illustrates the potential for 8-μm-period devices but also represents an important first step in the planned development of a wide-temperature-range device at 4-μm period. Devices with 8- and 4-μm period are expected to facilitate onboard memory systems of 128- and 512-megabit capacities, respectively.

Paul J. Hayes, 3535 506-61-03

Integrated Verification and Testing System for HAL/S Programs

The IVTS (integrated verification and testing system) is a large software system designed to support user-controlled verification analysis and testing activities for programs written in the HAL/S language being used on the Space Shuttle. The IVTS was developed under contract with Boeing Computer Services Company of Seattle, Washington. The Version 1.0 system is currently undergoing testing, evaluation, and enhancement of certain components to complete the detailed design capabilities.

Conceptually and functionally the IVTS is composed of a set of modular verification analysis tools of four major types: (1) static analysis, (2) dynamic analysis, (3) symbolic execution, and (4) documentation enhancement. Most of these major components contain several distinct tools that can be individually selected for execution by the system user. The IVTS contains a user interface component and a user command language, a data base, and a report-writer component, all of which support both interactive and batch mode usage.

ORIGINAL PAGE IS
OF POOR QUALITY

The IVTS is written predominately in Pascal for ease of portability and is designed to appear the same to users regardless of specific machine implementation. Other major design concepts are: (1) the analysis tools work only with previously compiled HAL/S programs and no compiler functions are duplicated; (2) program intent may be specified via "assertions" and checked against intermediate or final program results; (3) automated program instrumentation under user control supports object code testing and debugging; and (4) all communication between the IVTS and the user is in terms of the HAL/S source program.

Edmond H. Senn, 2062 506-61-23

Selection Criteria for Tunable-Diode Lasers Quantified

Experimental and analytical studies have been completed that permit prediction of expected performance of tunable-diode lasers in optical heterodyne receivers. The use of tunable-diode lasers has been limited primarily by the existence of optical noise over and beyond that expected from purely fundamental quantum noise inherent in lasers. Qualitative reasoning leads to the belief that the so-called "excess noise" must degrade the performance of systems using tunable-diode lasers as local oscillators. However, these studies have shown that reasonably well behaved "excess noise" can be modeled as a simple additive noise in the heterodyne process. The consequent decrease in available signal-to-noise ratio can thus be predicted and can be compared with instrument performance criteria. Shown in the figure is an example of the noise at the output of the detector-preamplifier in an optical heterodyne receiver for three cases: (1) detector-preamplifier alone, (2) 400-μamp induced photocurrent from a quantum-noise-limited CO_2 laser, and (3) 400-μamp induced photocurrent from a tunable-diode laser contaminated by well-behaved "excess noise." Simple calculations give the excess noise component compared to the ideal (CO_2 laser) value. Simultaneous measurements of signal-to-noise ratio achievable under these conditions show that the "excess noise" causes a simple additive effect in reducing signal-to-noise ratio, in agreement with theoretical considerations.

Utilizing the results of these studies, a simple instrument has been designed and developed that permits suppliers of tunable-diode lasers to screen their own devices. The instrument makes a direct measurement and read-out of the "excess noise" a simple process. Systematic selection procedures are now possible to ensure that suppliers provide devices that will respond to all essential requirements specified by instrumentation engineers.

Stephen J. Katzberg, 3535 506-61-73

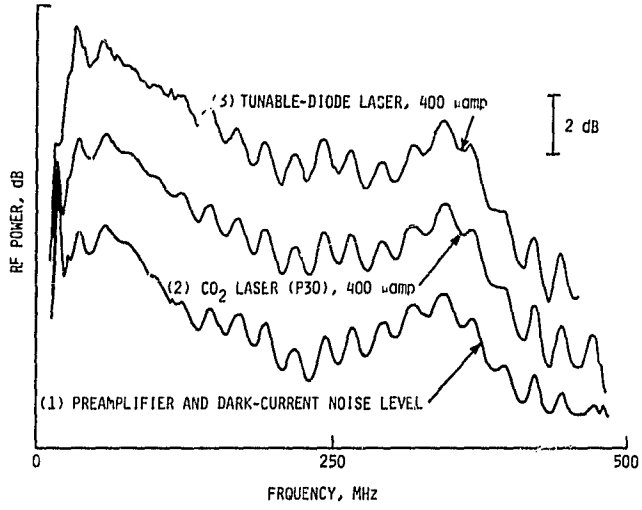

Residual excess noise measurements for a tunable-diode laser local oscillator.

Pointing/Solar-Tracking Unit

The Laser Heterodyne Spectrometer (LHS), an airborne sensing instrument under development at Langley, requires the delivery of a 3-in.-diameter beam of sunlight to the instrument's optical system. The optical axis of this beam must be maintained collinear to the instrument's optical axis within ±4 arc minutes during both ground and airborne operation. The stand-alone pointer/tracker system controls a mirror that can be rotated in elevation and azimuth to direct sunlight into the optical path of the LHS instrument. The range of motion for this mirror is 7.5° in elevation and 360° in azimuth.

The pointer/tracker system has two modes of operation. In the pointing mode the mirror's position is controlled relative to the unit's

ORIGINAL PAGE IS
OF POOR QUALITY

internal coordinate axes. This mode is used to direct test sources into the instrument and also during solar acquisition prior to tracking. Track mode is the primary operational mode. During track a part of the sunlight is directed into a telescope assembly that focuses the Sun's image onto a four-quadrant photodiode. The processed signals from this photodiode control and correct the mirror position to maintain the Sun's beam collinear to the instrument's optical axis, even in the presence of aircraft and solar motions.

All system operations are under microprocessor control. The pointer/tracker can be operated automatically with preprogrammed software routines, such as Sun Search, or manually either by entering commands through the control unit keyboard terminal or via an external interface. The pointer/tracker unit shown in the photograph and its control electronics and display unit (not shown) were designed and fabricated at Langley.

I. W. Jones, 4621 506-61-73

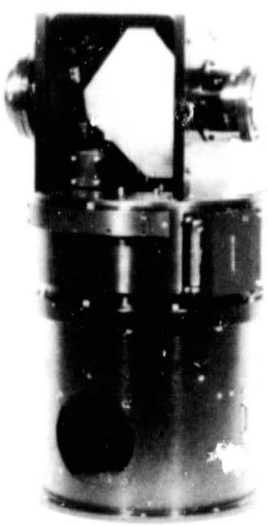

Pointer/solar-tracker unit.

Force Loop Augmentation for ASPS Magnetic Bearing Control

A force feedback loop has been successfully integrated with the magnetic bearing controls of the ASPS (annular suspension and pointing system) magnetic suspension. Revised predictions of 3-sigma on-orbit performance show an ASPS pointing stability of 0.005 arcseconds when supporting the Solar Optical Telescope at Goddard Space Flight Center.

This performance improvement is achieved via closure of the force loop around the gap position loop, thus eliminating all significant ASPS error sources (i.e., all errors related to rate of change of the magnetic gap (ΔG), errors due to unaccounted-for leakage flux, hysteresis error due to low-level residual flux, and errors due to variation in magnetic bearing coil parameters and system level calibration errors). Closure of the force loop also relaxes the repeatability requirement for the gap position sensor from 0.1 percent to 2 percent and allows the use of a change-coupled device (CCD) array digital gap sensor, which is inherently temperature insensitive. Implementation of the force loop is made possible by the development of a highly repeatable digital force sensor by Quartex, Inc. The sensor is based on the principle that the frequency of a vibrating quartz crystal varies as a function of compression or tension forces.

Prototype force sensors and gap position sensors have been evaluated in a magnetic-bearing laboratory dynamic test. Force sensor performance is 1 to 2 orders of magnitude better than specified. In addition, CCD gap sensor repeatability is better than 1 percent. Additional work is required on the force sensor overload protection mechanism designed to protect the fragile quartz crystals during Shuttle launch. Since the overload protection is external to the sensor, redesign will probably be postponed until flight development and flight qualification program phases are initiated.

C. R. Keckler, 4591 506-61-93

Surface Accuracy Measurement Sensor for Large Space Antennas

An anamorphic telescope-type engineering breadboard sensor for measurement of surface deformations of large space antennas was developed in a joint effort by Langley and TRW Space Systems Division. The sensor measures the deflection of a surface target, either a light-emitting diode or a retrodirective reflector, normal to the telescope's line of sight.

ORIGINAL PAGE IS
OF POOR QUALITY

A focal-plane photoelectric detector in the telescope receiver senses the target displacement normal to the electro-optical axis.

Target radiation entering the telescope is imaged on a linear-effect planar silicon photodiode that has a sensitive area 5 mm long by 2 mm wide. The detector is oriented with its long dimension along the direction of the target deflection to be measured. A cylindrical field lens is oriented with its axis in the direction of the target deflection. The image on the detector will move a distance proportional to the distance the target moves. Two current signals, one from each end of the detector, are produced by the photodiode, and the image position on the detector is proportional to the relative intensity of the signals; that is, the image position along the detector causes the signals to increase or decrease. Since the distance from the target to the telescope entrance aperture is known, the target deformations can then be calculated. Typically, at a distance of 21 m, angular sensitivities of 0.59 arcseconds and target deflection accuracies of 0.060 mm are obtained in tests on a mesh antenna model. The sensor has application for most large space structures where deflection measurements are desired to check alignment.

Charles G. Saunders, 3631 506-62-43

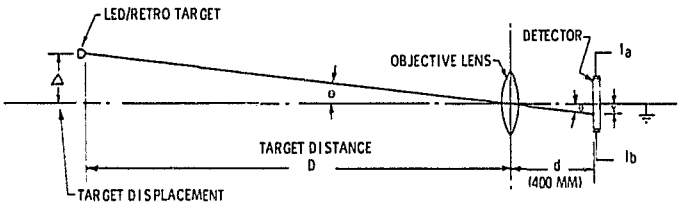

Optical schematic of surface deformation sensor.

IDEAS Computer-Aided Design System

IDEAS (interactive design and evaluation of advanced spacecraft) is an integrated system of computer-aided design and analysis software used to rapidly evaluate system concepts and technology needs for future advanced spacecraft such as large antennas, platforms, and space stations. The system was developed at Langley to meet a need for rapid cost-effective labor-saving approaches to the design and analysis of numerous missions and total spacecraft system options under consideration.

IDEAS consists of about 40 technical modules, efficient executive and data-base/file management software, and interactive graphics display capabilities. A single analyst at an interactive terminal can rapidly model the structure and design and analyze the total spacecraft and mission. The coupling of on-orbit environmental computational algorithms with analysis and design modules permits rapid evaluation of competing spacecraft. Parametric studies and technology-level trade-offs are easily accomplished using IDEAS. The user-friendly system guides the analyst through the computing session by displaying requests for processing paths and data inputs. Automatic formatting of data files relieves much of the tedium associated with conventional design and analysis efforts. Further, much of the repetitious computer system command instructions are directly coded into IDEAS, thereby freeing the analyst to concentrate on the spacecraft design tasks. Data and graphical summary information are presented to the analyst on graphics display terminals for immediate assessment and interactive modification of the spacecraft or

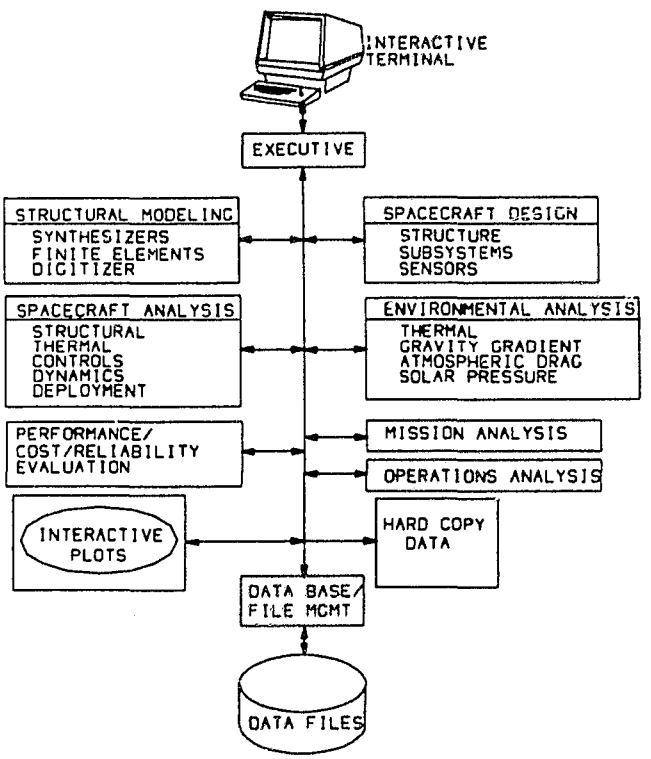

IDEAS system overview.

ORIGINAL PAGE IS
OF POOR QUALITY

mission design, as appropriate. Spacecraft concepts evaluated using IDEAS include microwave radiometer satellites, communication satellite systems, solar-powered lasers, power platforms, and orbiting space stations.

L. Bernard Garrett, 3666 506-62-43

SEADS Development Flight Instrumentation (DFI) Analysis

The Shuttle Entry Air Data System (SEADS) is the implementation of a new concept in air data systems that incorporates an array of flush orifices in the nose and forward fuselage of the flight vehicle and a new flow field modeling concept for analysis of the flight data and determination of the required air data parameters, including angle of attack, angle of side slip, dynamic pressure, total pressure, static pressure, and Mach number. Although this data reduction/analysis capability will not be fully implemented until SEADS' first flight, a developmental computational capability has been assembled and demonstrated. A much-simplified version of this developmental capability has been used to analyze flight data from the Orbiter's Development Flight Instrumentation (DFI) and determine dynamic pressure for STS-1 through STS-4. The results from this analysis confirm the basic concepts and techniques to be applied to the SEADS.

Additionally, aerodynamic analyses performed throughout NASA determined that the flight-derived vehicle aerodynamic coefficients for STS-1 through STS-4 were within 6 percent of the preflight data book values, except within the region from Mach 20 to 24 (185,000 to 245,000 ft). A review of this discrepancy and a statistical comparison of air data sources concluded that the dynamic pressure (q_∞) derived using the SEADS computational techniques and the in situ DFI pressure data was more accurate than the q_∞ available from other sources, namely the Best Estimate Trajectory (BET) and the real-time navigation system. This conclusion led to the incorporation of the q_∞ derived using the DFI pressure data and the SEADS computational technique into subsequent BET solutions. The figure compares q_∞ derived using the SEADS analytical technique with the BET q_∞ and the navigation q_∞.

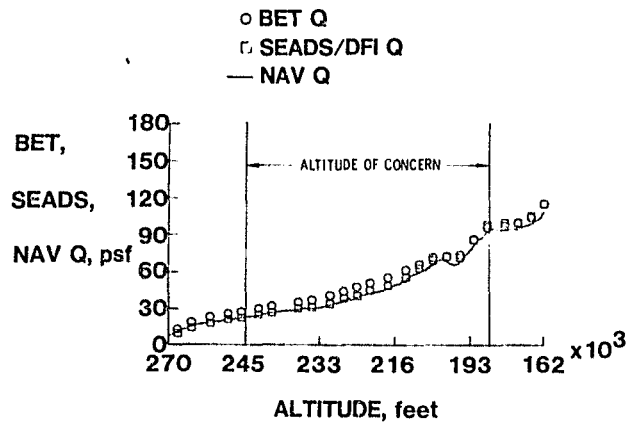

STS-3 DFI pressure analysis.

P. M. Siemers III, 3984 506-63-32

Space Science and Applications

Portable X-Ray Fluorescence Spectrometer

A portable battery-powered X-ray fluorescence spectrometer (XRFS) has been developed for use in geological exploration and is undergoing field evaluation by U.S. Bureau of Mines geologists. The instrument, developed under Langley direction in a cooperative venture with the Bureau of Mines, is a modification of the XRFS instrument that was used in the inorganic chemistry experiment on the Viking Mars Lander. It is intended for use in field geological exploration and survey expeditions and is able to rapidly characterize a minimum of 60 elements (including copper, uranium, and tungsten, for example) and their relative concentrations in rock formations. Potentially valuable seams or ore concentrations can thus be detected in situ and samples can be taken for subsequent detailed laboratory assay. No other portable self-contained instrument that can characterize so many elements exists for field use.

The instrument weighs less than 7.3 kg (16 lb), measures 28 cm by 13 cm by 28 cm (11 in. by 5 in. by 11 in.), and can easily be carried like a camera or tote bag. The self-contained unit employs conventional D-cells

ORIGINAL PAGE IS
OF POOR QUALITY

for power supply, Fe^{55} and Cd^{109} radioisotopes as X-ray sources, and proportional counter detector tubes. Function control is provided by an internal microprocessor. Both cathode ray tube (CRT) and liquid crystal display (LCD) are incorporated; the CRT provides a spectrum display and the LCD an alphanumeric display for element identification, status, instructions, etc.

Warren C. Kelliher, 3068 141-20-10

Portable battery-powered X-ray fluorescence spectrometer.

Waste-Water Disposal System

Extensive research and development were conducted at Langley during the late 1960's and early 1970's on regenerative life support systems, in support of extended-duration manned space missions. Reclamation and reuse of waste water was one of the significant technologies developed as a result of this research. This technology subsequently was instrumental to the design and incorporation of a household water reuse system in Langley's Technology Utilization House (Tech House). As a consequence of these technology program achievements, the Virginia State Department of Health expressed interest in utilizing NASA's expertise in life support systems to examine and abate problems associated with on-site waste-water disposal on land areas unsuitable for conventional septic-tank and drain field practices.

A cooperative project involving Langley, the Virginia Department of Health, and the Virginia Polytechnic Institute and State University was undertaken to determine the suitability of new concepts of on-site waste-water disposal on problem land sites. Four experimental waste water disposal beds were designed, placed in proximity to Tech House and connected to the Tech House septic-tank overflow pumping chamber. Two of the beds were shallow trenches, using lateral flow through the upper 2 ft of unsaturated soil as the disposal technique. These were located in a wooded area characterized by a high water table and poor drainage. The other two beds were above-surface mounds employing vertical and lateral flow through the mounds, which have the capacity for holding large quantities of waste water under unsaturated conditions (air and oxygen available), with evapotransportation occurring on the surface.

System tests were conducted over an 18-month period during which both dry and wet seasons were experienced. Collectively, the beds clearly demonstrated that alternatives to conventional on-site waste water disposal systems are available, and these alternative techniques offer potential solutions to on-site disposal on problem soils. In particular, the mound-type beds demonstrated the ability to handle double the initial design dose rates without becoming saturated or showing evidence of failure. The experimental data that were collected are being reduced and analyzed. Upon completion, the results will provide state officials with basic design parameters for waste water disposal beds that can serve to modify current regulations governing on-site disposal systems.

Warren D. Hypes, 2871 141-20-10

Explosive Seam Welding Applied to Reactor Repair

An explosive seam welding technique developed at Langley Research Center provides a simplified alternative to a difficult remote-fusion weld operation associated with the replacement of fuel channels in a nuclear reactor. Full replacement of these fuel channels is a massive and complex undertaking. Previous experience in this regard dictates that emphasis be placed on reducing both downtime and radiation exposure

ORIGINAL PAGE IS
OF POOR QUALITY

during the repair. One of the many replacement operations requires connection of a channel annulus bellows to an end fitting. The current standard joining approach involves making a fusion weld using a specially developed robotic tool. At best this technique involves a cumbersome spatial arrangement of the special tooling assembly, coupled with difficulty of access to the fuel channels within the reactor.

At the request of Foster Wheeler Development Corporation and Atomic Energy of Canada, Ltd., an alternative to fusion welding using an explosive seam weld technique developed at Langley has been demonstrated to be applicable to the bellows flange ring attachment. The explosive welding mechanism is a high-velocity oblique-plate collision process that effaces the metal oxide films and forces the metal surfaces into intimate contact at very high pressure (approximately 1 million psi), allowing atomic-level metallurgical bonding at the interface. In the bellows flange ring weld application the ribbon explosive and detonator are preassembled to the end fitting attachment ring outside the reactor. The explosive and the detonator remain attached throughout subassembly installation and are detonated when required to connect the bellows and the end fitting.

During the course of the project, various explosive-welding parameters were examined to establish limits of the variables involved in the welding process. Further tests on reactor grade materials were performed, culminating in full-scale demonstrations on actual bellows assemblies, as illustrated. No adverse effects on the bellows assembly were observed and no appreciable geometry change was measured.

Laurence J. Bement, 4621 141-20-10

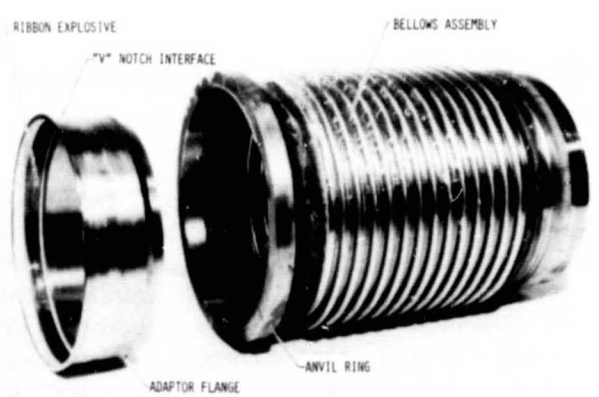

Explosive joining setup for reactor.

Accuracy and Resolution of Earth Radiation Measurements

The Earth Radiation Budget Experiment (ERBE) includes remote measurements at satellite altitude that are reduced to estimate the radiation budget at the top of the Earth's atmosphere. The accuracy and resolution of these estimates are two of the ERBE mission objectives. The wide-field-of-view measurement is the sum of all the radiation over a large area, and by its very nature it gives a smoothed representation of the true field. These measurements must be unsmoothed, or enhanced, to estimate the true field. A numerical filter technique has been developed to accomplish this by processing a sequence of measurements along the orbital track. The measurements are formulated in a matrix equation that is inverted to give the inversion weights for the filter. The amount of data that is processed at one time is the degree of the filter.

The questions of accuracy and resolution are best answered by numerical simulation of the data gathering and estimation process. The orbital geometry was defined and a typical longwave radiation field was chosen and taken as "truth." Synthetic measurements were calculated over this assumed radiation field and were then corrupted with random measurement errors. Applying the numerical filters to these synthetic measurements produced estimates at the top of the atmosphere that were compared to the true radiation field to establish the

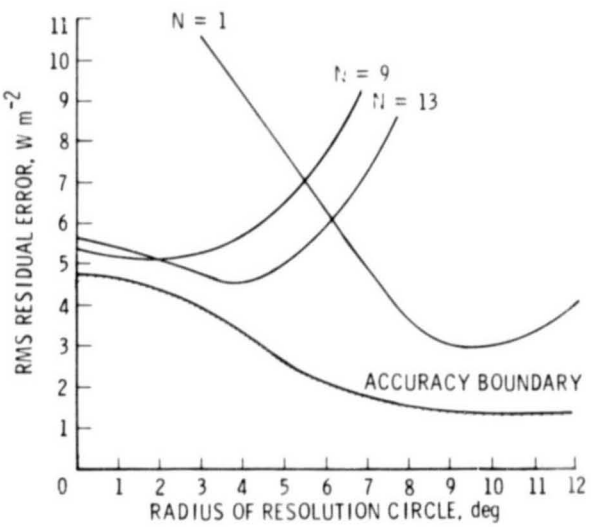

Accuracy and resolution of numerical filter.

ORIGINAL PAGE IS
OF POOR QUALITY

accuracy. This led to statements of confidence on how well the radiant exitance can be estimated for small regions.

A plot of error versus resolution shows the performance of the numerical filter for different degrees. A 1st-degree filter (N=1) that processes one measurement at a time gives good accuracy (2.8 W m^{-2}) for large areas. For medium areas, a 13th-degree filter gives better accuracy than the 1st-degree filter, and for small areas a 9th-degree filter is better than either of the other two filters for estimating the radiant exitance. In all cases, the simulation studies have shown that a well-designed numerical filter gives accuracies that are very near the theoretical accuracy boundary.

Richard N. Green, 2977 146-10-06

Radiative Effects of Clouds

Clouds influence the Earth's radiation balance and, ultimately, both weather and climate by reflecting solar energy and trapping heat radiated from the surface. Quantification of the regional and global effects of clouds is quite limited at present due to a lack of comprehensive observations and analyses of cloudiness and its radiative properties. This is one of the primary reasons for the continuing debate concerning the importance of clouds in climate modeling. Does an increase in cloudiness cause warming or cooling of the Earth's surface? Theoretical and empirical answers to this question have ranged from a slight warming to no effect to considerable cooling, but both types of results are based on very uncertain cloud effects. Until the effects of clouds are better understood and taken into account, large uncertainties in climate predictions will remain.

To increase the knowledge of the influence of clouds on the radiation balance, regional and zonal cloud and surface radiative properties have been derived at Langley for 20 percent of the Earth for the month of November 1978. This study utilized hourly high-resolution visible and infrared window data from the Geostationary Operational Environmental Satellite (GOES). Parameters derived from the GOES data include the cloud amounts, infrared fluxes, and albedo (fraction of incident solar radiation reflected from the Earth-atmosphere system) at three levels in the atmosphere, as well as the longwave flux and albedo over clear areas. The plot of zonal clear-sky and total (clear and cloudy together) albedos shows the increase in albedo due to cloud cover. Total albedo is more than double the clear-sky albedo. The clear-sky albedo is nearly constant south of 10°N due to higher solar elevations and a predominance of ocean regions. Higher clear-sky albedos north of 10°N result from lower Sun elevation and the relatively bright North American land mass. The more jagged appearance of the total albedo curve reveals the variable effects of clouds. The increased cloudiness of the Intertropical Convergence Zone is indicated by a sharp peak at 7°N. For this entire data set it was found that the cloud albedo effect (solar radiation blocked by the cloud tops) outweighs the infrared effect (infrared radiation trapped under the clouds), so that a net cooling of the Earth-atmosphere system was caused by the presence of clouds. Analyses of GOES data from other months are continuing in order to determine whether the net effect of the clouds remains constant or changes with the time of year.

Patrick Minnis, 2977 146-10-06

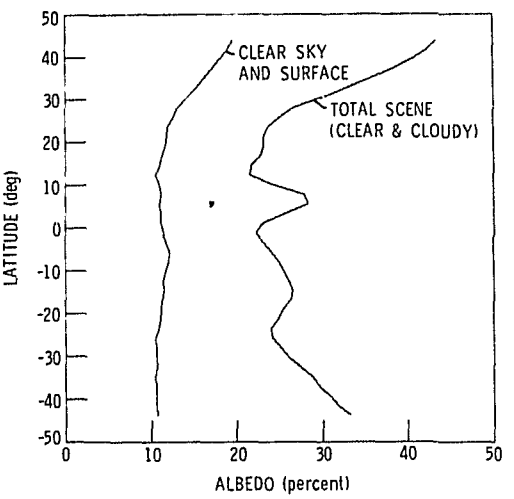

GOES-derived zonal albedos for November 1978 (longitude 30°W to 120°W).

Longitudinal Variability of Earth-Emitted Radiation

Because of the variation with latitude of radiation incident on the Earth, there is a variation of Earth-emitted radiation with

ORIGINAL PAGE IS
OF POOR QUALITY

latitude. There are also important variations of Earth-emitted radiation in the longitudinal direction. These variations of Earth-emitted radiation have been computed for large spatial scales using data from the wide-field-of-view (WFOV) radiometers on the Earth Radiation Budget (ERB) instrument aboard the Nimbus 6 spacecraft. These variations may be described in terms of Fourier series, whereby the variation is expressed as the sum of waves in the longitudinal direction. The power for each wave is one-half the amplitude squared and is shown for each wave number as a function of latitude for July 1975. The major feature is a strong wave-1 and wave-2 peak in the region from 20°N to 50°N. This is due to high levels of emitted radiation in the Sahara, Arabian, and Karakum Deserts and in the western U.S., low levels near India and the Tibetan Plateau, and variations of exitance over the subtropical North Pacific Ocean. The wave numbers 1 and 2 are absent in January. From 20°N to 20°S there is considerable structure, with wave numbers 1 through 4 active. Comparison of the July and January spectra indicates that this activity follows the Sun. In July there is a strong wave-1 peak at 75°S, associated with Antarctica. This continent is displaced from the South Pole along the 70°E meridian, and much of the terrain is at high elevation (above 4 km). The effect of this is to induce the strong wave 1 when there is little or no solar insolation during June and July. Study of these types of variations in Earth-emitted radiation is very important for advancing the understanding of our climate.

G. Louis Smith, 2977 146-10-06

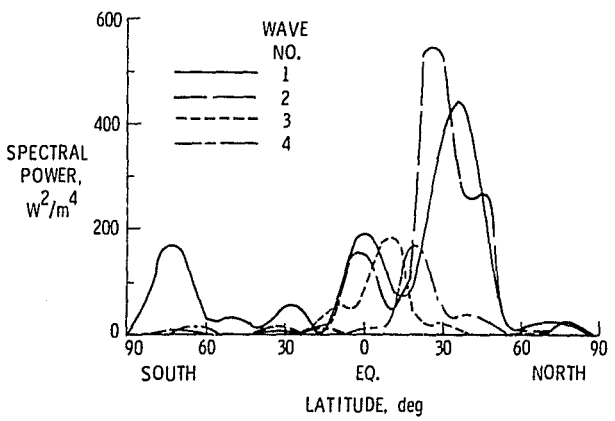

Latitudinal distribution of spectral power for July 1975.

Lidar Measurements of Stratospheric Volcanic Plumes

The 48-inch lidar system at Langley has been used to make routine observations of stratospheric aerosols for more than a decade. A smaller dual-wavelength aircraft-mounted system has been constructed in order to conduct satellite ground truth experiments and volcanic plume survey measurement missions. Lidars measure the vertical profile of laser backscattering ratio, which is greater than 1 in the presence of aerosol particles. By measuring this backscattering ratio after major volcanic eruptions, the lidar system is able to monitor the effluent injected into the stratosphere, and therefore provides valuable data for estimating atmospheric transport and the potential climatic impact of such an eruption.

A special airborne mission was flown to Costa Rica in February 1982. One of its principal objectives was to study the so-called "mystery cloud" of early 1982. Overwhelming evidence from these measurements indicates that the source of this layer was volcanic. Furthermore, the results show that the amount of particulates from this eruption appears to be greater than that from Mount St. Helens. A similar mission was flown in July 1982 near the coast of Venezuela to study the stratospheric effects of the eruption of the Mexican volcano El Chichon on April 3 and 4, 1982. The data show that this may be the most significant eruption of this century in terms of stratospheric effects and potential for radiative perturbation. Record backscattering ratios of 50

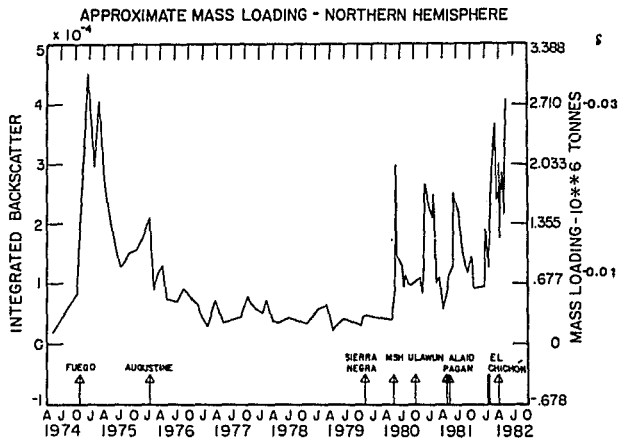

Lidar measurements of peak backscattering over LaRC (37°N).

ORIGINAL PAGE IS
OF POOR QUALITY

were measured from a broad aerosol layer between 22 and 33 km. This layer persisted over the region from 25°N to the southernmost measurement point, 12.5°N.

M. Patrick McCormick, 2065 146-10-06

The Earth's Atmosphere: Past, Present, and Future

Human activities may be perturbing the composition and chemistry of the atmosphere. In order to accurately assess their impact on the present and future atmosphere, we must first understand the natural processes or mechanisms that control the composition and chemistry of the atmosphere, including the level of solar ultraviolet (UV) radiation, which initiates photochemical reactions in the atmosphere, the emission of volcanic gases, lightning, precipitation, and the biogeochemical cycling of gases. In an effort to better understand these natural processes and their variations with time, photochemical models originally developed to study the impact of human activities on the present and future atmosphere have been utilized to study the evolution of the atmosphere over geological time.

It is widely believed that gases in the early atmosphere, energized by solar UV radiation and atmospheric lightning, formed the complex organic molecules, the precursors of living systems. Calculations made at Langley indicate that a mixture of methane (CH_4) and ammonia (NH_3), long believed to be the composition of the early atmosphere, would have been photochemically and chemically unstable and very short lived if such an atmosphere had existed in the early history of the Earth. Instead, an early atmosphere of carbon dioxide (CO_2) and nitrogen (N_2) resulting from volcanic emissions is favored by the Langley calculations. These findings suggest that the atmospheres of the Earth, Mars, and Venus all had a common origin, the volcanic release of gases trapped in the solid interior of the planets during their formation some 4.5 billion years ago. Today, the atmospheres of Mars and Venus are predominantly carbon dioxide (approximately 95 percent) with a few percent nitrogen. On Earth the bulk of the atmospheric carbon dioxide ended up in the form of carbonates due to the action of life, leaving relatively inert nitrogen to accumulate as the major atmospheric constituent (78 percent by volume). Oxygen, the next most abundant atmospheric species (21 percent by volume), resulted from the conversion of carbon dioxide and water vapor by photosynthetic organisms.

The level of oxygen in the early atmosphere prior to the evolution of photosynthetic organisms is another important question. The formation of atmospheric oxygen (O_2) is initiated by the photolysis of atmospheric carbon dioxide and water vapor by solar ultraviolet radiation, with the subsequent release of atomic oxygen (O). For many years it was believed that the early Sun emitted levels of UV comparable to or less than those of the present Sun. However, recent theoretical calculations performed at the Goddard Institute for Space Studies, as well as astronomical measurements of a half-dozen young Sun-like stars obtained with the International Ultraviolet Explorer satellite, have changed that idea. These calculations and measurements indicate that the early Sun emitted orders of magnitude more UV radiation than it presently emits. In collaboration with these astronomers, Langley photochemical models have been used to assess the effects of these high UV fluxes on the composition of the early atmosphere. The Langley calculations indicate that such fluxes acting on volcanic carbon dioxide and water vapor resulted in orders of magnitude more atmospheric oxygen and ozone in the early atmosphere than was previously believed, but these high levels of O_2 and O_3 were insufficient to protect the surface of the Earth from the greatly enhanced levels of UV radiation that appear to have been emitted by

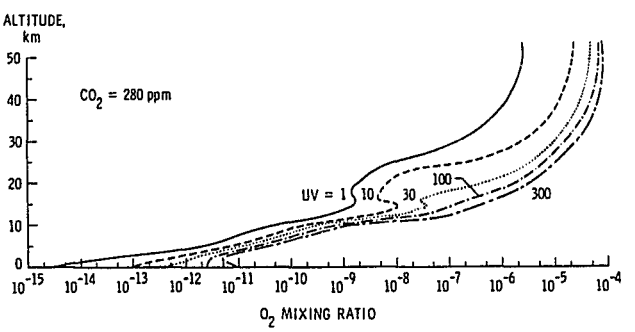

Vertical distribution of oxygen (O_2) in the prebiological early atmosphere for levels of solar UV radiation from 1 to 300 times the present value, based on photochemical calculations.

ORIGINAL PAGE IS
OF POOR QUALITY

the early Sun. These high levels of solar UV radiation incident on the surface of the Earth during its early history may have had important implications for the origin and evolution of life on our planet.

Joel S. Levine, 2187

146-20-10
307-02-02

Lidar Measurements of Ozone and Aerosols in the Upper Troposphere

The first airborne differential absorption lidar (DIAL) measurements of O_3 and aerosol profiles in the tropopause region of the atmosphere were made on August 6, 1981, in a flight over Maine. This was the first flight experiment conducted with the DIAL system operating in a zenith-viewing mode from the Lockheed Electra. Loring Air Force Base, Maine, was selected for the tropopause experiment because of its location on the northern side of the jet stream. The flight path went from northern Maine (47°03'N/69°28'W) to the coast of Maine (44°37'N/67°93'W) at an aircraft altitude of 7620 m. A return flight was made along this leg at 8230 m altitude. At the start of the flight an ozonesonde was released at Caribou, Maine, at 2200 EDT, and the flight was completed by flying over the ozonesonde launch site at 2348 EDT. The ozonesonde data showed a lower tropopause at an altitude of 11.1 km. Two prominent O_3 concentrations in these layers were twice the average concentration outside the layers. The depth of the lower layer was about 4500 m, and the upper layer had a depth of only 350 m. A comparison of the DIAL O_3 measurement profile and the ozonesonde data is shown in the figure, along with the potential-temperature data from the ozonesonde. The DIAL data represent the average O_3 profile obtained from 300 DIAL shots along a 6-km horizontal path. The horizontal bars designate the standard deviation of the average O_3 profile. The magnitude and relative position of the O_3 layers are in excellent agreement between the DIAL and ozonesonde measurements. The absolute altitude agreement for these layers is within 100 m. Ozone features in the minimum between the two layers are also accurately determined by the DIAL system.

Lidar measurements of aerosol scattering at a wavelength of 600 nm were made simultaneously with the O_3 DIAL measurements. The layers that were found to have enhanced O_3 concentrations also had increased levels of aerosol scattering. This direct correlation between O_3 and aerosol scattering may indicate that these layers were actually of tropospheric origin. A cross-sectional map of these layers is being constructed from the entire DIAL data set over Maine to determine their extent and characteristics.

Recent DIAL measurements of O_3 and aerosols in the tropopause and lower stratosphere regions have shown the potential for mapping thin atmospheric layers (300 m depth) having enhanced or depleted concentrations of O_3 or aerosols. These measurements were made at ranges up to 6 km above the aircraft altitude. For a 210-m vertical resolution and 6-km horizontal resolution, the average O_3 profile uncertainty was found to be about 5 percent at 3.5 km range to 15 percent at 6 km range. The aerosol distribution can be determined with a vertical and horizontal resolution of 20 m. Simultaneous information on O_3 and aerosol distributions may be important in determining the origin of some atmospheric layers and the gas-to-particle

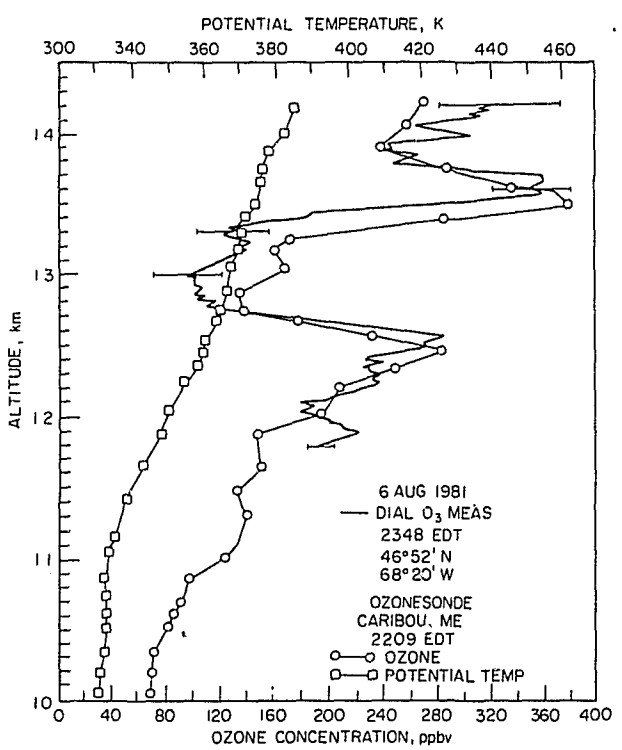

DIAL ozone measurement over Maine.

conversion that may be taking place in them. In addition, the capability for obtaining the temporal variation of a tropopause folding event will provide new understanding of this important stratosphere/troposphere exchange mechanism.

E. V. Browell, 2576 146-20-10

Scatterometer Simulation Program

Analyzing the design performance of scatterometers, which are used for determining wind speed and direction over the oceans, can be time consuming and limited in scope when simplified analysis programs are used. These programs only provide first-order estimates on performance and trade-offs between scatterometer designs. To remedy this situation a detailed simulation program was developed. This program simulates a scatterometer design and its orbital flight over a realistic wind field. The simulation routine generates a data base of noisy Earth-located values of σ^o (radar scattering coefficient, a function of wind speed and direction seen by the scatterometer) similar to one that an actual scatterometer would generate as it flies over the ocean. The σ^o data from the various antennas used in the scatterometer are grouped together in resolution bins and passed through a wind vector inversion algorithm, which converts the σ^o data to wind vector solutions. These solutions are compared to the original wind field in a statistical routine that evaluates the accuracy and performance of the particular design under study. Monto Carlo techniques are used to simulate random errors introduced by communication noise, attitude pointing errors, and model function uncertainties.

Using this simulation, program detail performance and trade-off studies can be conducted to provide wind speed and direction accuracy, alias removal skill, wind gradient sensitivity, and model function error sensitivity for various scatterometer antenna configurations and Doppler filter processing techniques. Such a study was conducted in early 1982 to determine the best scatterometer design and performance that could be accommodated on the TIROS-N satellite, where weight, space, power, and data rate are limited. The simulation study results indicated that a configuration could be flown that would meet minimum user requirements but would have certain limitations, such as higher wind speed and direction gradient sensitivity, lower resolution, and degraded low wind speed accuracy.

This simulation not only provides a tool for evaluating the performance of a particular scatterometer design, but can also be used to generate satellite scatterometer data to be used in evaluating data-processing algorithms, such as the alias removal algorithm and improved versions of the wind vector inversion algorithm. The simulation will be invaluable in the design and evaluation of any future scatterometers to be flown in space.

Emedio Bracalente, 3631 146-40-05

Aircraft Microwave Radar Measurement of the Sea Surface

The Langley Airborne Microwave Scatterometer was flown during the December 1980 Storms Transient Response Experiment over the North Pacific Ocean to refine our understanding of the relationship between sea surface normalized radar cross section (NRCS) and the wind and/or wind stress. The scatterometer was carried aboard the NASA/JSC C-130 aircraft, which normally flew at altitudes above 1500 m. A second aircraft flew formation below the C-130 in the near-surface turbulent boundary layer in order to measure wind speed and surface stress.

The 4 days of flights have been divided into about 60 straight segments, each typically 50 km long. For each segment the NRCS, and the low-altitude wind data were processed to obtain the cross correlation between the two. For each segment, the resulting lag (4.3 km for the example shown in the first figure) was used to align the data sets for construction of a scatter plot between wind and NRCS. The second figure is the scatter plot from the same segment, and shows the variation in NRCS for wind speeds between 14 and 21 m sec^{-1} for a crosswind radar look at 40^o incidence angle, horizontal polarization. From analyses of similar plots from all 60 segments, covering a wide range of incidence angles, azimuths, and wind speeds, a clearer understanding is emerging of

ORIGINAL PAGE IS
OF POOR QUALITY

the relationship between high-altitude radar measurements of the sea surface and the near-surface wind.

William L. Grantham, 3631 146-40-05

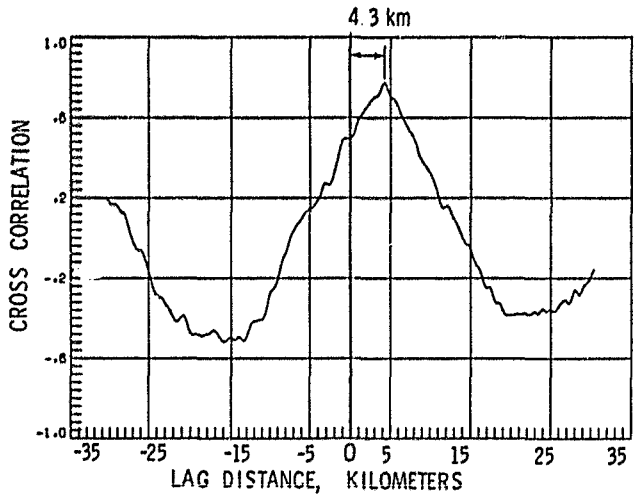

Cross correlation between sea surface NRCS and near-surface wind speed.

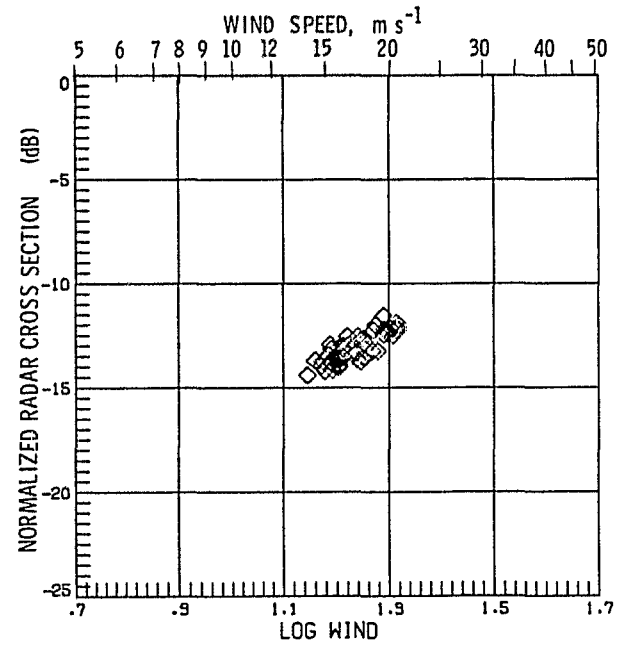

Scatter plot of sea surface NRCS and near-surface wind speed after lag correction.

MOCS Warm-Core Ring Experiment

LaRC's MOCS (Multichannel Ocean Color Sensor) was flown on the NASA Wallops P-3 aircraft on missions over a warm-core ring that drifted southward just off the continental shelf from New Jersey to North Carolina over a 4-month period. These flights were a joint experiment by marine and NASA scientists to study the dynamics of warm-core rings. These rings, which form from eddies that break off from the Gulf Stream, can be as much as 300 kilometers in diameter. Marine scientists are trying to determine the physical and biological consequences of these "hurricanes" in the ocean. Two questions being asked are whether these rings disturb fish populations and whether they collect and transport significant amounts of coastal pollution.

For the first time, in April 1982, remote data pertinent to marine scientists were

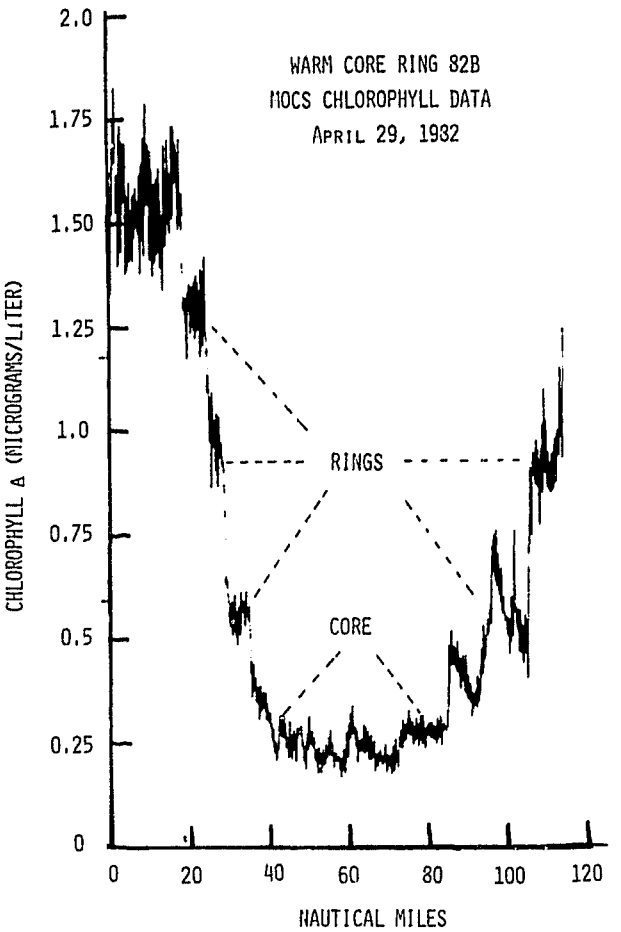

MOCS chlorophyll data.

ORIGINAL PAGE IS
OF POOR QUALITY

collected by MOCS and transmitted in real time to the R/V Knorr, a Woods Hole Oceanographic Institute ship. In the past, a ship could search for days to locate optimum areas for study, whereas the transmitted remote data can immediately guide ships to regions where extensive sea truth can be collected. A new algorithm that was calibrated during the 1981 Nantucket Shoals Experiment was used to convert MOCS data into chlorophyll a concentrations along flights paths over the ring. The chlorophyll a levels measured on this and subsequent flights were confirmed by ship measurements. Shown in the figure is an example of MOCS data collected during one pass across the ring. The data clearly demonstrate its fine structure, which suggests the existence of concentric rings of chlorophyll a levels about the core. Because the ring structure changes continually as it rotates once every 3 days, it is not possible for a ship to collect the cross sectional data that were obtained by MOCS. The new algorithm discovered at Langley can be applied to problem solving in other unrelated programs, particularly in research involving spectral analysis of data.

Gary W. Grew, 3761 307-01-02

DE-I Spin-Scan Ozone Imaging Experiment

Using the imaging instrumentation aboard the recently launched Dynamics Explorer Spacecraft (DE-I), total-column ozone densities were obtained in the sunlit hemisphere by measuring the intensities of backscattered solar ultraviolet radiation with multiple filters and multiple photometers. The high-apogee altitude (23,000 km) of the eccentric polar orbit allows high-resolution global-scale images of the terrestrial ozone field to be obtained within 12 minutes. Previous ozone-monitoring spacecraft have required much longer time periods for comparable spatial coverage because of their lower altitudes (less than 1200 km). The much higher altitude of DE-I also provides the unique opportunity for continuous imaging of features for hours at a time. Near perigee, high-resolution images can be gained with pixel size as small as 3 km to view mesoscale atmospheric perturbations. Utilizing these data, the effects of planetary-scale, synoptic-scale, and mesoscale dynamical processes that control the distribution of ozone near the tropopause can be studied. Preliminary results show short-term variations (less than 1 day) in the synoptic ozone field, and these variations appear to be in accord with meteorological data. Initial results have demonstrated excellent agreement with ground-based ozone measurements.

The regions of high ozone values shown in this 12-minute image obtained on October 1, 1981, are found to correspond closely to 250-mb pressure lows and to regions of low tropopause altitudes, as defined by meteorological charts, for the same day. The sharp ozone gradient between high and low ozone centers (closely spaced contour lines) is consistent with the location of the main jet stream. Owing to the high inverse correlation (greater than 0.9) seen to date between ozone and tropopause height, it is expected that analysis of these data will make possible a better understanding of the time evolution of the dynamics of the Earth's atmosphere near the tropopause.

Gerald M. Keating, 2084 146-60-01

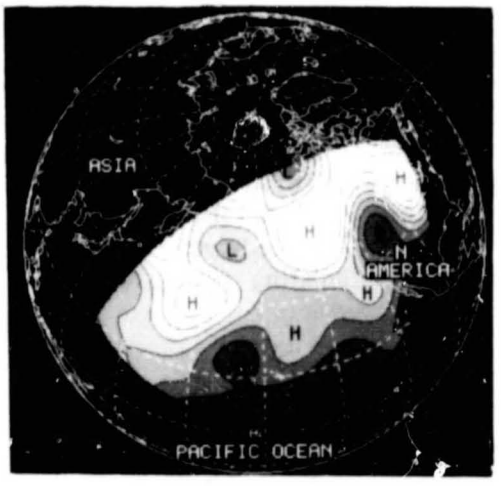

DE-I measurements of total ozone over the globe.

Catalyst for Closed-Cycle Operation of High-Energy Pulsed CO_2 Laser

CO_2 lidar has great potential for remote sensing of trace gases and aerosols and the determination of their transport from satellites

ORIGINAL PAGE IS
OF POOR QUALITY

and aircraft. For these applications a high-energy pulsed laser must be developed that will operate for long periods without having the laser gas mixture replenished. An important step has been taken in this technology with the development of a new catalyst that will recombine the dissociation products of CO_2.

High-energy pulsed CO_2 lasers normally require a supply of laser gas mixture constantly flowing through the laser cavity, because each pulse dissociates the CO_2 into CO and O_2. These product gases do not recombine at room temperature, and attempts have therefore been made to recombine the CO and O_2 over a catalyst at high temperature to overcome the need to carry bulky gas cylinders for resupplying the laser. For rare-isotope lasers (e.g., CO_2^{18}) the gas mixture is expensive. Recombining the CO and O_2 to CO_2 is more economical.

A more suitable catalyst would regenerate CO_2 from CO and O_2 at low temperatures. The catalyst must be efficient at low concentrations of CO and O_2 (less than 0.1 percent), and must be applicable to rare-isotope CO_2 chemistry. A promising new catalyst system has been developed at Langley that incorporates various oxidation states of copper, ranging from pure copper to Cu_2O and CuO. This catalyst has been tested in the laboratory with surrogate gas mixtures and was found to convert CO to CO_2 at 50°C. The catalyst is prepared by heating CuO in a reducing or inert atmosphere at high temperatures for several hours. Preliminary tests with a 0.7-J/pulse CO_2 laser have demonstrated closed-cycle operation in a prototype gas-recirculating system using this new catalyst system.

Robert S. Rogowski, 2818 307-01-02

Three-Dimensional Model Simulations of Ozone Distribution

An increasing awareness has developed that technological developments and increasing energy demands have the potential to alter atmospheric composition, with consequent undesirable effects upon environmental quality and global climate. An example is the possibility of depleting ozone as a result of aircraft engine emissions, halocarbons, fertilizers, and other chemicals. Extensive modeling efforts are being conducted at Langley to study the dynamical, chemical, and radiative processes that maintain the composition and structure of the atmosphere. Recently, a comprehensive treatment of stratospheric chemical processes has been incorporated into a three-dimensional general-circulation/transport model. This model simulates the spatial and temporal distribution of ozone and other important atmospheric constituents. In contrast with past three-dimensional modeling efforts, which simulated only ozone transport while prescribing other species distributions, the present model simulates the simultaneous transport of ozone and numerous other species important to the ozone budget.

Initial simulations have been conducted and are being analyzed. Shown in the figure is a comparison of total ozone (in Dobson units) after the initial 60 days of simulation with a comparable monthly mean for November 1974 obtained from the Nimbus 4 BUV (Backscattered Ultraviolet) Experiment. Good agreement between the observed and simulated distributions can be seen with respect to the location and magnitude of a number of individual features. These preliminary results are encouraging, but it should be noted that a large variability exists in the November monthly means from the 7 years of BUV data. The

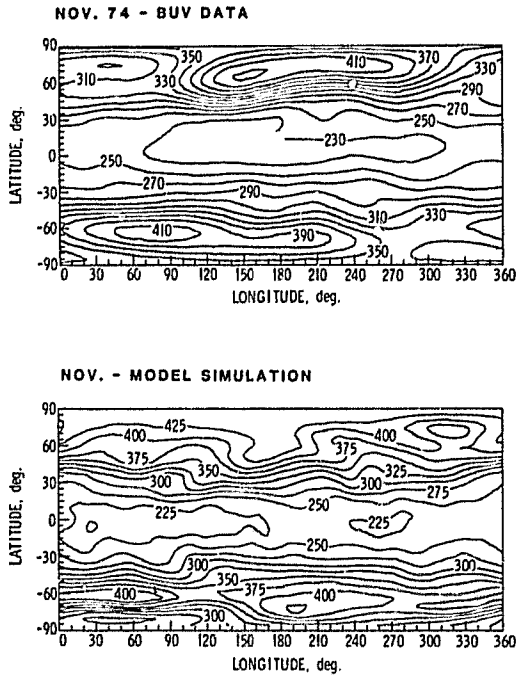

Total ozone monthly mean for November (Dobson units).

ORIGINAL PAGE IS
OF POOR QUALITY

model simulations are being extended through the Northern Hemisphere winter, where data for ozone as well as other species are available from the Nimbus 7 experiments (LIMS and SAMS) for more extensive comparisons.

William L. Grose, 2906 147-30-01

Influence of Solar Cycle on Atmospheric Variations

It has been demonstrated that changes in the middle atmosphere zonal flow can give rise to significant differences in the nature of vertical and horizontal planetary wave propagation. This can lead to significant changes in tropospheric planetary wave structure, even when the tropospheric forcing for such waves is constant. It has also been suggested that changes in solar UV flux with solar cycle can give rise to varying thermal and wind structure in the middle atmosphere. An initial attempt has been made to connect these concepts. A middle-atmospheric radiative computation was carried out for the observed winter and summer solstice conditions. The net radiative heating was determined for a stationary temperature field, thus allowing the dynamic heating to be inferred. Assuming that this dynamic heating remains unchanged with varying solar UV input, a new temperature structure was calculated that included, in an approximate way, the effect of changed ozone distribution. Geostrophic mean zonal flows were then determined for solar maximum and minimum conditions. Changes in the mean zonal flow of 10 to 20 m/sec were found in the middle-latitude upper stratosphere and lower mesosphere, with lesser changes at lower altitudes. A linear quasi-geostrophic calculation was then carried out for stratospheric planetary waves to assess the change in their structure for fixed tropospheric forcing, but using the computed mean zonal wind structure for solar maximum and minimum conditions.

Results suggest that large changes occur in the upper stratosphere in the amplitude of wave numbers 1 and 2 in the geopotential fields from solar minimum to solar maximum. Changes in the troposphere are more moderate, generally less than 10 percent. The figure illustrates the geopotential height difference field (solar minimum to solar maximum conditions) in meters for wave numbers 1 and 2 combined at 500 mb (approximately 5.5 km). Such changes may, in part, explain how climatic variations would be associated with the 11-year solar cycle.

Linwood B. Callis, Jr., 2985 147-30-01

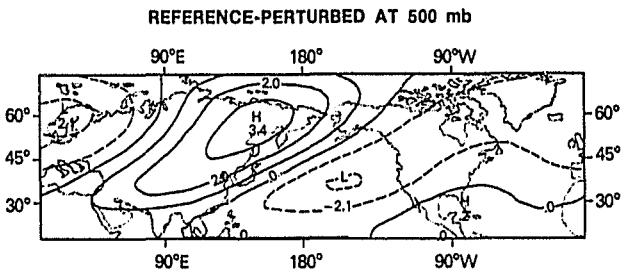

Geopotential height difference (m) over a solar cycle.

Analysis of Infrared Atmospheric Spectra

Expansion of the quantitative measurement data base on stratospheric phenomena lies at the heart of research to improve our understanding of the upper atmosphere and its susceptibility to change. Since virtually all molecular chemical species of stratospheric importance have infrared spectral features, high-resolution atmospheric spectra provide a powerful tool for addressing this need. Analysis of such spectra can yield simultaneous data on species, pressure, and temperature, as well as spectral information needed in the design of advanced atmospheric sensors, particularly for space application.

In collaboration with the University of Denver, comprehensive analyses have been undertaken of 5- to 12-μm atmospheric transmittance spectra obtained with the high-resolution (approximately 0.02 cm^{-1}) Denver balloon interferometer. Stratospheric spectra in the 5- to 8-μm region from a 1979 balloon flight have been studied to obtain important data on the O_2-continuum absorption centered near 1556 cm^{-1} (6.43 μm). The figure compares measured transmittances (solid symbols) from the Denver spectra and O_2 continuum transmittances (dashed curves) calculated from published absorption coefficients based on extrapolation of laboratory data to

ORIGINAL PAGE IS
OF POOR QUALITY

stratospheric conditions. Solar zenith angles and tangent altitudes are listed for the four spectra shown. This research shows that most of the atmospheric absorption in this spectral region is due to the O_2 continuum, and that it can be reasonably represented using extrapolated laboratory data. Corrections for this O_2 band are required in interpreting limb radiance data in the 6-μm region, and the results of this research have been significant in analyses of the H_2O and NO_2 channels of the Nimbus 7 Limb Infrared Monitor of the Stratosphere (LIMS) experiment.

These atmospheric spectra are also being studied to derive data on stratospheric species and temperature profiles. Absorption features near 1880 cm^{-1} (5.32 μm) in the 1979 spectra have provided quantitative data on N_2O. These results can be coupled with previous retrievals of NO, NO_2, HNO_3, H_2O, and O_3 from the same spectra by University of Denver and associated researchers. Similarly, analysis of temperature-dependent CO_2 features in 8- to 12-μm spectra from a 1981 Denver balloon flight indicate that this spectral region can be used to derive complementary data on stratospheric temperature profiles.

R. K. Seals, Jr., 2576 147-30-01

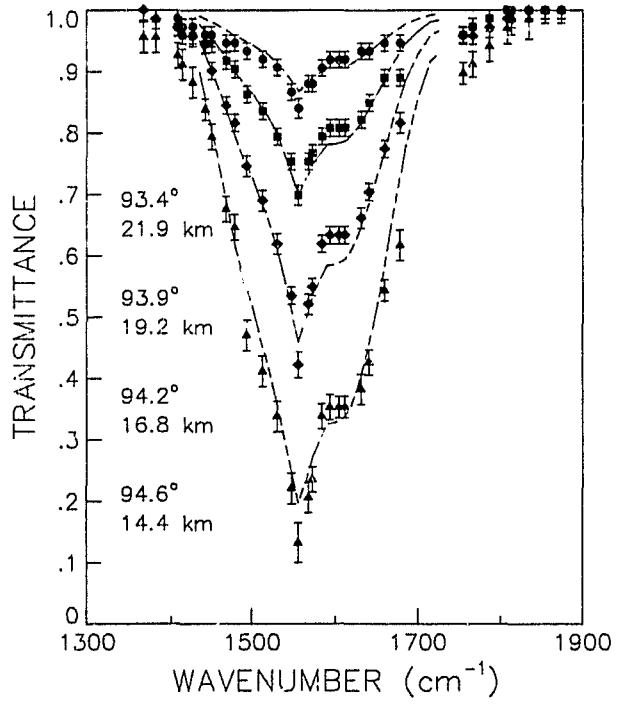

Observed background transmittance in 1979 Univ. of Denver spectra compared to calculated values for O_2 continuum only.

Estimation of Atmospheric Planetary Waves From Satellite Data

The increasing accuracy and resolution of data obtained from meteorological satellites are now providing a more detailed picture of the stratosphere than was previously possible. Unfortunately, the characteristics of the satellite system that account for its extensive coverage also introduce ambiguities into the data when a global map, or snapshot, of the data is produced. These problems arise because the atmosphere is in motion and the measurements are not made simultaneously around the globe.

Two methods of estimating the synoptic field have been examined. Both of these methods, Kalman filtering and complex demodulation, have been tested using simulated data from a general circulation model of the stratosphere. By testing the methods with the simulated data, we have been able to determine the effects of measurement errors, missing measurements, and time variations in the data fields, as well as the limitations imposed by the sampling rate. In general, these methods were used to recover the model data within the error limitations imposed on the data. However, periods of missing data (half a day or more) resulted in larger errors in the estimates.

These methods are now being used to obtain global field estimates of temperature, geopotential height, and trace species from data taken by the LIMS instrument on the Nimbus 7 satellite. These fields will be used in the analysis of stratospheric dynamics, transport, and chemistry.

Kenneth V. Haggard, 3431 307-02-02

Remote Sensing Optics of Turbid Waters

Laboratory experiments directed at quantifying the optical behavior of typical constituents of turbid coastal waters were completed in early 1982. Using facilities of the Langley Marine Upwelled Spectral Signature Laboratory (MUSSL), test waters of controlled composition were illuminated with an artificial solar simulator, and the intensity of radiation returned from the water was measured as a

ORIGINAL PAGE IS
OF POOR QUALITY

function of wavelength by a spectrometer scanning the 500- to 800-nm spectral interval. The measurement is analogous to the detection of radiation upwelled from a natural water body by a passive remote-sensing device, such as a multispectral scanner. Upwelled radiant intensity was normalized by the source intensity to produce a dimensionless percent "spectral reflectance" that can be manipulated and compared with results obtained under differing illumination conditions.

Experiments were focused on effects of particulate organic material suspended in the test water. In natural coastal waters such material is derived primarily from mechanical and biological breakdown of plant material. This particulate organic "detritus" is found in significant concentrations and could potentially impact remote-sensing signatures of turbid coastal waters. In the laboratory, particulate organic material was simulated by grinding dried grasses collected from marsh environments, which would be likely to contribute detritus to tidal waters. This material was added in varying concentrations to a filtered deionized base water and its effect on spectral reflectance was monitored.

The simulated organic detritus was unexpectedly benign over a range of concentrations from near zero to approximately 20 g/m^3, producing little or no change in water reflectance at any wavelength. At visible wavelengths (such as 550 nm, shown in the figure), effects of inorganic particulates and of dissolved organic carbon (humic acid) seem far more likely to influence remotely sensed water color. This suggests that remote-sensor measurements of naturally turbid waters, such as those found near the coast and in estuaries, rivers, reservoirs, and some lakes, can potentially be interpreted by means of a simple two-component model of constituent effects (incorporating inorganic particulates and dissolved organics).

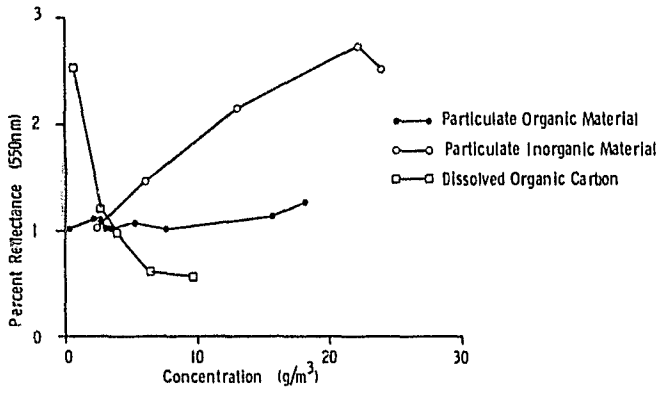

Reflectance cross sections for individual water constituents (550 nm).

D. S. Bartlett, 2871 307-02-02

Measuring Methane Fluxes From Wetland Environments

Methane (CH_4) is an important component of the biogeochemical cycle of carbon, and plays a potentially critical role in the geochemistry of carbon cycling. Recent analysis indicates a possible increase in atmospheric CH_4 of 0.1 ppm (from 1.6 to 1.7 ppm) over the past decade. Because sources of CH_4 are very poorly characterized, with particularly large uncertainties in estimates of natural source strengths, it is impossible to assess potential sources for an increase in global tropospheric CH_4 at present.

Wetland are hypothesized to be a major source of CH_4 in the atmosphere. A recent assessment of existing techniques and data for CH_4 flux from wetland environments suggests that the uncertainty in estimates of this source may exceed a factor of 10. Inland and coastal wetland habitats are ecologically and topographically complex, posing unique problems for quantitative monitoring of gas fluxes at water, plant, and soil interfaces with the atmosphere.

A technique for making field measurements of methane fluxes as a function of air velocity at a water-atmosphere interface has been developed and tested. The method uses a partitioned chamber placed over the water surface, where the air velocity along the surface can be controlled. The detection system is a nondispersive infrared absorption instrument developed at Langley that uses a concentrated sample of CH_4 to provide a selective filter for radiation absorbed in a gas mixture containing trace amounts of CH_4.

CH_4 fluxes as low as 2×10^{-3} (± 0.05) g m^{-2} day^{-1} were measured in this way, and additional CH_4 flux data were determined as functions of air velocity from 0.9 (± 0.1) m sec^{-1} to 4.4 (± 0.37) m sec^{-1}. Emission rates of gas across an air-water interface are controlled by shear stress of winds in the overlying gas. Our objective was to develop a relatively simple

ORIGINAL PAGE IS
OF POOR QUALITY

field system that had the capability of quantitatively controlling air velocity over the water surface within the chamber sampling area. This technique has the important advantage of including a continuous monitoring system so that data can be observed on site. Measurements obtained in coastal wetland creeks demonstrate that the CH_4 flux passing through a water-atmosphere interface can be quantified as a function of air velocity over the water surface.

D. I. Sebacher, 2871 199-30-36

MAPS Shuttle-Borne Remote Measurements of Carbon Monoxide

The MAPS (Measurement of Air Pollution from Satellites) experiment, flown as part of the OSTA-1 payload aboard the second flight of the Space Shuttle during November 1981, was the first attempt to measure a pollutant gas in the troposphere from an orbiting platform. The experiment measured carbon monoxide in two broad layers, one centered near 8 km altitude and another centered near 12 km altitude. On the global scale, carbon monoxide is a chemically active gas in the troposphere, with a mean mixing ratio of 10^{-7} by volume. It is produced both as a result of natural processes and as a result of man's technological and agricultural activities. Measurements taken at the surface and from aircraft show that the mixing ratio varies with latitude, longitude, altitude, and season. The long-range goal of the MAPS program is to define these variations on the global scale.

During the flight of STS-2, the MAPS experiment acquired 32 hours of nadir-viewing data between 38°N and 38°S latitude. This represents approximately 1 million km of data along the flight track. Instrument performance was excellent, with signal-to-noise ratios being about 150 to 1. An example of the reduced data for the layer centered near 8 km altitude is shown in the figure. The large noise spikes result from the presence of clouds in the field of view, and they will be removed with further data processing. The clear column mixing ratios are represented by the points along the lower edge of the trace. It can be seen that the CO mixing ratio increases toward the north and east until the vicinity of Cyprus is reached. From that point on, the mixing ratio falls very rapidly. (The small oscillations in the data, most clearly seen over the Arabian Sea, are an instrumental effect.) When the data reduction is complete, the MAPS experiment will have produced the first truly global measurements of carbon monoxide. The data will be highly useful to the understanding of man's possible impacts on the atmosphere.

Henry G. Reichle, Jr., 2576 618-22-31

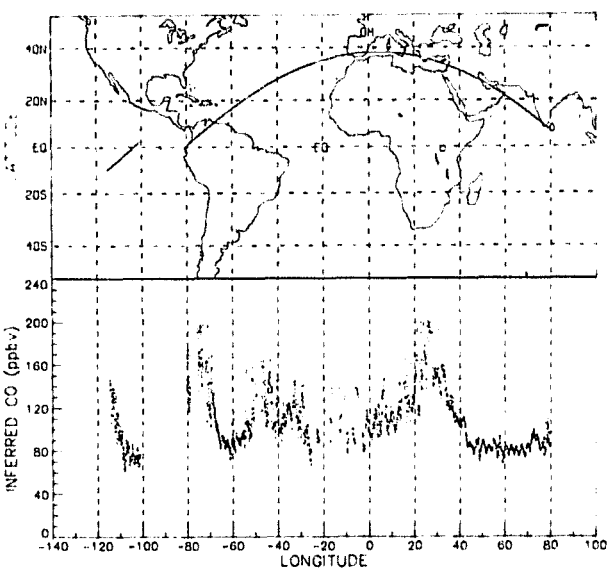

Middle-tropospheric carbon monoxide mixing ratio as determined by the MAPS experiment.

Stratospheric Phenomena Revealed by Nimbus 7 LIMS Data

The LIMS experiment was launched on Nimbus 7 for the purpose of sounding the upper-atmosphere composition and structure on a global scale. The instrument operated virtually without flaw from the time of turn-on (October 25, 1978) until turn-off (May 28, 1979), when the solid cryogen used for detector cooling had depleted as planned. Approximately 7000 radiance profiles were collected almost continuously each day. (The duty cycle was 11 days on and 1 day off.) The profiles were ground-processed to yield vertical profiles of temperature, ozone (O_3), water vapor (H_2O), nitrogen dioxide (NO_2), and nitric acid (HNO_3). Measurements were made at about 85-km

ORIGINAL PAGE IS
OF POOR QUALITY

intervals along the orbit track over the latitude range from approximately 64°S to 84°N. The vertical resolution was about 2 km for all measurements except NO_2 and H_2O, which had a value of about 4 km. The approximate altitude range of the measurements extended from 15 km to 70 km for temperature, 65 km for O_3, and 50 km for H_2O and HNO_3. The NO_2 data cover from about 20 km to 50 km. The measurement accuracy in the midstratosphere is estimated to be approximately 1 to 2 K for temperature, 15 percent for HNO_3, and 20 percent for O_3, H_2O, and NO_2. Precision of the measurements is approximately 0.3 K for temperature, about 4 percent for HNO_3, about 1 percent for O_3, 8 percent for H_2O, and about 5 percent for NO_2.

These data represent one of the most sophisticated and comprehensive data sets ever assembled on the upper atmosphere in terms of number and type of parameters, geographic coverage, spatial resolution, accuracy, precision, and simultaneity of measured parameters. The experiment operated during the time when a major stratospheric warming occurred in the Northern Hemisphere winter. This phenomenon, which is believed to be due to upward-propagating waves, results in large changes in temperature (on the order of 40 K) over time scales of 1 week. LIMS data display these changes prominently, not only in temperature but also in ozone. Ozone levels increased dramatically during the warming to achieve "spring-like" levels that remained as the spring season arrived. LIMS data also clearly show the division of the polar vortex into two vortices centered on either side of the pole during the warming. The circulation returned to the normal single-vortex condition after the warming was over. The 30-mb surface nitric acid levels show peak values centered in one quadrant of the globe prior to the warming, but during the event the concentration of HNO_3 is more diffuse and the region of high concentration is much less distinct. Other phenomena now apparent from the LIMS data are the presence of a rapid decrease in NO_2 concentration at high latitudes in winter and the presence of a low water vapor concentration in the tropics extending from about 35°S to 35°N and from 100 mb to 10 mb during all seasons. The NO_2 decrease is very sharp in the latitudinal direction, with mixing ratios changing by a factor of 3 over a 10° latitude range at the 10-mb level. This feature represents one of the greatest challenges to theory, and LIMS data will provide an extensive base of information for its study. The low water vapor levels in the tropics, as shown in the figure, have been suggested from single profiles measured previously from balloons, and these have now been confirmed by LIMS results. The area of decreased mixing ratio moves northward as the spring season approaches. All of these phenomena and several others that have been identified are the focus of scientific investigations being conducted by Langley scientists and other members of the LIMS science team. The data promise to shed new light on key upper-atmosphere processes that up to now have been only moderately understood.

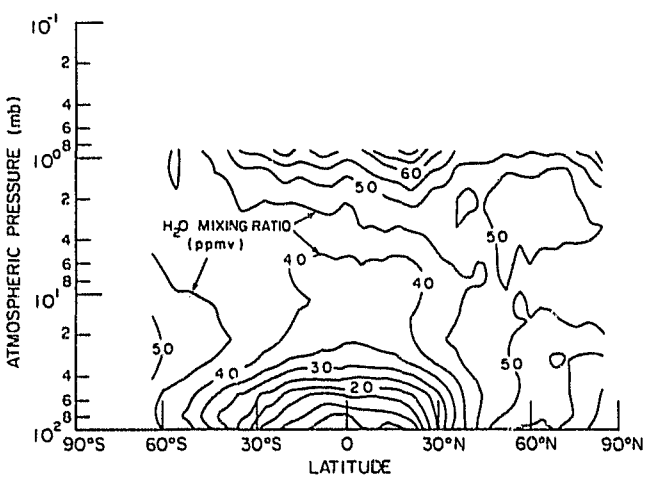

LIMS water vapor zonal mean cross section for February 21-25, 1979, obtained using research algorithm.

James M. Russell III, 2576 665-10-40

Satellite Observations of Stratospheric Aerosols

For the purpose of monitoring global stratospheric aerosols in a nearly continuous manner, NASA has been conducting two satellite experiments: SAM II (Stratospheric Aerosol Measurement) and SAGE (Stratospheric Aerosol and Gas Experiment). Both Langley experiments provide highly resolved vertical profiles of aerosol extinction at 1.0 μm wavelength. The measurements of aerosol extinction by SAM II are limited to polar regions in the latitude bands from 64° to 80°

ORIGINAL PAGE IS
OF POOR QUALITY

for both hemispheres, while SAGE covers latitudes between 79°S and 79°N (depending on the season).

Global background values of the stratospheric peak extinction are observed to be about 1 to 2 × 10^{-4} km^{-1}. However, numerous stratospheric clouds with 1 to 2 orders of magnitude enhancement of the peak extinction have been observed by SAM II and SAGE. The enhancement observed by SAM II is due to the presence of polar stratospheric clouds (PSC's), which are strongly correlated with low temperature. The occurrence of PSC's is more prevalent in the Antarctic region during the cold wintertime. It was observed, for example, that in the Antarctic stratosphere there were 1030 clouds in 1980 in comparison with 810 clouds in 1979. Much smaller numbers of clouds have been observed in the Arctic stratosphere, but the number of clouds was also higher in 1980 than in 1979, due to a colder winter period. The enhancement of aerosol extinction observed by SAGE can usually be traced to the eruption of volcanoes. Since SAGE provides global coverage in about 1 month, the transport, dispersion, and mass loading of stratospheric plumes created by major volcanic eruptions can be determined from SAGE measurements. For example, Mount St. Helens erupted on May 18, 1980, and produced a 100-percent enhancement in the northern hemispheric aerosol mass. SAGE has monitored a volcanic eruption about every 6 months since its February 1979 launch. The global aerosol data set that is evolving for the first time is proving to be extremely valuable in understanding the role aerosols play in radiation balance, water vapor budgets, and heterogeneous chemistry, and in studying atmospheric circulations.

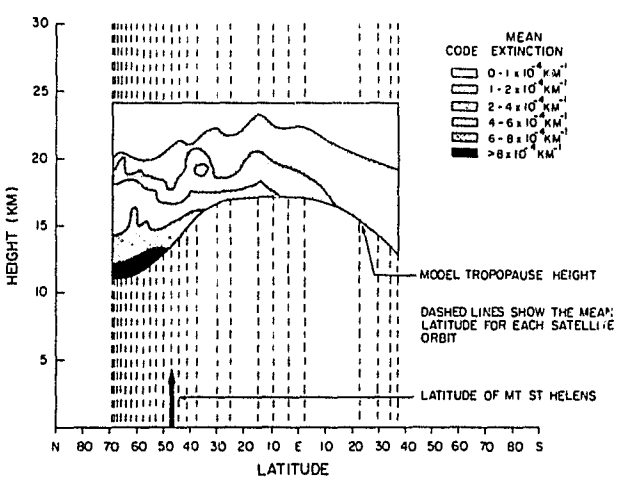

SAGE extinction measurements (zonal mean) for July 1 to August 12, 1980.

M. Patrick McCormick, 2065 665-10-40

Space Transportation Systems

Gap Heating in Shuttle Thermal Protection System

An analytical study has been performed to investigate the cause of excessive heating in the tile-to-tile gaps of the Shuttle Orbiter thermal protection system (TPS) during the initial flight. The excessive heating was evidenced by visible discoloration and charring of the filler bar and strain isolation pad (SIP) used in the attachment of tiles to the aluminum substrate. The study concentrated on determining if tile-to-tile steps and gaps measured after flight created a pressure disturbance around a stepped tile and caused hot-gas flow in the gaps during entry. Techniques based on existing experimental data were developed to predict the local pressure disturbances. In addition, a technique was devised to approximate the energy potential of the air flowing from the local boundary layer into the tile-to-tile gap. A tile flow model, developed previously to determine the pressure loading on a tile during ascent, was modified to account for compressibility in the flow in the tile-to-tile gaps during entry. The flow model predicts mass flow rates and pressure distributions in the tile-to-tile gaps, in the SIP, and within the tiles. It utilizes analogies between conventional heat conduction and internal gas flow in the calculation procedure. With the flow rates established, a thermal model of adjacent tiles, the tile-to-tile gap, filler bar, and SIP was used to predict temperature distributions throughout the system while maintaining an energy balance on the air flowing through the tile array.

Combinations of tile step heights and tile-to-tile gaps that could cause varying degrees of damage to the filler bar on the lower fuselage and wing were determined. The

ORIGINAL PAGE IS
OF POOR QUALITY

magnitudes of the predicted step heights and gaps were comparable to the step heights and gaps observed in damaged regions after the first several flights of the Shuttle. The results indicate that the tolerances on steps and gaps maintained during tile installation must also be maintained in flight. If the tolerances cannot be maintained, tile-to-tile gap filler would be an alternative.

Dewey M. Smith, 4508 986-15-10

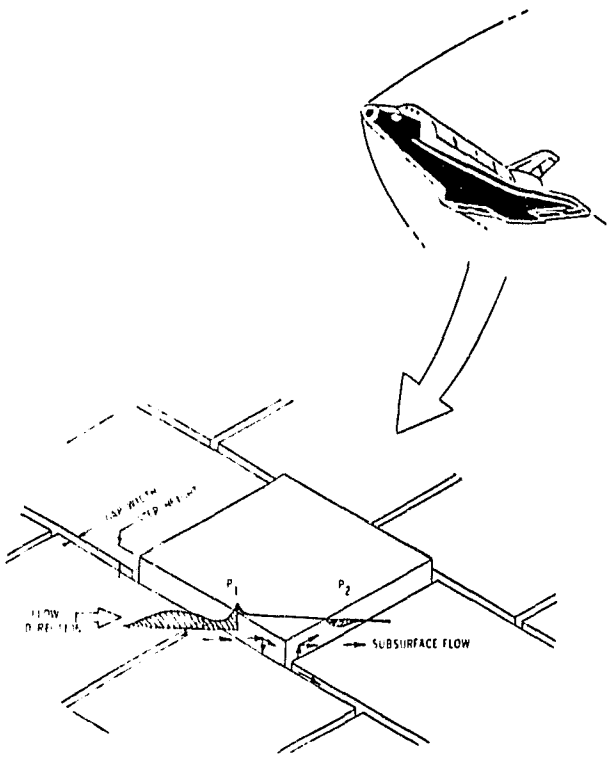

Stepped tile model.